Isotope Insights into the **Phosphorus Cycle** of **Marine Sediments**

Dissertation

zur Erlangung des Doktorgrads der Naturwissenschaften

(Dr. rer. nat.)

am Fachbereich für Geowissenschaften

Universität Bremen

vorgelegt von

Tobias Karl Magnus Goldhammer

Oktober 2009

1. Gutachter PD Dr. Matthias Zabel

2. Gutachter Prof. Dr. Kai-Uwe Hinrichs

Tag des Dissertationskolloquiums: 26. Oktober 2009

What is a scientist after all?

It is a curious man looking through a keyhole, the keyhole of nature - trying to know what's going on.

Jacques-Yves Cousteau

Preface

This study was funded by Deutsche Forschungsgemeinschaft (DFG) via DFG Research Center and Excellence Cluster "MARUM – The Ocean in the Earth System" and part of the Project B2 "Simulation of biogeochemical processes in the marine subsurface: understanding carbon-flow and identification of process-specific biosignatures". The project has been supervised by PD Dr. Matthias Zabel (MARUM and University of Bremen), and Dr. Timothy G. Ferdelman (MARUM and Max-Planck-Institute for Marine Microbiology, Bremen). The research was conducted at Geochemistry and Hydrogeology Group, Department of Geosciences, University of Bremen, and at Biogeochemistry Group, Department of Biogeochemistry, Max-Planck-Institute for Marine Microbiology, Bremen, from July 2006 to September 2009.

The present dissertation focuses on identifying the microbial contribution to marine phosphorus biogeochemistry and comprises six parts. The first is an introduction into the topic, the scientific rationale of the study, and the approaches followed. The second to fourth form the main part of the dissertation, comprising three research articles, two submitted to international journals for publication, and one as a draft close to submission. The fifth gives a short conclusion and perspectives for future research. The sixth is an appendix containing abstracts of four additional research manuscripts published or prepared during the period of the project, and an overview of (co-)supervised student projects.

Thesis Abstract

The aim of the present dissertation was to investigate the microbial contribution to biogeochemical phosphorus (P) cycling in marine sediments. This essential nutrient controls marine primary production on geologic and recent time scales. Regeneration of phosphate (P_i) from organic matter and sequestration in phosphorites are major processes in the ocean's P cycle, in which the benthic microbial community has decisive influence on the source-sink balance. Two isotopic methods elucidated these biogeochemical transformations of P_i in detail and allowed new insights that extended the scope of investigations of P_i concentrations and pools alone.

Oxygen isotopes of dissolved P_i ($\delta^{18}O_P$) have proven a suitable biosignature for microbial P_i regeneration and cycling. We refined and validated a micro extraction protocol for the separation and mass spectrometry of ultra low P_i samples (< 1 µmol) of marine pore waters. We obtained a novel dataset on $\delta^{18}O_P$ from two sediment cores off Morocco. With increasing depth, isotopic equilibration of P_i with water indicated thorough microbial P_i turnover, while disequilibria at the top pointed to P_i release from organic matter.

In a comprehensive study on benthic P_i cycling in the Benguela upwelling system, we combined pore water inventories and modeling with the investigation of $\delta^{18}O_P$, in order to detect the microbial control on P_i regeneration and the influence of different sedimentary settings of mineralization and P_i availability. Pattern of $\delta^{18}O_P$ in the sediments were more complex than expected from geochemical evidence. Isotope disequilibria were preserved at low P_i deep-sea sites, and thorough equilibria at sites with high mineralization and P_i concentration. Bottom water data pointed to a discontinuity between water column and pore water P_i. An isotope mass balance model, considering enzyme and substrate systems, allowed us to estimate the P_i recycling efficiency of the benthic community. We believe that different microbial P_i uptake strategies, controlled by ambient P_i availability, strongly influence the preservation of pore water $\delta^{18}O_P$.

We finally sought to elucidate the role of microorganisms in authigenic phosphorite formation, and applied a radioisotope tracer (^{33}P) to track sedimentary P_i transfers in incubation experiments. Our results constitute the first direct evidence that the presence of live bacteria is pivotal to phosphorite precipitation. Sequestration of P_i outbalanced regeneration under anoxic conditions, and P_i uptake by *Thiomargarita namibiensis* strongly suggested that these large sulfur bacteria provide a transient P_i reservoir. The unique physiology of P_i uptake and release in these bacteria may antagonize the positive feedback between enhanced P_i regeneration, stimulated primary production, and anoxia in bottom waters of upwelling regions.

Kurzfassung

Mit der vorliegenden Dissertation möchte ich einen Beitrag zur Aufklärung der Rolle von Mikroorganismen im biogeochemischen Phosphorkreislauf in marinen Sedimenten leisten. Die Verfügbarkeit von Phosphor als lebenswichtigem Nährstoff bestimmt die Primärproduktion der Weltmeere - sowohl heute als auch über geologische Zeiträume. Die Freisetzung von Phosphat aus organischem Material und die Festlegung in Phosphoriten sind dabei Schlüsselprozesse im marinen Phosphorkreislauf. In beiden Prozessen ist die Aktivität von Mikroorganismen im Meeresboden entscheidend für die Bilanz aus Quellen und Senken. Zwei isotopenorientierte Methoden wurden angewandt, um diese biogeochemischen Umwandlungsprozesse des Phosphats detailliert zu beleuchten. Dieser Ansatz ermöglichte neuartige Einblicke, die mit einer einfachen Inventarisierung von Phosphatkonzentrationen und –vorratsmengen nicht möglich gewesen wäre.

Das Verhältnis der stabilen Sauerstoffisotope (^{18}O) im gelösten Phosphatmolekül beinhaltet wichtige Informationen über mikrobielle Phosphatregeneration und -stoffwechsel. Ein speziell angepasstes Mikroextraktionsverfahren ermöglichte nun erstmalig, sehr geringe Phosphatmengen aus marinen Porenwasserproben (< 1 µmol) für die Massenspektrometrie verfügbar zu machen. Der erste Datensatz von ^{18}O im Porenwasserphosphat wurde aus zwei Sedimentkernen vor der marokkanischen Küste gewonnen. Dabei deutete ein mit der Tiefe zunehmendes isotopisches Gleichgewicht zwischen Phosphat und Wasser einen regen mikrobiellen Umsatz an, während in den obersten Sedimentschichten eine Abweichung von diesem Gleichgewicht auf vermehrte Phosphatfreisetzung aus der organischen Material hinwies.

In einer zweiten, umfangreichen Studie des benthischen Phosphorkreislaufs im Auftriebsgebiet des Benguelastroms vor der Küste Nambias wurden die geochemische Zusammensetzung des Porenwassers bestimmt und Umsatzraten modelliert, und mit einer Analyse des Phosphat-^{18}O kombiniert. Dabei sollte untersucht werden, welche mikrobielle Kontrollgrößen auf die Regeneration von Phosphat Einfluß nehmen, und ob unterschiedliche geochemische Randbedingungen in Bezug auf Mineralisationsprozesse oder Phosphatverfügbarkeit eine Rolle spielen. Die Verteilungsmuster der Phosphat-^{18}O-Daten waren weit komplizierter zu interpretieren, als die Ergebnisse der geochemischen Porenwasseranalysen erwarten ließen. In Tiefseesedimenten mit niedrigen Phosphatkonzentrationen waren isotopische Ungleichgewichte ausgeprägt, während in Schelfsedimenten mit hoher Mineralisationsrate und hohen Phosphatgehalten im Porenwasser isotopische Gleichgewichte vorherrschten. Messungen in Bodenwasserproben deuteten zunächst auf eine Entkopplung von Phosphatumsetzungsprozessen in Wassersäule und

Sedimenten hin. Mit einer Isotopenmassenbilanz, die spezifische Effekte verschiedener Enzyme und Substrate berücksichtigt, konnte die Effizienz des mikrobiellen Phosphat-Recyclings abgeschätzt werden. Unsere Ergebnisse deuten darauf hin, dass unterschiedliche Transportsysteme für die zelluläre Phosphataufnahme die Konservierung der Sauerstoffisotopensignatur beeinflussen. Die Ausprägung dieser Transportsysteme wird dabei entscheidend durch die Verfügbarkeit von Phosphat kontrolliert.

In einem zweiten isotopenorientierten Ansatz sollte die Rolle von Mikroorganismen in der Bildung von authigenen Phosphoriten näher untersucht werden. Dazu wurden Inkubationsexperimente mit Radioisotopenmarkierungen durchgeführt, um Phosphattransfers in Sedimenten beobachten und quantifizieren zu können. Diese Studie lieferte einen einzigartigen direkten Beleg für die Stimulation der Phosphoritbildung durch lebendige Mikroorganismen im Sediment. Die Festlegungsraten von Phosphat in der Apatitfraktion, und damit die Stärke dieser Phosphatsenke, übertraf unter anoxischen Bedingungen die potentielle Freisetzungsrate aus organischem Material bei weitem. Die beobachtete Phosphataufnahme des großen Schwefelbakteriums *Thiomargarita namibiensis* ließ vermuten, dass diese Bakterien einen temporären Zwischenspeicher für Phosphat darstellen. Ihre besondere Physiologie, die Phosphataufnahme und -abgabe beinhaltet, kann so einem positiven Rückkopplungsprozess entgegen wirken, der ansonsten einen Kreislauf aus erhöhter Phosphatfreisetzung unter anoxischen Bedingungen, stimulierter Primärproduktion, und dadurch verstärkten anoxischen Verhältnissen im Bodenwasser von Auftriebsgebieten bedingt.

Table of Contents

List of Figures

List of Tables

I

Introduction

I.1 The marine phosphorus cycle - setting the stage

I.1.1 Phosphorus as an essential nutrient

Phosphorus (P) is one of the essential nutrients for life on this planet. All known living organisms synthesize phosphorylated biomolecules to support cell structure and function (Pasek 2008). Information transfer within cells and during replication is mediated by nucleic acids (RNA, DNA), in which nucleotide phosphoesters provide the structural backbone. Energetic coupling of catabolic and anabolic pathways is accomplished by coenzymes (NADP+), or by oxidative phosphorylation and dephosphorylation of adenosine phosphates (AMP, ADP, ATP), a mechanism that utilizes the high amounts of energy that are stored in the phosphoanhydride bonds. Intracellular polyphosphates stored in granules are considered as a primeval precursor of the ATP system, but are still prevalent in prokaryotes today (Kornberg 1995). The structural integrity of the cell is often maintained by phospholipids (such as bacterial lecithine). A non-comprehensive compilation of biologically important phosphorus compounds can be found in Figure I.1.

Phosphorus occurs in natural systems almost exclusively in the form of ortho-phosphate (PO_4^{3-}, abbreviated as P_i), and phosphorus biogeochemistry is phosphate biogeochemistry in most instances. Under ambient conditions at the Earth's surface, phosphorus does usually not undergo redox reactions (Schink and Friedrich 2000). Phosphorus has the oxidation state of +5 in the phosphate molecule, and the reduction requires extremely low redox potentials (between -515 and -922 mV). These are energetically unfavorable in organisms, so that the occurrence of phosphonates and phosphites, as secondary metabolites, is the exception (Schink et al. 2002).

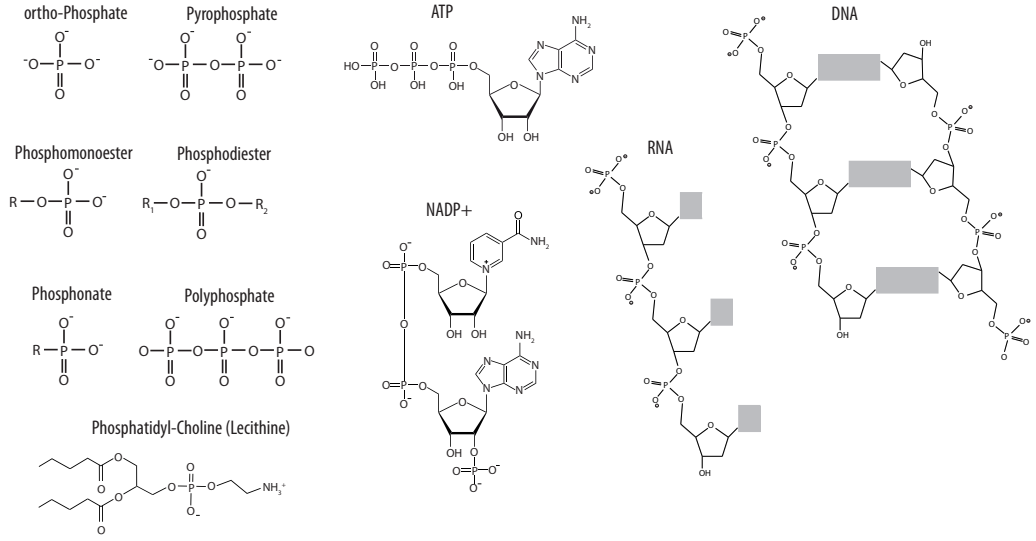

Figure I.1: Physiologially important, phosphorylated biomolecules that are widespread in organisms

I.1.2 Pathways and fluxes of phosphorus in the ocean

The availability of P will strongly influence the productivity and structure of ecosystems (Paytan and McLaughlin 2007). The marine phosphorus cycle is thus tightly coupled to global biogeochemical cycles of other major elements, such as carbon and oxygen (Berner 1990, Colman et al. 2000). It is accepted that P is the ultimate limiting nutrient in the ocean, and its source-sink balance controls production over geologic timescales (Bjerrum and Canfield 2002, Redfield 1958, Van Capellen and Ingall 1994). But recently, evidence has accumulated that phosphorus limitation in the ocean is a much more relevant phenomenon than previously thought also on short timescales (Paytan and McLaughlin 2007). So what are the important fluxes and transformations of phosphorus in the ocean? We will examine these on the basis of Figure I.2A.

The major P source to the ocean is continental weathering (Delaney 1998). Dissolved and particulate inorganic phosphate (P_i and PIP) and dissolved and particulate organic phosphorus (DOP and POP) are brought into the oceans by river transport (Föllmi 1996). The organic fraction stems from terrestrial and/or aquatic organisms. The atmospheric deposition of dust-associated PIP and POP is of importance at continental margins of the subtropics, and often the only external phosphorus source in the remote oligotrophic ocean (Benitez-Nelson 2000, Paytan and McLaughlin 2007). In the river load, PIP comprises grains of apatite and other minerals, and adsorbed P_i on iron (Fe)

or manganese (Mn) oxyhydroxides. This fraction is usually deposited in the coastal environments and bypasses the oceanic cycle (Paytan and McLaughlin 2007, Figure I.2A, Table I.1). Dissolved P_i is instantly consumed in primary production in the surface waters, and the uptake of P_i by photosynthetic phytoplankton transfers it to the POP pool.

Hence, the P_i concentrations in surface waters are usually depleted (Delaney 1998). Incorporation of P_i into planktonic biomass occurs in the traditional C:P ratio of 106:1 found by (Redfield 1958) that is reflected in the well-known sum formula of photosynthesis

$$106\ CO_2 + 16\ HNO_3 + H_3PO_4 + 122\ H_2O \rightarrow C_{106}H_{263}O_{110}N_{16}P + 138\ O_2 \qquad \text{Equation I.1}$$

Much of the POP formed in the photic zone is aggregated and sinks towards the sea floor. During this sinking, starting already in the upper water column, microbial remineralization processes regenerate P_i from POP. Diffusion and, more important, advective

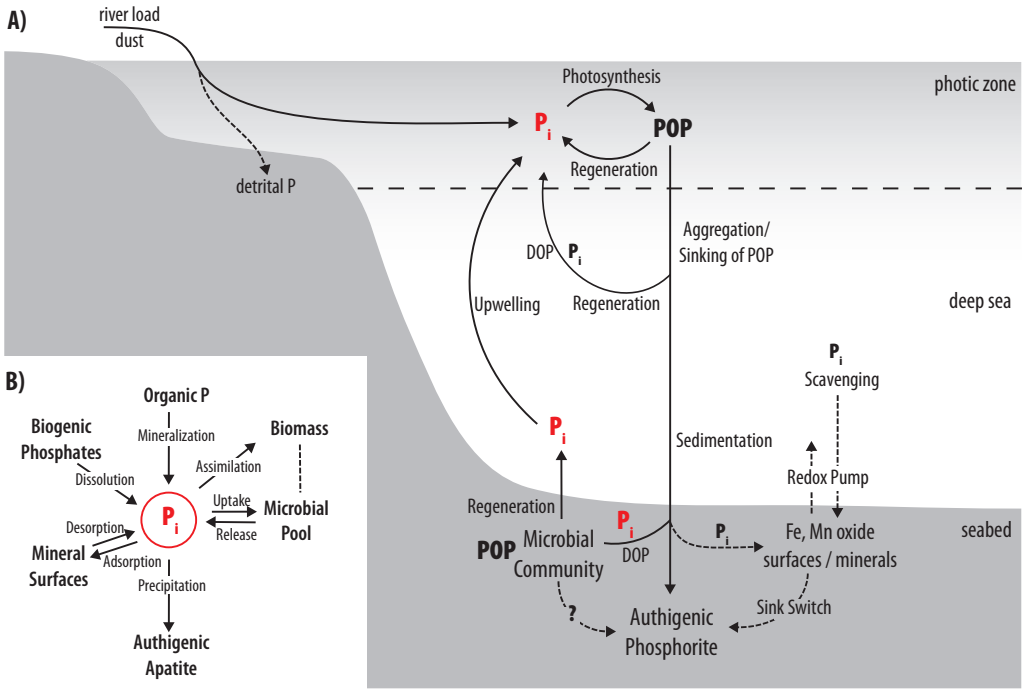

Figure I.2 Phosphorus cycling in the ocean. **(A)** Scheme of important transformations, fluxes and regeneration pathways of dissolved phosphate (P_i) between the water column and the seabed. The present dissertation focuses on the sedimentary transformations of P_i mediated by the microbial community (bottom left). **(B)** P_i in pore water of the sediment connects various processes and P pools. Inspired by Paytan and McLaughlin (2007) and Compton et al. (2000)

Table I.1 Present day phosphorus fluxes to the ocean and turnover fluxes within the ocean (in 10^{12} g a^{-1}). The inorganic flux (DIP, PIP) has doubled anthropogenically. Data from Benitez-Nelson (2000), Compton et al. (2000), Föllmi (1996), and Paytan and McLaughlin (2007)

Influx	10^{12} g a^{-1}	Internal Turnover	10^{12} g a^{-1}
P_i	0.8 – 1.4	Burial of detrital PIP	-16.5
DOP	0.2	Burial of P_i (shelves)	-2.35
POP	0.9	Burial of P_i (ocean basins)	-2.35
PIP (Fe bound)	1.3 – 7.4	P_i fixation in OM	-102.5
PIP (detrital)	14.5 – 20.5	P_i regeneration	96.8
Total	17.7 – 30.4	Total	-26.9

transport with intermediate and deep ocean currents in upwelling systems bring P_i back into the photic zone (Figure I.2A), where it is again available for primary production. About 5 to 10 % of the downward P flux finally reaches the sea floor and is transformed in the subsurface (Compton et al. 2000, Föllmi 1996). Sequential extractions of bottom P flux material have revealed an average composition of 40 % POP, 25 % authigenic PIP, 21% labile and Fe oxyhydroxide associated P_i, and 13 % detrital PIP (Faul et al. 2005). The Fe oxyhydroxide associated P_i has been scavenged from the water column by sinking minerals, and plays a role for oceanic settings where input of iron or manganese is pronounced (Compton et al. 2000).

The seabed is the main reservoir for oceanic phosphorus (Föllmi 1996), and processes of sedimentary burial and transformation are diverse. For simplification, we distinguish three process complexes that are described in the following.

Redox dependent transformations of iron and manganese phases

The first are the Fe- and Mn-associated transformations that include adsorption of P_i on mineral surfaces and diagenetic sequestration of P in phases such as vivianite (Krom and Berner 1980, Slomp et al. 1996). Reductive dissolution of Fe and Mn oxyhydroxides releases P_i back to the pore water and the overlying water column. In contrast, a "cap" of Fe and Mn oxyhydroxides in the top layers of the sediments will absorb P_i that is diffusing upwards along a concentration gradient. Hence, redox conditions (*i.e.*, the presence of anaerobic or aerobic bottom waters) are decisive for the P_i flux balance into or out of

the sediments. This control is indeed so effective in Fe dominated systems, that flux studies with benthic chambers have stimulated a seldom challenged paradigm that anoxia generally enhance benthic P reflux to the water column (Ingall and Jahnke 1994, Ingall and Jahnke 1997, Slomp et al. 1996, Van Capellen and Ingall 1994).

Microbial mineralization of organic matter

The second complex is the burial and regeneration of P_i during mineralization of organic matter (OM). Organic matter is the dominant shuttle of P transfer from the water column to the sediments (McManus et al. 1997). Microbial breakdown of particulate into dissolved OM transforms POP to DOP, and subsequent mineralization is the most fundamental source for dissolved P_i in the pore water (Berner 1990, Föllmi 1996). In the classic scheme of Froelich et al. (1979), available terminal electron acceptors (TEA) are consumed in the order of the Gibb's free energy produced in their reaction (Table I.2).

During microbial respiration of OM, P is preferentially regenerated, and the C:P ratio of OM increases with depth (Ingall and Van Capellen 1990). Thus, refractory OM buried deep in the subsurface has C:P ratios typically much higher than Redfield (Algeo and Ingall 2007, Anderson et al. 2001, Ingall and Van Capellen 1990), and the C:P of the mineralization products (CO_2 and P_i) is much smaller than Redfield (Anderson and Sarmiento 1994). There are two plausible reasons for this preferential regeneration. First, P limitation is widespread in planktonic communities in the surface and deeper

Table I.2 Remineralization of Redfield organic matter by different terminal electron acceptors, after Froelich et al. (1979). The order is controlled by the yield of Gibb's free energy (ΔG_r) of the reaction, here reported per mole of "Redfield-molecule"

Pathway	Reaction (sum equation)	ΔGr kJ mol^{-1}
Oxygen consumption	$(CH_2O)_{106}(NH_3)_{16}(H_3PO_4) + 138\ O_2 \rightarrow 106\ CO_2 + 16HNO_3 + 122\ H_2O + H_3PO_4$	-56367
Mn oxide reduction	$(CH_2O)_{106}(NH_3)_{16}(H_3PO_4) + 236\ MnO_2 + 476\ H^+ \rightarrow 236\ Mn^{2+} + 106\ CO_2 + 8\ N_2 + 366\ H_2O + H_3PO_4$	-54600
Nitrate reduction (to ammonium)	$(CH_2O)_{106}(NH_3)_{16}(H_3PO_4) + 84.8\ HNO_3 \rightarrow 106\ CO_2 + 42.2\ N_2 + 16\ NH_3 + 148.4\ H_2O + H_3PO_4$	-48593
Fe oxide reduction	$(CH_2O)_{106}(NH_3)_{16}(H_3PO_4) + 212\ Fe_2O_3 + 848\ H^+ \rightarrow 424\ Fe^{2+} + 106\ CO_2 + 16\ NH_3 + 530\ H_2O + H_3PO_4$	-24915
Sulfate reduction	$(CH_2O)_{106}(NH_3)_{16}(H_3PO_4) + 53\ SO_4^{2-} \rightarrow 106\ CO_2 + 16\ NH_3 + 53\ S^{2-} + 106\ H_2O + H_3PO_4$	-6715
Fermentative Methanogenesis	$(CH_2O)_{106}(NH_3)_{16}(H_3PO_4) \rightarrow 53\ CO_2 + 53\ CH_4 + 16\ NH_3 + H_3PO_4$	-6185

water column (Dyhrman and Palenik 1999, Sundareshwar et al. 2003, Tanaka et al. 2004, Thingstad et al. 1998) and may also occur in sediments. Microbial communities of marine environments that receive little external input of P must effectively recycle P_i from the organic pool. Second, it is also known that microorganisms in the deep-sea and in sediments are limited in OM as a carbon source (Sander and Kalff 1993). Remaining P_i headgroups in OM prevent C uptake and metabolism (Colman et al. 2005). In this case, dephosphorylation of OM will effect preferential regeneration of P_i as a by-product of C mineralization.

Formation of phosphorites

The third complex is the formation of authigenic phosphate minerals, usually termed phosphogenesis (Föllmi 1996). The sequestration and burial of P in these phases is a true sink and considered as the ultimate removal from the marine cycle (Compton et al. 2000, Froelich et al. 1982). Phosphorites are sediments containing more than 18 % of pyrophosphate (Föllmi 1996, and references therein). The importance of phosphogenesis for the global P cycle is highlighted by the existence of giant ancient phosphorite deposits. Their depositional settings are supposedly similar to sites of modern phosphogenesis (Filipelli and Delaney 1992). They often coincide with organic-rich facies in the geological record, and are linked to episodes of high productivity, intense rock weathering, and P accumulation in sedimentary basins (Föllmi 1996).

The chemical basis of phosphogenesis is the reaction of dissolved P_i in the sediment pore water with calcium (Ca^{2+}) that produces insoluble calcium-phosphate minerals, such as francolite, carbonate fluorapatite (CFA), or hydroxyapatite (HAp). The initially amorphous precipitates are metastable nuclei for further mineral growth and diagenetically consolidated with proceeding burial (Blackwelder 1916, Föllmi 1996, Van Capellen and Berner 1991). The formation of authigenic phases depends on the interstitial P_i enrichment. The most important source of pore water P_i is microbial breakdown of OM. The magnitude of diffusive escape of pore water P_i to the water column often depends on redox conditions in the overlying waters (Colman et al. 2000, Ingall and Jahnke 1994), especially in iron dominated systems as illustrated above. In sediments rich in organic matter, highest P_i accumulations occur in the uppermost part of the sediments near the benthic interface (Föllmi 1996), due to the fact that microbial remineralization (and preferential P regeneration) is most intense in freshly deposited sediments (Froelich et al. 1979). The chemical controls on phosphate precipitation have been elaborated in detail (e.g. Froelich 1988, Van Capellen and Berner 1991). However, the observation that pore waters are frequently supersaturated in P_i respective to calcium phosphates, but do

not precipitate (Föllmi 1996), has stimulated hypotheses of a biological contribution to this process (e.g. Gächter et al. 1988, Nathan et al. 1993). Today, there is growing evidence that the role of microorganisms for phosphorite formation is not restricted to the liberation of P_i from organic matter, but includes active engagement in P_i concentration and precipitation, for instance by precipitation of apatite on ubiquitous polyphosphate grains of planktonic origin (Diaz et al. 2008, Schulz and Schulz 2005). However, the challenging note of Föllmi (1996) - "the direct and active participation of microorganisms in apatite formation has not yet been positively demonstrated" – holds true until today.

Focus of the dissertation: sedimentary pore water phosphate

We have to keep in mind that several cross-linkages exist between these three complexes. We therefore regard the dissolved P_i pool in the pore water of sediments as an interface between the fundamental transformations (Figure I.2B). Redox-dependent adsorption and desorption on mineral surfaces, dissolution of biogenic phosphates (e.g. fish bones), mineralization of OM, microbial uptake and release as well as incorporation into living biomass, and the precipitation of authigenic apatite influence the pore water P_i pool. The present dissertation aims to elucidate the contribution of benthic microbial communities to two important aspects of this network: the regeneration of phosphate by mineralization of organic matter in the sediments, and the authigenic formation of apatites.

I.1.3 Hot spots of global phosphorus biogeochemistry: regions of oceanic upwelling

Nutrient availability and primary production are not equally distributed across the global ocean. The shallow coastal waters at continental margins support abundant life due to their proximity of external nutrient input from the continents, while remote regions of the open are much lower in production (Longhurst et al. 1995). The impact of nutrients on ecosystem production becomes particularly evident at those subtropical eastern boundaries of the ocean basins, where trade winds and oceanic currents force nutrient rich, deep water masses to ascend. The flux of P_i with upwelling currents may be as high as 95 % of the ocean's standing P stock (Benitez-Nelson 2000, Föllmi 1996). Though the main upwelling systems at the continental margins of the Pacific (California and Humboldt current) and the Atlantic (Canary and Benguela current) cover only a small portion of the global ocean's volume (0.1%), they account for as much as 5 % of the global marine primary production (Carr 2002). Among these, the Benguela system off-

shore Namibia is the most productive (Carr 2002). Some reasons why upwelling regions may be perceived as hot spots of P biogeochemistry are highlighted below.

High rates of mineralization and alternating redox conditions

Sedimentation of organic matter is high beneath the productive coastal waters, and the surface shelf sediments often exhibit high contents in organic carbon. This leads to remarkable rates of benthic mineralization in the upwelling regions (Seiter et al. 2005) and intense microbial activity. Accordingly, concentrations of P_i in the pore waters and flux rates across the sediment-water interface are high. Oxygen is episodically depleted in the bottom waters, and periodic switches between anoxic and oxic conditions are characteristic of the system (e.g. Brüchert et al. 2003). Both P_i regeneration and redox cycles are known to impact on P cycling (Figure I.2A).

Sites of modern phosphogenesis

Although phosphorite formation is somewhat widespread in the world's ocean (Baturin 1988, Ruttenberg and Berner 1993), it is evident that phosphogenesis is most pronounced in modern upwelling systems (Föllmi 1996). For example, the continental margins of Peru and Chile, and of Southwest Africa and Namibia, are regions where large phosphorite deposits have formed within the past ~300,000 years (Baturin and Bezrukov 1979, Baturin et al. 1972, Veeh and Burnett 1973). These systems are considered as modern analogues to ancient phosphorite deposits (Filipelli and Delaney 1992).

Peculiar benthic communities

Among the microbial communities that inhabit the sediments of upwelling regions, dense populations of large sulfur bacteria are probably the most curious organisms. They belong to the filamentous genera *Thioploca* and *Beggiatoa*, and the spherical species *Thiomargarita namibiensis* (Schulz and Jorgensen 2001). Their peculiar physiology has raised a debate about their role in benthic P cycling, especially in the formation of authigenic phosphates.

For example, *Thiomargarita namibiensis* is a non-motile sulfide oxidizer that has developed a unique strategy to cope with the spatial and temporal separation of electron acceptors and donors. Under oxic bottom water conditions, it oxidizes sulfide with oxygen and nitrate (Schulz 2006), and may use up to 98 vol. % of the vacuole for nitrate storage. Under anoxic conditions, sulfide is taken up and kept in inclusions of elemental sulfur, and acetate (as C source) is stored in glycogen. The storage of nitrate and sulfide

respective acetate unites electron acceptor and donors. Additionally, under the energetically favorable oxic conditions, dissolved P_i is assimilated and stored in polyphosphate granules. These serve most likely as an energy backup for enduring anoxia (Schulz 2006). Breakdown of the polyphosphates yields energy (Kornberg 1995), and P_i is released to the surrounding pore water. The ability to accumulate P_i and induce high pore water oversaturation with respect to apatite, and co-occurrence of high cell numbers and authigenic phosphate has stimulated the hypothesis that *Thiomargarita namibiensis* is responsible for phosphorite formation on the Namibian shelf (Schulz and Schulz 2005). Yet, the actual mode of this mechanism remains elusive, and direct observations have not been made.

I.1.4 The role of microorganisms: open questions and aims of this thesis

Investigations of the benthic phosphorus cycle have focused on the identification and quantification of sources and sinks, and have provided detailed inventories of sedimentary P pools (Delaney 1998, Ruttenberg and Berner 1993, Schenau and de Lange 2001). However, though there is consensus on the microbial contribution to P transformations, there is little to no information on the manner and rate of the underlying processes. With this dissertation, we try to shed some light on those parts of the benthic P cycle, where we consider the microbial contribution most relevant: the balance between P_i regeneration and microbial uptake in mineralization of organic matter (1), and the recent formation of authigenic phosphorites (2). In particular, we aimed to answer the following set of

Research questions

(1) Are there *isotopic signatures* of microbial mineralization of organic matter? How is microbial activity related to P_i release from OM? What is the balance between P_i regeneration and actual microbial uptake? Can we learn something about potential P limitation of benthic communities, as known for pelagic communities?

(2) Can we find direct evidence for the *role of bacteria* (and more specific – large sulfur bacteria) *in phosphorite formation*? Are living microorganisms fundamental to the ultimate burial of P in the seabed? What are potential rates of recent P_i sequestration? Are these rates relevant for the benthic P budgets?

Structure of the thesis

The dissertation addresses these questions in three manuscripts that are presented in Chapters II and III (theme 1) and Chapter III (theme 2). Chapter I describes the effort of refinement, validation and first application of a micro extraction protocol for the first analysis of oxygen isotopes in marine pore water P_i. The analysis of two sediment cores from the Moroccan margin offshore Cape Ghir revealed the balance of microbial regeneration and uptake of P_i on basis of this isotopic biosignature. Chapter III presents a comprehensive study of benthic microbial P_i regeneration across a transect in the Benguela upwelling system, combining classic geochemical profiling, steady state pore water modeling, and novel phosphate oxygen isotope data. Chapter IV reports the results of an experimental study of active microbial phosphorite formation in the Benguela upwelling system that uses an innovative combination of sequential extraction of P_i pools and radioisotope methods to investigate the role of large sulfur bacteria in this process.

I.2 Isotopic tools and methods

To elucidate the contribution of the microbial community to benthic P cycling, we used a set of biogeochemical methods that deserve a few comments. Our efforts were motivated by the challenge that was once put into the humorous notion: "Biogeochemical cycles work in practice, but we do not know if they will ever work in theory". Tackling benthic microbial P turnover made soon clear that the target processes were under the radar of conventional P_i inventories and flux calculations. We therefore applied two isotopic tools – first, the measurement of P_i oxygen isotopes in natural systems, and second, a ^{33}P phosphate radiotracer in sediment incubation experiments.

I.2.1 Phosphate oxygen isotopes

The oxygen isotope composition of P_i in biogenic phosphates (mostly shells and fishbones) has a long history of use as a palaeothermometer (Kolodny et al. 1983, Longinelli and Nuti 1973, Luz et al. 1984). It has become evident only recently that the decisive imprint of biological P turnover makes it also a superb isotopic biosignature for unraveling microbial P_i dynamics in natural systems (Blake et al. 2001). The P-O bonds in the P_i molecule (Figure I.1) are stable under ambient conditions in the oceans. Only enzymatic activity can exchange oxygen atoms with the surrounding water and alter the P_i oxygen composition (reported as $\delta^{18}O_P$, Blake et al. 1997, Tudge 1960). This mechanism is par-

ticularly involved in the hydrolytic cleavage of phosphoester bonds (Blake et al. 2005). Phosphoesters are a class of compounds that forms the majority of naturally occurring organic P (Figure I.1). Their hydrolysis is the most important reaction mechanism in biological P cycling, including preferential regeneration of P_i from organic matter, P_i uptake for the synthesis of phosphorylated biomolecules, and various intracellular turnover reactions. Figure I.3 displays three examples of oxygen exchange reactions in hydrolysis of a phosphomonoester, phosphodiester, and a nucleic acid (in this case, RNA), involving different enzymatic systems.

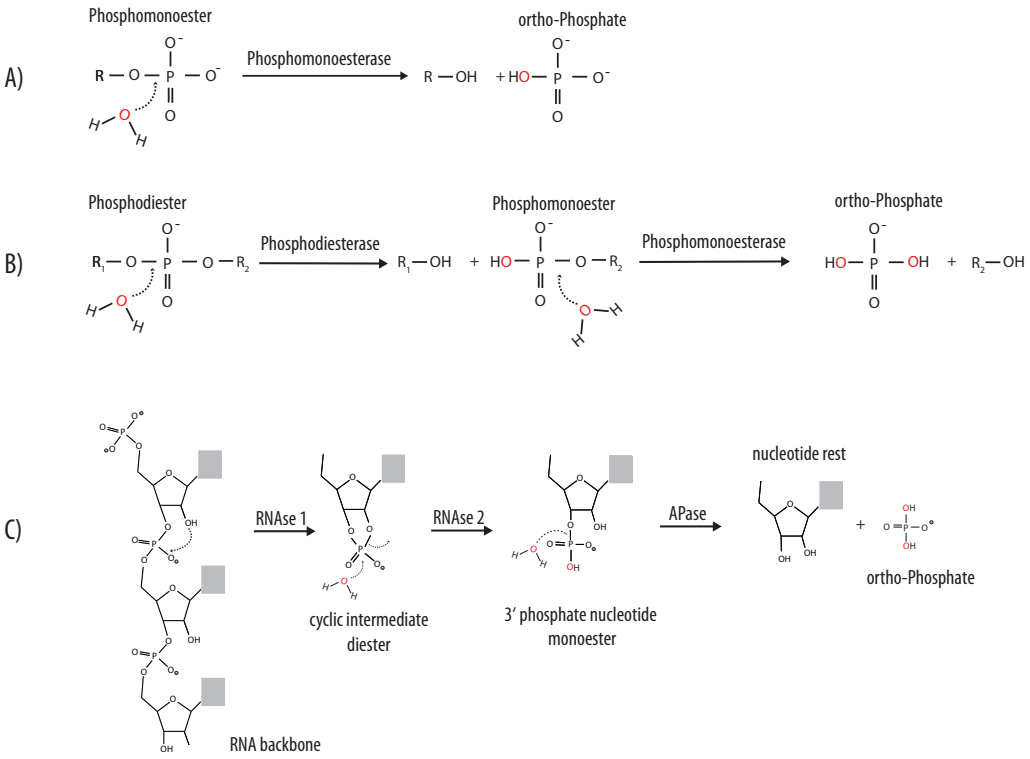

Figure I.3 Enzyme-mediated phosphoester breakdown mechanisms that involve oxygen exchange between P_i and water. **(A)** Hydrolysis of a phosphomonoester. **(B)** Two-step hydrolysis of a phosphodiester, involving a phosphodiesterase and phosphomonoesterase. **(C)** Hydrolysis of a nucleic acid (here: RNA). The first step is the endomolecular hydrolysis of the RNA backbone and formation of an intermediate, cyclic phosphodiester. The second step is the hydrolysis of the cyclic intermediate into a 3' phosphate nucleotide phosphomonoester. These two steps are catalyzed by endonucleases (phosphodiesterases) such as RNAse. The third step is a regular phosphomonoester hydrolysis of the nucleotide phosphomonoester, liberating ortho-P_i and involving a phosphomonoesterase, e.g. APase. Modified after Blake et al. (2005) and Liang and Blake (2009)

Two antagonistic and distinct isotope effects are defining the $\delta^{18}O_P$ value. The first is microbial uptake, transformation and release of P_i that creates an isotopic equilibrium between P_i and water through a cascade of phosphorylation and dephosphorylation steps, e.g. mediated by the enzyme pyrophosphatase (PPase, Blake et al. 2005). The second is extracellular degradation of P_{org} that causes a kinetic fractionation during rapid hydrolysis, e.g. mediated by the enzyme alkaline phosphatase (APase, Blake et al. 2005, Figure I.4).

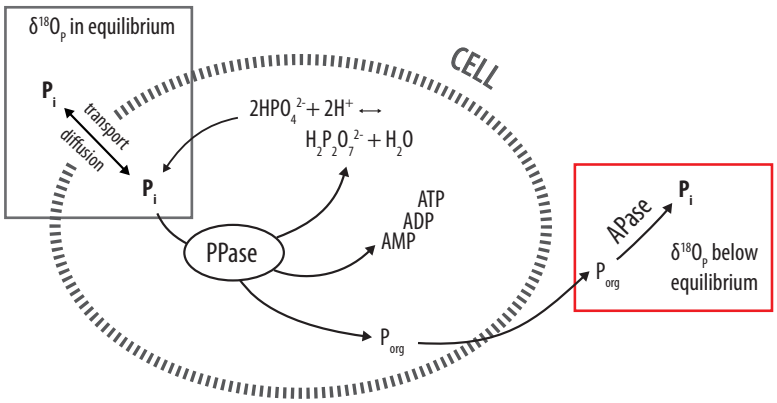

Figure I.4 Simplified cellular phosphate (P_i) turnover and resulting $\delta^{18}O_P$ signatures. Modified after Blake et al. (2005), for further details, see text.

Laboratory studies have investigated enzyme mechanisms and the isotope effects of different cultures (Blake et al. 2005, Liang and Blake 2006), reconstructed signals of various P substrates (Liang and Blake 2009), and distinguished biological processes from geochemical reactions (Blake et al. 1998, Liang and Blake 2007). These investigations form the basis for the systematic application of P_i oxygen isotopes. The first field studies of marine, estuary, and riverine $\delta^{18}O_P$ have disentangled the balance of P_i release and uptake (Colman et al. 2005, McLaughlin et al. 2006b), and identified external P_i sources (McLaughlin et al. 2006a).

We have refined a micro extraction protocol for the separation of P_i from complex aqueous media (Colman 2002), and were able to analyze $\delta^{18}O_P$ on pore water samples, where P_i yields were previously too small for isotope ratio mass spectrometry.

I.2.2 Radiotracer labeling with ^{33}P

Earlier studies of P transformations in the oceans have focused on the identification and balance of P sources and sinks (Benitez-Nelson 2000, Delaney 1998, Ruttenberg and Berner 1993). Elaborated protocols exist that allow an accurate speciation of the sedimentary P pools (Ruttenberg 1992, Ruttenberg et al. 2009, Schenau and de Lange 2000). However, to our knowledge no studies exist that have elucidated rates and pathways of sedimentary transformations of P. Much of this deficit comes from to the fact that P_i is the almost exclusive form of P in sediments, and it is impossible to assess short-term transformations from one pool to another on the basis of concentration data alone. Several researchers have successfully used the cosmogenic radioisotopes ^{32}P and ^{33}P to determine P turnover rates in the water column. Though they could show that P_i turnover between the dissolved and particulate pool is very rapid (Benitez-Nelson and Karl 2002, Sorokin 2002), the wide application of this method is complicated by the huge amounts of seawater that need to be processed in order to measure the radionuclides at natural abundance (Paytan and McLaughlin 2007).

In this context, it remains curious why it has been seldom attempted to make use of artificial radioisotope tracers to determine and quantify P turnover. Radioisotopic methods are generally used to measure potential in situ rates of many important processes that proceed in aquatic ecosystems with the participation of microbial communities (Sorokin 1999). The classic example is the measurement of bacterial sulfate reduction rates (SRR, (Fossing and Jørgensen 1989, Jørgensen 1977)) by labeling sediment incubations with ^{35}S-sulfate.

In the present dissertation, we applied ^{33}P labeled phosphate as a radiotracer in incubation experiments. The isotope ^{33}P is a soft beta emitter with a half-life of 25.4 days and can be handled securely in the laboratory. By analyzing the distribution of ^{33}P before and after incubation, typically by sequential extraction of P pools (Ruttenberg 1992), we traced the transfer of P_i from the pore water into sedimentary phases, and calculated potential rates for this transfer. By producing digital autoradiographs, two-dimensional images of beta radiation on an object slide (Charpak et al. 1989), we also captured bacterial P_i uptake. The method has proven to be highly sensitive and enabled the detection of the microbial turnover of smallest P_i quantities.

I.3. References

Algeo TJ, Ingall ED (2007) Sedimentary C_{org}:P ratios, paleocean ventilation, and Phanerozoic atmospheric pO_2. Palaeogeography, Palaeoclimatology, Palaeoecology 256:130-155

Anderson LA, Sarmiento JL (1994) Redfield ratios of remineralization determined by nutrient data analysis. Global Biogeochemical Cycles 8:65-80

Anderson LD, Delaney ML, Faul KL (2001) Carbon to phosphorus ratios in sediments: Implications for nutrient cycling. Global Biogeochemical Cycles 15:65-79

Baturin GN (1988) Disseminated phosphorus in oceanic sediments - a review. Mar Geol 84:95-104

Baturin GN, Bezrukov PL (1979) Phosphorites on the sea floor and their origin. Mar Geol 31:317-332

Baturin GN, Merkulova K, Chalov PI (1972) Radiometric evidence for recent formation of phosphatic nodules in marine shelf sediments. Mar Geol 13:M37-M41

Benitez-Nelson CR (2000) The biogeochemical cycling of phosphorus in marine systems. Earth-Science Reviews 51:109-135

Benitez-Nelson CR, Karl DM (2002) Phosphorus cycling in the North Pacific Subtropical Gyre using cosmogenic P-32 and P-33. Limnology and Oceanography 47:762-770

Berner RA (1990) Diagenesis of phosphorus in sediments from non-upwelling areas. Phosphate Deposits of the World 3:27-33

Bjerrum C, Canfield DE (2002) Ocean productivity before about 1.9 Gyr ago limited by phosphorus adsorption onto iron oxides. Nature 417:159-162

Blackwelder E (1916) The geologic role of phosphorus. PNAS 2:190-495

Blake RE, Alt JC, Martini AM (2001) Oxygen isotope ratios of PO_4: An inorganic indicator of enzymatic activity and P metabolism and a new biomarker in the search for life. PNAS 98:2148-2153

Blake RE, O'Neil JR, Garcia GA (1997) Oxygen isotope systematics of biologically mediated reactions of phosphate: 1. Microbial degradation of organophosphorus compounds. Geochim Cosmochim Ac 61:4411-4422

Blake RE, O'Neil JR, Garcia GA (1998) Effects of microbial activity on the $\delta^{18}O$ of dissolved inorganic phosphate and textural features of synthetic apatites. American Mineralogist 83:1516-1531

Blake RE, O'Neil JR, Surkov AV (2005) Biogeochemical cycling of phosphorus: insights from oxygen isotope effects of phosphoenzymes. American Journal of Science 305:596-620

Brüchert V, Jørgensen B, Neumann K, Riechmann D, Schlösser M, Schulz HN (2003) Regulation of bacterial sulfate reduction and hydrogen sulfide fluxes in the central namibian coastal upwelling zone. Geochim Cosmochim Ac 67:4505-4518

Carr ME (2002) Estimation of potential productivity in Eastern Boundary Currents using remote sensing. Deep-Sea Res II 49:59-80

Charpak G, Dominik W, Zaganidis N (1989) Optical imaging of the spatial distribution of beta particles emerging from surfaces. PNAS 86:1741-1745

Colman AS (2002) The oxygen isotope composition of dissolved inorganic phosphate and the marine phosphorus cycle. PhD Thesis, Department of Geology & Geophysics, Yale University, New Haven

Colman AS, Blake RE, Karl DM, Fogel ML, Turekian KK (2005) Marine phosphate oxygen isotopes and organic matter remineralization in the oceans. PNAS 102:13023-13028

Colman AS, Holland HD, Glenn CR, Prévôt-Lucas L, Lucas J, Dalrymple RW (2000) The global diagenetic flux of phosphorus from marine sediments to the oceans: redox sensitivity and the control of atmospheric oxygen levels. In: Marine authigenesis: from global to microbial. SEPM Special Publication 66

Compton J et al. (2000) Variations in the global phosphorus cycle. In: Marine authigenesis: from global to microbial. SEPM Special Publication 66

Delaney ML (1998) Phosphorus accumulation in marine sediments and the oceanic phosphorus cycle. Global Biogeochemical Cycles 12:563-572

Diaz J et al. (2008) Marine polyphosphate: A key player in geologic phosphorus sequestration. Science 320:652-655

Dyhrman ST, Palenik B (1999) Phosphate stress in cultures and field populations of the dinoflagellate Prorucentrum minimum detected by a single-cell alkaline phosphatase assay. Applied and Environmental Microbiology 65:3205-3212

Faul KL, Paytan A, Delaney ML (2005) Phosphorus distribution in sinking oceanic particulate matter. Marine Chemistry 97:307-333

Filipelli GM, Delaney ML (1992) Similar phosphorus fluxes in ancient phosphorite deposits and a modern phosphogenic environment. Geology 20:709-712

Föllmi KB (1996) The phosphorus cycle, phosphogenesis and marine phosphate-rich deposits. Earth-Science Reviews 40:55-124

Fossing H, Jørgensen B (1989) Measurement of bacterial sulfate reduction in sediments: Evaluation of a single-step chromium reduction method. Biogeochemistry 8:205-222

Froelich PN (1988) Kinetic Control of Dissolved Phosphate in Natural Rivers and Estuaries - a Primer on the Phosphate Buffer Mechanism. Limnology and Oceanography 33:649-668

Froelich PN, Bender ML, Luedtke NA, Heath GR, DeVries T (1982) The marine phosphorus cycle. American Journal of Science 282:474-511

Froelich PN et al. (1979) Early oxidation of organic matter in pelagic sediments of the eastern equatorial Atlantic: suboxic diagenesis. Geochim Cosmochim Ac 43:1075-1090

Gächter R, Meyer J, Mares A (1988) Contribution of bacteria to release and fixation of phosphorus in lake sediments. Limnology and Oceanography 33:1542-1558

Ingall ED, Jahnke R (1994) Evidence for enhanced phosphorus regeneration from marine sediments overlain by oxygen depleted waters. Geochim Cosmochim Ac 58:2571-2575

Ingall ED, Jahnke R (1997) Influence of water-column anoxia on the elemental fractionation of carbon and phosphorus during sediment diagenesis. Mar Geol 139:219-229

Ingall ED, Van Capellen P (1990) Relation between sedimentation rate and burial of organic phosphorus and organic carbon in marine sediments. Geochim Cosmochim Ac 54:373-386

Jørgensen BB (1977) The sulfur cycle of a coastal marine sediment (Limfjorden, Denmark) Limnology and Oceanography 22:814-832

Kolodny Y, Luz B, Navon O (1983) Oxygen Isotope Variations in Phosphate of Biogenic Apatites. 1. Fish Bone Apatite - Rechecking the Rules of the Game. Earth and Planetary Science Letters 64:398-404

Kornberg A (1995) Inorganic polyphosphate: toward making a forgotten polymer unforgettable. Journal of Bacteriology 177:491-496

Krom MD, Berner RA (1980) Adsorption of phosphate in anoxic marine sediments. Limnology and Oceanography 25:797-806

Liang Y, Blake R (2009) Compound- and Enzyme-specific Phosphodiester Hydrolysis Mechanisms Revealed by $\delta^{18}O$ of Dissolved Inorganic Phosphate: Implications for marine P cycling. Geochim Cosmochim Ac 73:1-49

Liang Y, Blake RE (2006) Oxygen isotope signature of P_i regeneration from organic compounds by phosphomonoesterases and photooxidation. Geochim Cosmochim Ac 70:3957-3969

Liang Y, Blake RE (2007) Oxygen isotope fractionation between apatite and aqueous-phase phosphate: 20-45°C. Chemical Geology 238:121-133

Longhurst A, Sathyendranath S, Platt T, Caverhill C (1995) An estimate of global primary production in the ocean from satellite radiometer data. Journal of Plankton Research 17:1245-1271

Longinelli A, Nuti S (1973) Revised phosphate-water isotopic temperature scale. Earth and Planetary Science Letters 19:373-376

Luz B, Kolodny Y, Kovach J (1984) Oxygen isotope variations in phosphate of biogenic apatites, III. Conodonts. Earth and Planetary Science Letters 69:255-262

McLaughlin K, Cade-Menun BJ, Paytan A (2006a) The oxygen isotopic composition of phosphate in Elkhorn Slough, California: A tracer for phosphate sources. Estuarine Coastal and Shelf Science 70:499-506

McLaughlin K, Chavez F, Pennington JT, Paytan A (2006b) A time series investigation of the oxygen isotopic composition of dissolved inorganic phosphate in Monterey Bay, California. Limnology and Oceanography 51:2370-2379

McManus J, Berelson WM, Coale KH, Johnson KS, Kilgore TE (1997) Phosphorus regeneration in continental margin sediments. Geochim Cosmochim Ac 61:2891-2907

Nathan Y, Bremner JM, Loewenthal RE, Monteiro P (1993) Role of bacteria in phosphorite genesis. Geomicrobiology Journal 11:69-76

Pasek MA (2008) Rethinking early Earth phosphorus geochemistry. PNAS 105:853-858

Paytan A, McLaughlin K (2007) The oceanic phosphorus cycle. Chem Rev 107:563-576

Redfield AC (1958) The biological control of chemical factors in the environment. American Scientist 46:205-221

Ruttenberg KC (1992) Development of a sequential extraction method for different forms of phosphorus in marine sediments. Limnology and Oceanography 37:1460-1482

Ruttenberg KC, Berner RA (1993) Authigenic apatite formation and burial in sediments from non-upwelling, continental margin sediments. Geochim Cosmochim Ac 57:991-1007

Ruttenberg KC, Ogawa N, Tamburini F, Briggs RA, Colasacco ND, Joyce E (2009) Improved, high-throughput approach for phosphorus speciation in natural sediments via the SEDEX sequential extraction method. Limnology and Oceanography: Methods 7:319-333

Sander BC, Kalff J (1993) Factors controlling bacterial production in marine and freshwater sediments. Microbial Ecology 26:79-99

Schenau S, de Lange GJ (2000) A novel chemical method to quantify fish debris in marine sediments. Limnology and Oceanography 45:963-971

Schenau S, de Lange GJ (2001) Phosphorus regeneration vs. burial in sediments of the Arabian Sea. Marine Chemistry 75:201-217

Schink B, Friedrich M (2000) Bacterial metabolism - Phosphite oxidation by sulphate reduction. Nature 406:37-37

Schink B, Thiemann V, Laue H, Friedrich M (2002) Desulfotignum phosphitoxidans sp nov., a new marine sulfate reducer that oxidizes phosphite to phosphate. Archives of Microbiology 177:381-391

Schulz HN (2006) The genus Thiomargarita. Prokaryotes 6:1156-1163

Schulz HN, Jorgensen BB (2001) Big bacteria. Annual Review of Microbiology 55:105-137

Schulz HN, Schulz HD (2005) Large sulfur bacteria and the formation of phosphorite. Science 307:416-418

Seiter K, Hensen C, Zabel M (2005) Benthic carbon mineralization on a global scale. Global Biogeochemical Cycles 19

Slomp CP, Epping EHG, Helder W, Van Raaphorst W (1996) A key role for iron-bound phosphorus in authigenic apatite formation in North Atlantic continental platform sediments. Journal of Marine Research 54:1179-1205

Sorokin YI (1999) Radioisotopic methods in hydrobiology. Springer, Berlin

Sorokin YI (2002) Dynamics of inorganic phosphorus in pelagic communities of the Sea of Okhotsk. Journal of Plankton Research 24:1253-1263

Sundareshwar PV, Morris JT, Koepfler EK, Fornwalt B (2003) Phosphorus limitation of coastal ecosystem processes. Science 299:563-565

Tanaka T, Rassoulzadegan F, Thingstad TF (2004) Orthophosphate uptake by heterotrophic bacteria, cyanobacteria, and autotrophic nanoflagellates in Villefranche Bay, northwestern Mediterranean: Vertical, seasonal, and short-term variations of the competitive relationship for phosphorus. Limnology and Oceanography 49:1063-1072

Thingstad TF, Zweifel UL, Rassoulzadegan F (1998) P limitation of heterotrophic bacteria and phytoplankton in the northwest Mediterranean. Limnology and Oceanography 43:88-94

Tudge AP (1960) A method of analysis of oxygen isotopes in orthophosphate - its use in the measurement of paleotemperatures. Geochim Cosmochim Ac 18:81-93

Van Capellen P, Berner RA (1991) Fluorapatite crystal growth from modified seawater solutions. Geochim Cosmochim Ac 55:1219-1234

Van Capellen P, Ingall ED (1994) Benthic phosphorus regeneration, net primary production, and ocean anoxia: A model of the coupled marine biogeochemical cycles of carbon and phosphorus. Palaeoceanography 9:677-692

Veeh HH, Burnett WC (1973) Contemporary phosphorites on the continental margin of Peru. Science 181:844-845

II

Marine sediment pore-water profiles of phosphate oxygen isotopes using a refined micro-extraction technique

Tobias Goldhammer[1], Thomas Max[2], Benjamin Brunner[1,2], Florian Einsiedl[3], Matthias Zabel[1]

[1]MARUM – Center for Marine Environmental Sciences, University of Bremen, Bremen, Germany, [2]Max-Planck-Institute for Marine Microbiology, Bremen, Germany, [3]Department of Environmental Engineering, Technical University of Denmark, Kongens Lyngby, Denmark

Manuscript submitted to *Limnology and Oceanography: Methods*, 02.10.2009

Abstract

Phosphorus cycling in the ocean is influenced by biological and geochemical processes that are reflected in the oxygen isotope signature of dissolved inorganic phosphate (PO_4^{3-}, abbreviated P_i). Extending the P_i oxygen isotope record from the water column into the seabed is difficult due to low P_i concentrations and small amounts of marine pore waters available for analysis. We obtained the first pore water profiles of P_i oxygen isotopes using a refined protocol based on the original micro-extraction designed by Colman (2002). This refined and customized method allows the conversion of ultra-low quantities (0.5 – 1 µmol) of pore water P_i to silver phosphate (Ag_3PO_4) for routine analysis by mass spectrometry. A combination of magnesium hydroxide co-precipitation with

ion exchange resin treatment steps is used to remove dissolved organic matter, anions and cations from the sample before precipitating Ag_3PO_4. Samples as low as 200 mg were analyzed in a continuous flow isotope ratio mass spectrometer setup. A series of tests with external and lab internal standards validated the preservation of the original phosphate oxygen isotope signature ($\delta^{18}O_P$) during micro extraction. Pore water data on $\delta^{18}O_P$ has been obtained from two sediment cores of the Moroccan margin. The $\delta^{18}O_P$ values are in a range of + 19.49 to + 27.30 ‰.

We applied a simple isotope mass balance model to disentangle processes contributing to benthic P cycling, and found evidence for P_i regeneration outbalancing microbial demand in the upper sediment layers. This highlights the great potential of using $\delta^{18}O_P$ to study microbial processes in the subseafloor and at the sediment water interface.

II.1 Introduction

Phosphorus (P) is one of the essential nutrients for life on Earth. The oceanic cycle of phosphate (P_i) controls marine primary productivity on both geologic and recent timescales (Benitez-Nelson 2000, Froelich et al. 1982, Paytan and McLaughlin 2007), and is linked to global carbon biogeochemistry and atmospheric oxygen levels (Colman et al. 2000). In those regions of the oceans where input of inorganic P_i is limited, it must be biologically recovered from organic matter (OM) to maintain the supply to the pelagic and benthic communities. Pathways and rates of biological P_i recycling thus directly control the P supply state of the marine ecosystem. So far, research has focused on budgets and standing stocks of P_i in the water column and marine sediments, and provided insight into P_i partitioning between different sedimentary fractions, but transformations and fluxes in and between those compartments are still poorly understood (Benitez-Nelson 2000). Despite the recognition of the seabed's decisive role for OM remineralization and P_i recycling, as well as for effective burial of P_i in the marine sediments, it remains difficult to characterize the biological contribution to P_i turnover in this main reservoir of the marine P cycle. Since P is mostly resistant to redox transformations (Schink and Friedrich 2000) and does not change its molecular form when passing from one compartment to another, it has been almost impossible to reconstruct such transitions from P_i concentration data only.

Only recently, the oxygen isotopic signature of dissolved inorganic phosphate ($\delta^{18}O_P$) has been proposed to yield information on biological P cycling (Blake et al. 2001). The P-O bond is stable under ambient conditions of the Earth's surface and ocean, and only

the activity of enzymes of living organisms can alter the phosphate oxygen isotope signature by exchanging oxygen atoms with surrounding media (Blake et al. 1997, Tudge 1960). Hydrolysis of phosphoesters is the most crucial process (Blake et al. 2005, Liang and Blake 2009). Experimental studies elucidated enzymatic mechanisms involved in this hydrolysis and determined the respective isotope effects for different cultures (Blake et al. 2005, Liang and Blake 2006), reconstructed signatures of different P_i substrates (Liang and Blake 2009), and discriminated biological processes from geochemical reactions (Blake et al. 1998, Liang and Blake 2007). Field investigations of marine, estuary, and riverine water $\delta^{18}O_P$ have disentangled the balance of P_i release and uptake (Colman et al. 2005, McLaughlin et al. 2006b), and identified external P_i sources (McLaughlin et al. 2006a). This new "inorganic biomarker" (Blake et al. 2001) should thus prove useful for characterizing P_i dynamics in marine sediments, where the pore water P_i pool connects diagenetic mineralization of organic matter, microbial uptake and release, adsorption/desorption and precipitation/dissolution reactions with solid phase minerals.

For analysis of $\delta^{18}O_P$ by isotope ratio mass spectrometry (IRMS), it is necessary to convert P_i into a pure phase without isotopic alteration. Ideally, that compound excludes external oxygen sources, and is non-hygroscopic and stable under laboratory conditions. Silver phosphate (Ag_3PO_4) has been proven a convenient P_i phase for this purpose (Firsching 1961, O'Neil et al. 1994) and has since then gradually substituted the earlier fluorination technique (Kolodny et al. 1983, Tudge 1960). Commonly, Ag_3PO_4 is reduced with carbon at high temperature (> 1200 °C) in a thermal combustion elemental analyzer (TCEA) to yield carbon monoxide (CO) for analysis by IRMS (Colman 2002, McLaughlin et al. 2004, O'Neil et al. 1994). TCEA and mass spectrometer are linked via a continuous flow interface, and the CO gas is measured instantaneously after formation (Kornexl et al. 1999).

Two detailed protocols for isolating, purifying and precipitating small quantities of P_i from complex matrix solutions such as fresh and ocean waters have been published lately (Colman 2002, McLaughlin et al. 2004). Unlike the open ocean water column, where sample size is only restricted by pump performance and bottle capacity, pore water of marine sediments is difficult to obtain and sample volumes are very limited. Retrieving undisturbed sediment involves drilling a core with typical diameter of a few centimeters, yielding pore water samples around a few tens of mL. For common sedimentary P_i concentrations (10^0 – 10^2 µM), this results in not more than 1 µmol P_i in the initial sample, which is at the low end of what aforementioned protocols may handle. Based upon similar principles, the procedures outlined by Colman (2002) and McLaughlin et al. (2004) involve a series of precipitations, resin treatments, and concentration steps

to remove dissolved organic phosphorus (DOP) and interfering ions from the sample. With respect to obtaining P_i from marine porewaters, neither of the two methods shows a considerable advantage over the other, and we assume that both may be equally appropriate. Here we present a refined version of the protocol by Colman (2002), tailored for the conversion of ultra low quantities (< 1µmol) of pore water P_i to Ag_3PO_4 for routine IRMS analysis (Figure II.1). We tested the method with external reference materials and

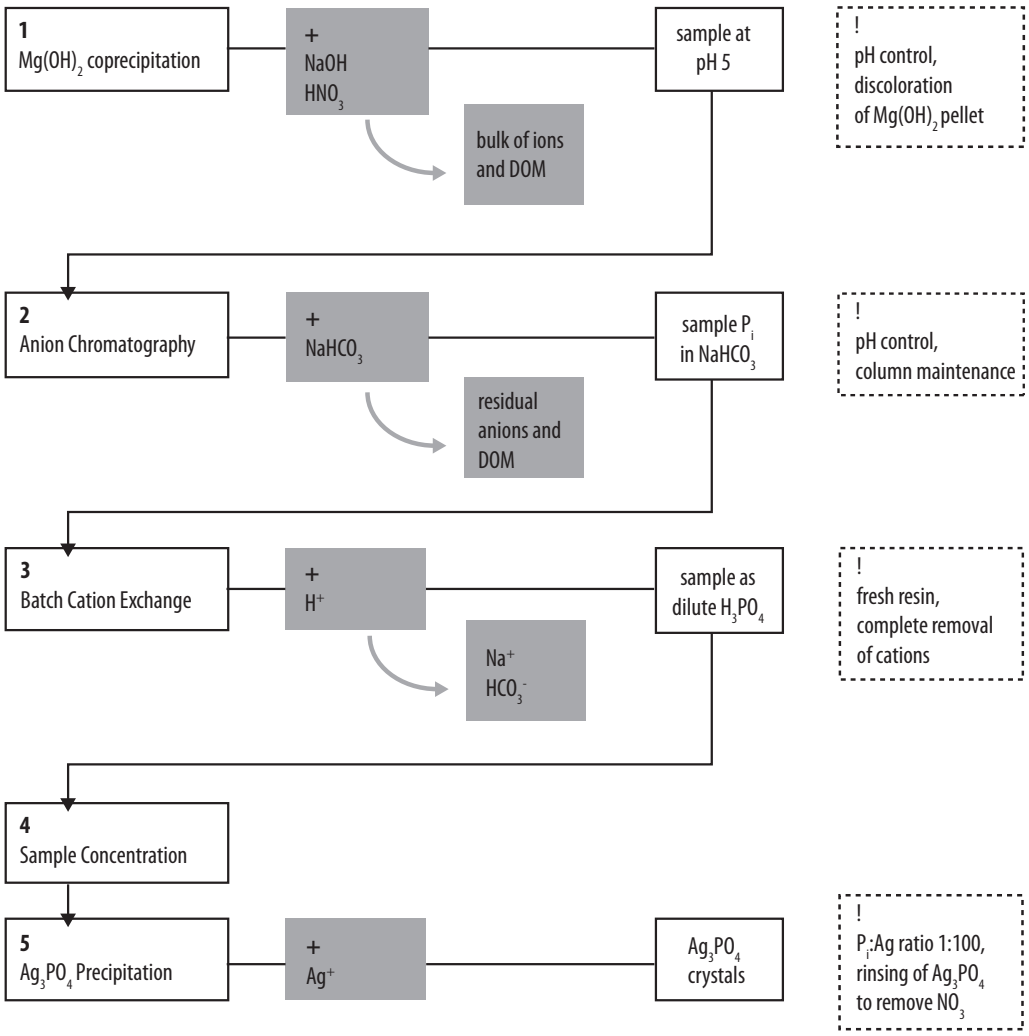

Figure II.1 Flow diagram of refined micro extraction sequence for pore water P_i based on Colman (2002). Panels show in sequence: the added reagents (+), the removed components, and the resulting sample status for each treatment step. Aspects deserving special attention are noted in separate boxes on the right. The detailed experimental procedure is described in the text

internal laboratory standards, both pure and in matrices simulating natural samples, and successfully obtained the first dataset on pore water $\delta^{18}O_P$ from two sediment cores of the Northwest African continental shelf.

II.2 Materials and Procedures

II.2.1 Labware

For sample and solution handling, we used 250, 125 and 60 mL HDPE sample bottles (Nalgene), 50 mL PP Falcon centrifuge tubes (Sarstedt), 30 mL PPCO Oak Ridge centrifuge flasks (Nalgene), 26 mL PS test tubes with stoppers (Sarstedt), 20 mL scintillation vials, and 2.0 mL Eppendorf reaction cups. All flasks were triple-washed with nitric acid (HNO_3, 1 mol L^{-1}) and rinsed with deionized water (H_2O, Milli-Q) prior to use. The anion separation line comprised 60 mL syringe barrels, 6 mL reservoir cartridges (Varian Bond Elut) with frits and connectors, various Luer stopcocks and adaptors, Tygon tubing (ID 1.6 mm, OD 3.2 mm), and two-stop pump tubes (Ismatec, color code orange-orange, ID 0.89 mm). Furthermore, we employed Rhizon suction samplers with Luer connectors (Rhizosphere Research, Wageningen), filter cartridges (0.22 µm, Millipore Steriflip Express Plus Membrane), filter membranes (0.2 µm, cellulose acetate, Sartorius), disposable PS cuvettes (2.5 mL, Brand), 25 mL PTFE beakers, and disposable petri dishes (Greiner). For IRMS sample preparation, we used silver cartridges (3.5 mm * 5 mm, Hekatech) annealed at 600 °C prior to use. Powder-free latex gloves were worn to avoid sample contamination.

II.2.2 Chemicals and reagents

We used potassium phosphate (KH_2PO_4, ACS grade, Merck), 1 mol L^{-1} sodium bicarbonate ($NaHCO_3$, ACS grade, Merck), silver nitrate ($AgNO_3$, puriss. p.a., Riedel-de Haën), ammonium nitrate (NH_4NO_3, Fluka Ultra BioChemika), sodium hydroxide solution (NaOH, 1 mol L^{-1}, Merck), phosphate standard solution (1000 mg KH_2PO_4 L^{-1}, Merck CertiPur), pH indicator strips (Merck), anion exchange resin AG1-X8 (hydroxide form, 100-200 mesh, biotechnology grade, Biorad), cation exchange resin AG50W-X8 (hydrogen form, 100-200 mesh, biotechnology grade, Biorad), and ultra pure HNO_3 (67 %) freshly prepared by sub-boiling distillation.

II.2.3 Equipment

Equipment used in this study included a tabletop centrifuge with exchangeable rotors (Sigma 2-16) capable of spinning up to 15,000 rpm, a test tube vortexer (IKA Basic), a peristaltic pump (Ismatec IPC 12), a horizontal shaker plate (Heraeus), a drying cabinet (Memmert), a thermostatic heating block with wells for 25 mL PTFE beakers and argon line, a thermostatic heating plate (diameter 14 cm) with a quartz bath accommodating 2 mL micro reaction cups, a spectral photometer (Merck SQ 118), a micro balance (Sartorius), and a temperature conversion elemental analyzer (Thermo Finnigan TC/EA) linked via a continuous flow interface (Thermo Finnigan ConFlo II) to an isotope ratio mass spectrometer (Thermo Finnigan Delta plus).

II.2.4 Refined separation protocol for pore water phosphate after Colman (2002)

Sample handling and standard aqueous phase analyses

It is first essential to obtain filtered, uncontaminated pore water samples for analysis of the oxygen isotope composition of phosphate and concentratios of phosphate and other ions. Pore water samples from sediment cores are taken with Rhizon suction samplers (Rhizosphere Research, Wageningen) immediately after core retrieval. In contrast to conventional squeeze sampling of the pore water, the Rhizon technique yields a practically sterile sample, leaves cells intact, and avoids the pressure-related release of adsorbed P_i (Dickens et al. 2007, Seeberg-Elverfeldt et al. 2005). The samples are stored at 4 °C until further processing. Dissolved inorganic phosphate was quantified photometrically (Merck SQ 118, 820 nm) by using the phosphomolybdenum blue method modified after Hansen and Koroleff (1999) and Murphy and Riley (1962). Anions were determined by ion chromatography (Metrohm 861 Advanced Compact IC, column A Supp 5, conductivity detection after chemical suppression). Cations were measured by inductively coupled plasma optical emission spectrometry (ICP-OES, Perkin Elmer Optima 3300R). The oxygen isotope composition of water ($\delta^{18}O_w$) was determined on selected samples after equilibration with CO_2 using mass spectrometry.

Step 1 – Multiple phosphate co-precipitation with magnesium hydroxide (Figure 1)

The first step of the micro extraction procedure isolates phosphate from the other ions in solution. Strict separation of pore water P_i from other P pools is a prerequisite for the proper interpretation of the isotopic signatures. In this protocol, we strip P_i from the

solution by magnesium-induced coprecipitation (MagIC, (Colman 2002, Karl and Tien 1992)), leaving the bulk of DOM and ions behind. Pore water samples are transferred to 30 mL centrifuge tubes. Addition of 1 mL of a 1 M NaOH solution to each tube raises the pH to approximately 10 and induces the precipitation of magnesium hydroxide ($Mg(OH)_2$). Samples are vigorously vortexed for 30 s. In presence of excess Mg^{2+} (typical pore water concentrations were 55 mM), $Mg(OH)_2$ rapidly flocculates and quantitatively adsorbs dissolved HPO_4^{2-}. The flock is separated from solution by centrifuging at 10,000 rpm for 15 min. This high rotation speed ensures complete settling of the fine crystalline $Mg(OH)_2$. This is not achieved at lower speeds (e.g. 3000 rpm, Colman 2002). The supernatant solution is discarded after checking for absence of P_i. The whitish pellet is re-dissolved with 10 mL of 0.1 M HNO_3. The above procedure including coprecipitation of P_i with $Mg(OH)_2$, vortexing, centrifugation and re-dissolution is repeated three times. In presence of high DOM, which is indicated by coloration of the pore water sample and stained pellet, the procedure has to be repeated until the discoloration disappears. After final re-dissolution of the pellet, the sample pH is adjusted to 6 with NaOH. At this pH the main P_i species is $H_2PO_4^-$. At this step, the P_i concentration of the pro-

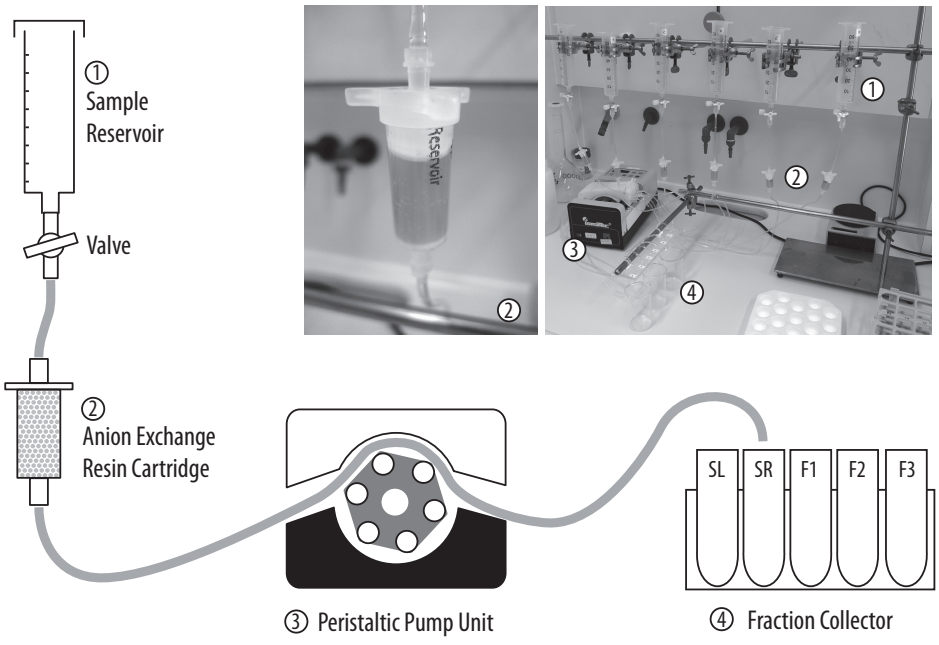

Figure II.2 Preparative anion chromatography setup. The sample is transferred into the 60 mL syringe barrel reservoir (1), loaded onto the anion exchange resin column (2), mounted before the peristaltic pump (3), and sample fractions are collected with a tube rack fraction collector (4). The preparation line comprises six parallel units in simultaneous operation (photograph on top right) and could be extended according to the maximum capacity of the peristaltic pump

cessed sample is recorded photometrically. When initial sample volumes exceed 30 mL, samples can be evenly split between several centrifuge tubes and merged after the first co-precipitation and re-dissolution step.

Step 2 – Preparative anion chromatography

The second step of the micro extraction procedure leads to a further purification of the phosphate samples by removing residual DOM and anions (Colman 2002). For this step, 3.0 g of anion exchange resin AG1X8 is washed into cut-to-fit SPE cartridges and connected to a simple peristaltic pump system (Figure II.2). Gas bubble free packing of the columns ensures steady flow rates. Prior to sample processing, each column is conditioned with 60 mL of 1 M $NaHCO_3$ and rinsed with 40 mL H_2O at a flow rate of 1.5 mL min^{-1}. Pump rate in the following steps is 1.5 mL min^{-1}, and the pump timer is used to control fraction volumes. The sample is transferred into 60 mL syringe barrel reservoirs and loaded onto the column, and the sample load (Figure II.2: fraction SL) is collected. Subsequently, the sample reservoir is flushed with 10 mL of H_2O (Figure II.2: fraction SR). Dissolved inorganic phosphate is eluted from the column with a fresh solution of 0.15 M $NaHCO_3$ in a 20 mL fraction (Figure II.2: F2) collected in 50 mL Falcon tubes. A 8 mL pre- (Figure II.2: F1) and 12 mL post-run (Figure II.2: F3) is discarded. The proper performance of Step 2 can be confirmed by checking for absence of P_i in fractions SL, SR, F1 and F3 and quantitative recovery of P_i from F2.

Step 3 – Cation exchange in batch mode

The third step of the micro extraction procedure removes HCO_3^- and Na^+ from the samples and converts the sample P_i from $H_2PO_4^-$ to H_3PO_4. This is achieved by the exchange of Na^+ for H^+, which subsequently reacts with HCO_3^- to form CO_2 that bubbles off spontaneously (Colman 2002). The cation exchange resin AG50WX8 is freshly converted to H^+ form by 30 min of batch reaction with 1M HNO_3 on a horizontal shaker, followed by a triple rinse with H_2O. Approximately 3.0 g of resin is added to the samples. This induces rapid release of CO_2. After the initial CO_2 pulse, sample tubes are slowly agitated on the shaker and opened every 30 min to release CO_2. Two hours of reaction guarantee complete removal of $NaHCO_3$ from the sample. This is a crucial prerequisite for the subsequent precipitation of Ag_3PO_4 (Step 4). A Steriflip membrane filter unit is used to separate the resin from the sample. The filter is rinsed with 2 mL of H_2O. The sample has a mildly acidic pH of 5 – 6 after this treatment step.

Step 4 – Sample concentration

The fourth step of the micro extraction procedure serves to concentrate P_i to a level where it can be precipitated as silver phosphate (Ag_3PO_4). This step reduces the sample volume from approximately 25ml to 0.5 - 1 mL. The samples are transferred to PTFE beakers, and evaporated gently in a 60 °C heating block under a slow argon stream. Volume reduction is completed after 8 – 10 h. The sample is pipetted into a 2.0 mL micro reaction cup, together with a 200 µL H_2O rinse of the PTFE beaker. The sample is now ready for precipitation of Ag_3PO_4 (Step 5).

Step 5 – Silver phosphate precipitation

The fifth and last step of the micro extraction procedure is the precipitation of Ag_3PO_4. This step is crucial to obtain precipitates that can easily be handled in the preparation for oxygen isotope analysis by IRMS. Excess Ag^+ is added to the samples in form of a 0.2 M $AgNO_3$ solution buffered in 0.35 M NH_4NO_3 and 0.74 M NH_4OH (O'Neil et al. 1994), according to a P_i:Ag ratio of approximately 1:100. This corresponds to 0.5 mL of silver amine solution for a 1 mL sample containing 1 µmol P_i. Interestingly, the 1:10 ratio used in Colman (2002) did not yield satisfactory results for our small samples. The precipitation cups are then kept in a 50 °C sand bath in a dust-protection cabinet. Under these conditions, NH_3 slowly evaporates and liberates Ag^+ that reacts with P_i in solution. After a few hours, crystals of Ag_3PO_4 start to form on the liquid surface and the walls of the reaction cup. Complete precipitation of Ag_3PO_4 takes up to 60 h. This slow precipitation technique (Colman 2002) yields better results in crystal size and handling than the comparatively more rapid precipitation described by Dettmann et al. (2001). Using a 2 mL Eppendorf pipette, the crystals are carefully detached from the walls of the cup and transferred onto a 0.2 µm membrane filter. Thorough washing of the sample on the filter with H_2O on a vacuum system ensures removal of nitrate that may have persisted in the sample. This is essential, because nitrate, as an oxygen-bearing moiety, compromises oxygen isotope analysis by IRMS. The crystals on the filters are placed into a small petri dish, and dried at 60 °C for at least 12 h. The dry crystals are kept in envelopes of annealed aluminum foil in a dessicator for subsequent IRMS analysis.

II.2.5 Isotope ratio mass spectrometry

We use a continuous flow TC/EA IRMS setup (Figure II.3A) that follows the scheme used in Colman (2002), Laporte et al. (2009), or McLaughlin et al. (2004). The Ag_3PO_4 sample is carbothermically reduced in a glassy carbon reactor at 1450 °C yielding complete conversion of sample oxygen to CO. We achieve better results by operating the reactor without an additional graphite crucible in the reaction zone (Colman et al. 2000), but with an amendment of approx. 7 g of nickelized carbon to the glassy carbon granules (Kornexl et al. 1999, Figure II.3B). With this setup, very small amounts of Ag_3PO_4 (around 200 µg) can be analyzed. The capacity of the reactor is up to 150 consecutive samples, after which silver residues have to be removed from the glassy carbon granules.

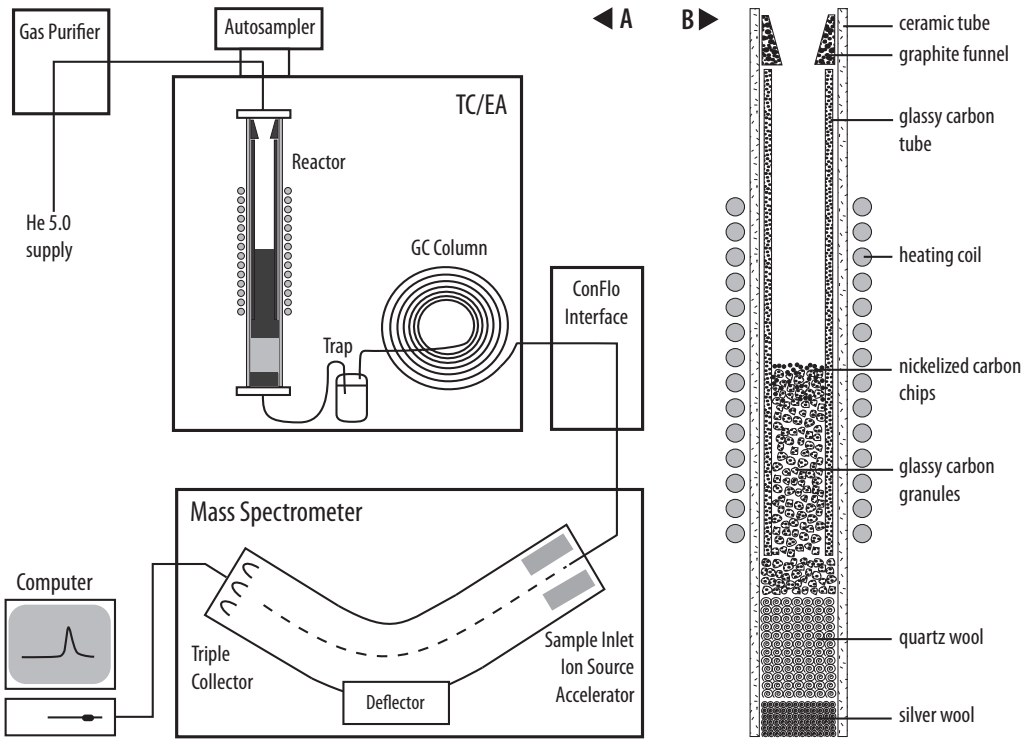

Figure II.3 (A) Instrumental setup for isotope ratio mass spectrometry. Helium from a building supply line (flow rate: 80 mL min^{-1}) is cleaned by a gas purifier. Samples are introduced into the TC/EA through an autosampler carousel. The reactor is operated at 1450 °C, the GC column at 90 °C. After passing the continuous flow interface (ConFlo), the CO sample gas enters the mass spectrometer, which simultaneously detects masses 28, 29 and 30. **(B)** Details of the TC/EA reactor. The graphite funnel ensures that the sample drops into the glassy carbon tube (ID 8.6 mm). Packing depth of the glassy carbon granules is approximately 20 cm. Approximately 7 g of nickelized carbon chips are added on top of the glassy carbon granules. The quartz wool plug at the bottom of the reactor tube keeps the keep carbon granules in place whereas the silver wool removes halogenides and sulfur from the gas stream

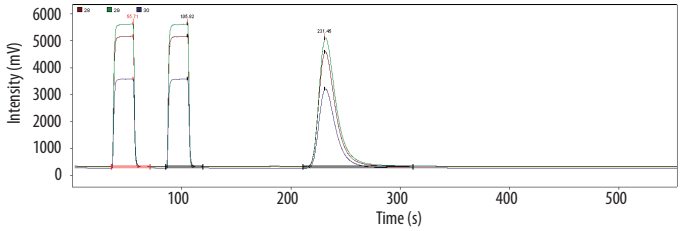

Figure II.4 Spectrum of Ag_3PO_4 sample run with two CO gas peaks from a laboratory CO tank (left) and sample peak (right) for masses 28, 39 and 30

The sample gas is carried by a continuous Helium (He) stream at 80 mL min^{-1}, passes a H_2O trap filled with hygroscopic magnesium perchlorate ($Mg(ClO_4)_2$), and a gas chromatography (GC) column held at 90 °C. The GC column separates gases that potentially interfere with the measurement (i.e. N_2 from CO). An open split (ConFlo) serves as interface between the high pressure system (TC/EA) and vacuum system (IRMS).

Silver phosphate samples are weighed into silver capsules. The minimum weight of samples is 200 µg. The silver capsules are tightly crimped to minimize included air (Vennemann et al. 2002). A single sample run takes 550 s and is comprised two injections of CO gas from a CO tank at 30 s and 80 s, sample insertion into the TC/EA at 125 s, and the arrival of sample CO in the mass spectrometer at approximately 200 s (Figure II.4). Peak integration of masses 28, 29, and 30 was based on a time-based background average from 120 to 140 s. Raw $\delta^{18}O_P$ values were calculated by the Isodat software (Isodat NT version 2.0) and normalized to VSMOW by a linear three-point calibration with external standards TU1, TU2, and USGS35 (Table II.1). Daily routine includes running the three standards in duplicates for calibration of sample $\delta^{18}O_P$ to VSMOW, then a batch of 15 to 20 samples, and finally again the three standards for instrument drift control. Usually drift can be neglected during a day's run.

Table II.1 External standard materials for calibration of measurements to VSMOW

Standard	Compound	$\delta^{18}O$ (‰VSMOW)	Method	Reference
TU1	Ag_3PO_4	+21.11 ± 0.57	high-temperature reduction IRMS	Vennemann et al. (2002)
TU2	Ag_3PO_4	+5.35 ± 0.62	high-temperature reduction IRMS	Vennemann et al. (2002)
USGS35	$NaNO_3$	+57.5 ± 0.4	high-temperature reduction IRMS	National Institute of Standards and Technology (2008)

II.3 Assessment

II.3.1 Standard materials and artificial samples

Mass spectrometer performance for low sample weights

We evaluated the performance of our IRMS setup with external oxygen isotope standards TU1, TU2, and USGS35 (Table II.1) to test the reproducibility and accuracy of the measurements at low samples weights. We found no remarkable difference in variability of uncalibrated $\delta^{18}O_P$ values of the standard TU1 for weight classes 100 – 200 µg, 200 – 300 µg and 300 – 400 µg (Figure II.5). Samples with lower weights showed higher deviations and were not considered for oxygen isotope measurements.

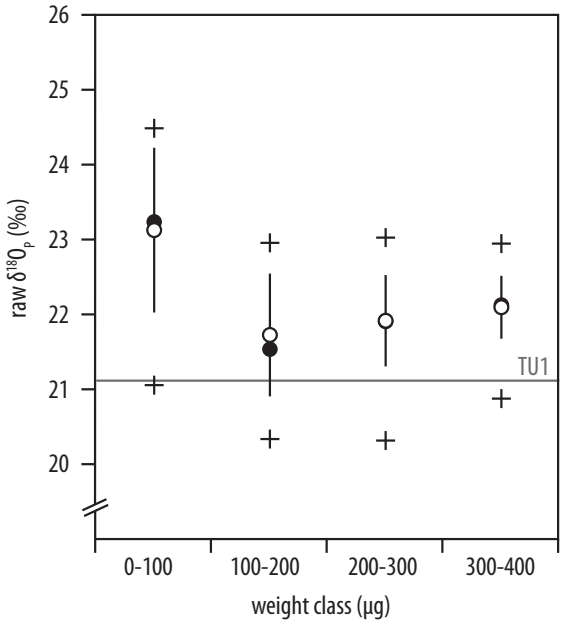

Figure II.5 Low Ag_3PO_4 weights do not compromise IRMS analyses. Shown are arithmetic mean (circle) with 1σ standard deviation (lines), median (dots), and minimum/maximum (crosses) of uncalibrated $\delta^{18}O_P$ values of repeated measurements of standard TU1 (referenced value: horizontal line) in different weight classes. Weight classes of 100 - 200 (n = 12), 200 - 300 (n = 35), and 300 - 400 µg (n = 30) appear similar, while 0 -100 µg (n = 14) show considerably higher variability and were thus considered too small for sample analysis

Preservation of isotopic signature during phosphate micro extraction

We tested our method to ensure that the presented purification procedure does not entail any alteration of the oxygen isotopic signature, neither by contamination nor by isotopic exchange. The micro extraction procedure was applied to materials of known (TU1, TU2) and unknown (BR2) isotopic composition that were dissolved in water and artificial sea water (ASW) to assess accuracy and reproducibility of the method (Table II.2). Additional tests were performed with artificial samples (BR1) varying in P_i concentration (0.5µmol/L to 100 µmol/L), pH (4.5 and 7.5), and matrix composition (water and North Atlantic Sea Water, Table II.2).

The test series comparing low pH (4.5) to high pH (7.5) was carried out to evaluate potential acid hydrolysis of DOP, which would result in incorporation of oxygen isotopes from water (Blake et al. 1997). We prepared samples of P_i standard BR1 (Merck Certipur solution) in sterile filtered stock North Sea water (NSW) with a P_i blank below detection

Table II.2 Test series for evaluation of the micro extraction protocol. Oxygen isotope values ($\delta^{18}O_P$) and recoveries are given as arithmetic means µ with standard deviation σ, each for n replicates

Material	Source P_i	Matrix and concentration	Preparation	*n*	$\delta^{18}O_P$ $\mu \pm \sigma$ ‰	recovery $\mu \pm \sigma$ %
BR1	Merck Certipur PO_4^{3-} solution	in H_2O 0.50 µmol L^{-1}	direct precipitation reference	7	8.29 ± 0.74	
		in NSW 50 µmol L^{-1} pH 4.5	micro extraction	9	6.97 ± 0.09	92 ± 2
		in NSW 100 µmol L^{-1} pH 4.5	micro extraction	6	7.41 ± 0.20	91± 3
		in NSW 50 µmol L^{-1} pH 7.5	micro extraction	6	7.95 ± 0.19	94 ± 5
		in NSW 100 µmol L^{-1} pH 7.5	micro extraction	6	8.83 ± 0.21	96 ± 4
BR2	Merck KH_2PO_4 ACS reagent	in H_2O 100 µmol L^{-1}	direct precipitation reference	12	12.19 ± 0.29	
		in ASW 100 µmol L^{-1}	micro extraction	4	12.08 ± 0.20	93 ± 3
TU1	Ag_3PO_4	in ASW 100 µmol L^{-1}	micro extraction	4	20.88 ± 0.04	93 ± 3
TU2	Ag_3PO_4	in ASW 100 µmol L^{-1}	micro extraction	4	5.50 ± 0.25	93 ± 2

limit of the phosphomolybdenum blue method (<-1 µmol L^{-1}) in two concentrations (50 and 100 µmol L^{-1}) and adjusted pH to 4.5 and 7.5, respectively, and subjected them to the micro extraction protocol. The $\delta^{18}O_P$ values of resulting Ag_3PO_4 were compared to those of directly precipitated Ag_3PO_4 from BR1 (Table II.2). Samples with pH 4.5 deviate from the direct reference, while the mean values of replicates from pH 7.5 were statistically not different to the direct reference. This discrepancy may reflect acid hydrolysis of DOP from NSW. We infer that the initial sample pH is crucial for the conservation of the original sample $\delta^{18}O_P$. Therefore, samples must be kept at pH higher than 4.5 until complete DOM removal after steps 1 and 2. When dissolving sample pellets with HNO_3 in step 1, it needs to be considered that excessive use of this acid, which is also an oxidizing agent, could have negative effects on the reliability of the presented method.

We also tested the full experimental protocol with a set of phosphate that covers a range of oxygen isotope compositions, BR2 (KH_2PO_4, Merck ACS grade reagent, $\delta^{18}O_P$ = 12.2 ‰), TU1 (Ag_3PO_4 standard, Vennemann et al. 2002, $\delta^{18}O_P$ = 21.1 ‰) and TU2 (Ag_3PO_4 standard, Vennemann et al. 2002, $\delta^{18}O_P$ = 5.4 ‰). Solution of BR2 was prepared as a 100 µmol L^{-1} solution in sterile filtered artificial seawater (ASW, Kester et al. 1967) that did not contain DOP. The standards TU1 and TU2 were dissolved in a solution of NH_4NO_3 and NH_4OH. From those solutions we prepared 100 µmol L^{-1} samples in ASW analog to BR2. The isotope composition of BR2 after from micro extraction was isotopically not distinguishable from directly precipitated reference Ag_3PO_4 (Table II.2), and both TU1 and TU2 matched the referenced $\delta^{18}O_P$ values (Table II.2, referenced values in Table II.1).

Mass recovery of P_i after extraction

Mean sample P_i recoveries were higher than 90% for artificial test samples (93 ± 4 %, n = 39), and in a similar range for natural samples (91 ± 19 %, n = 47). In light of the results of the test series, we conclude that the preparative loss of sample P_i is isotopically non-selective and does not compromise data quality.

II.3.2 Natural samples

The investigation area offshore Cape Ghir is located in a trade-wind driven upwelling system, where nutrient rich deep waters sustain high productivity in the coastal zone, and nutrients are transported several hundred km to the open ocean in filaments in the surface waters (Freudenthal et al. 2002). During the *R/V M.S. Merian* cruise 04/4a in March 2007, two sites on the Moroccan continental shelf were drilled on two loca-

tions just offshore Cape Ghir (GeoB11804-4, 30°50.73'N, 10°5.90'W and GeoB11807-2, 30°51.02'N, 10°16.10'W) using a remotely operated drill rig (MARUM MeBo). Drilling reached depths of 39 mbsf (GeoB11804-4) and 17 mbsf (GeoB11807-2). Immediately after retrieving the cores from the rig, we took pore water samples which were stored at 4 °C, and shipped back to Bremen for further processing. We successfully extracted P_i with the micro extraction procedure and precipitated Ag_3PO_4 even from samples containing only 0.4 µmol P_i, which corresponds to final Ag_3PO_4 weights of around 150 µg. These sample amounts are a factor of 0.2 to 0.5 lower than previously used for IRMS analyses (Colman 2002, McLaughlin et al. 2004), but yield similar variability as higher weights in a comparison of standard measurements (Figure II.5). It thus is feasible to use these low amounts of Ag_3PO_4 for determination of $\delta^{18}O_P$.

II.4 Discussion

At both investigated sites, pore water phosphate concentrations reach a maximum where sulfate profiles show a distinct change in their slope and sulfate values become low (Figure II.6). These concentration profiles indicate that P_i is released from the sediments to the overlying water column whereas sulfate is consumed in the upper sediment by organoclastic sulfate reduction, and sulfate reduction related to anaerobic oxidation of methane at 7 meters below surface (mbsf). There are two major sources for P_i in the pore water, release of phosphate during remineralization of organic matter (OM) and release of phosphate adsorbed to mineral phases during early diagenesis. During microbial respiration of OM, P is preferentially regenerated and the C:P ratio of OM increases with depth (Ingall and Van Capellen 1990). Sulfide produced during microbial sulfate reduction induces transformation of mineral phases, i.e. the reduction of iron and manganese. Phosphate incorporated or adsorbed to such phases is released to the pore water. The accumulation of dissolved phosphate in pore water, and the reflux to overlying bottom waters suggests that in the topmost sediments, phosphate release exceeds microbiological demand and geochemical sequestration.

Examination of the disequilibrium in the phosphate oxygen isotope composition provides more insight into the balance between biological demand, sequestration, and flux of P in the sediments. We can calculate the theoretical oxygen isotope composition of P_i at equilibrium with water according to the equation from Longinelli and Nuti (1973) by using a gradient of 0.01 °C m^{-1}, and the measured $\delta^{18}O_W$ that had an average of 0.26 ‰ (Equation II.1).

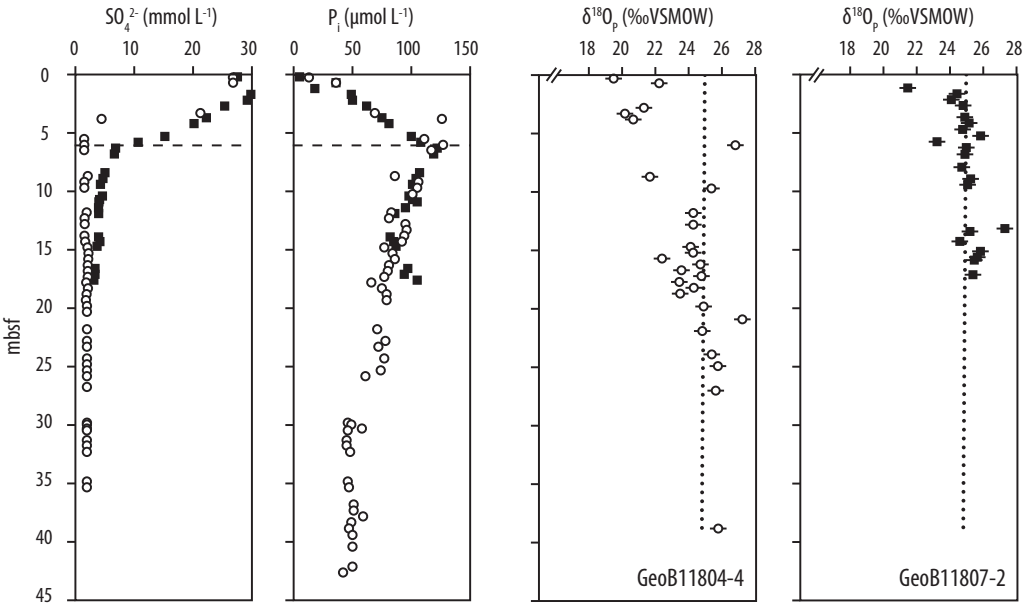

Figure II.6 Pore water profiles for sediment cores GeoB11804-4 (circles) and GeoB11807-2 (squares). Left panels: dissolved sulfate and phosphate concentrations for both cores. The dashed line at 6 mbsf indicates the sulfate penetration depth (SPD) at both sites. Right panels: pore water phosphate $\delta^{18}O_P$ referenced to VMSOW. For reason of clarity, the $\delta^{18}O_P$ have been corrected for water $\delta^{18}O$, and the temperature-dependent isotopic equilibria for a geothermal gradient of 0.05 °C m^{-1} have been calculated from the empirical relationship of Longinelli and Nuti (1973) and a water $\delta^{18}O$ of 0.26 ‰ (Equation II.1). Error bars are 1σ standard deviations from concomitant external standard analyses

$$\delta^{18}O_P = \left[(111.4 - T)/4.3\right] + \delta^{18}O_W \qquad \text{Equation II.1}$$

The comparison of the actual measurements to the calculated equilibrium isotope composition shows a remarkable offset at the core tops, whereas measured values overlap with the theoretical values at greater sediment depths (Figure II.6). The offset of pore $\delta^{18}O_P$ from the equilibrium isotope composition indicates that this disequilibrium is either caused within the sediment, or by exchange of P_i with the overlying water column. In the latter case, P_i from the overlying water column is in disequilibrium to the theoretical equilibrium values. Offsets in the oxygen isotope compositions of P_i to values lower than the theoretical equilibrium have been shown to be caused by the activity of extracellular enzymes such as alkaline phosphatase (APase) that liberate P_i from OM by phosphoester hydrolysis (Blake et al. 2005). These processes are in competition to the activity of endocellular enzymes such as pyrophosphatase (PPase), that equilibrate P_i oxygen with ambient water during synthesis and degradation of P biomolecules (e.g. ADP, ATP, polyphosphates, phospholipids, cf. Blake et al. 2005).

In sediments, bioavailable P_i is depleted whereas C:P ratios of OM increase with depth. This imposes a need for efficient P_i recycling within the microbial community. Such circumstances are expected to favor rapid microbial turnover of P_i and to drive $\delta^{18}O_P$ towards oxygen isotope equilibrium with water. This expectation is supported by the observed isotope trends in the investigated cores (Figure II.6). However, it is intriguing that this rapid equilibration does not lead to equilibrium oxygen isotope values in the top of the sediments. This implies that the influx of P_i depleted in ^{18}O relative to the equilibrium value is larger than the microbial turnover causing isotope equilibration, a hypothesis supported by the fact that P_i concentrations elevated in the upper part of the sediment column.

We can use a simple isotope mixing model to obtain a rough estimate of the relative importance of production of P_i by OM by phosphoester hydrolysis (APase pathway, offset from the equilibrium value) compared to the production of P_i that is equilibrated with pore water. We assume that inorganic processes, such as adsorption and desorption of P_i with iron and manganese oxyhydroxides (Blake et al. 2001) or precipitation and dissolution of apatite (Blake et al. 1998, Liang and Blake 2007) do not play a role. In a strict sense, this assumption is not correct. Nevertheless, it is reasonable to assume that these phases have an isotope composition that averages the values for full equilibrium and maximum disequilibrium. Therefore, P_i release from these phases will not strongly impact the isotope mass balance. We further assume that all P_i fed to the system by sinking OM from the photic zone has an oxygen isotope composition of 21 ‰, which is inferred from equation 1 using a temperature of 10 °C. Now, we can determine one end-member of the isotope mixing model. The oxygen isotope effect of APase regeneration pathway can be calculated after Liang and Blake (2006) as follows:

$$\delta^{18}O_{P,APase} = 0.25\left(\delta^{18}O_W - 30‰\right) + 0.75\left(\delta^{18}O_{Porg}\right) \qquad \text{Equation II.2}$$

The other end-member of the mixing model (PPase activity) corresponds to the temperature dependent isotope equilibrium between P_i and water (Equation II.1).

The two end-members of the isotope mixing model can now be combined in an isotope mass balance, which results in the measured isotope composition of P_i at a particular sediment depth:

$$\delta^{18}O_P = x\left(\delta^{18}O_{P,APase}\right) + (1-x)\left(\delta^{18}O_{P,PPase}\right) \qquad \text{Equation II.3}$$

The parameter x corresponds to the relative contribution of the two end-members in the isotope mixing model. Thus, by calculating the value of x, we can estimate the rela-

tive importance of the respective pathways (Figure II.7). As expected, the supply of P_i from APase activity is outcompeted by PPase towards core bottom, while up to 32 % of P_i in the upper sediment column exhibits the imprint of APase activity. However, considering that P_i concentrations decrease strongly towards the interface to the water column, where microbial activity is highest, it is striking that the oxygen isotope composition of P_i is not fully overprinted by isotope exchange. This indicates that the oxygen isotope composition of P_i in the pore water close to the sediment water interface is not just the result of mixing of P_i from the water column with P_i from deeper sediments, but that the microbial benthic P turnover is an important contributor to marine P cycling.

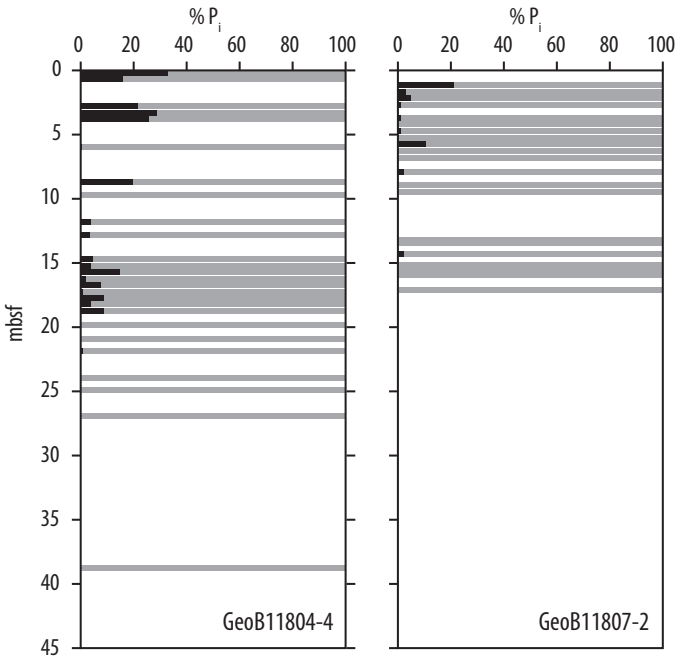

Figure II.7 Fraction of pore water P_i in isotopic disequilibrium with ambient H_2O (black) and in isotopic equilibrium with ambient H_2O (grey), derived from a two end-member mixing model. The disequilibrium fraction represents regenerated P_i that has not been equilibrated with pore water by microorganisms

Using oxygen isotope tools, we now stand on the cusp of new insights into the modern marine P cycle. At the moment though, we lack data on pore water $\delta^{18}O_P$ from other marine sites. It remains to be seen as to whether our novel data set represent general or specific pattern, and if our interpretation of the data using a simple end-member mixing model is an appropriate approach. To gain a more thorough understanding of phosphate

oxygen isotopes in marine sediments, we need a better knowledge on how sources and sinks of inorganic and on how sedimentary transformations affect P_i pools and their isotope composition. The role of interaction between P_i and solid-bound phosphate in various phases, such as iron minerals and phosphorites, has not yet been elucidated in natural systems, and high turnover rates and fluxes in the benthic boundary layer, where water column and sediments are coupled, may also contribute to yet unforeseen isotopic effects.

II.5 Comments and Recommendations

In line with earlier studies, we found sample pH being the important control on P_i recovery and isotope integrity (McLaughlin et al. 2004). Thus, monitoring pH during sample handling is prerequisite for successful extraction of P_i for isotope analysis. Considering the ultra low P_i quantities in pore water samples, we suggest employing a pH microelectrode with short response time instead of pH indicator strips that may induce sample loss and can be a source of sample contamination.

Proper handling, fresh conditioning and rinsing of the cation resin AG50WX8 before every application turned out to be crucial to the successful precipitation of Ag_3PO_4. Using resin prepared the previous day resulted in a reddish discoloration of the sample and made proper precipitation of Ag_3PO_4 impossible. We have not yet resolved the cause of this complication.

Though the micro extraction method is manually elaborate, it was possible to achieve throughput rates of about 6 pore water samples per day. The volume reduction of the sample (Step 4) is very time-consuming. Therefore, we recommend the use an automated evaporator to speed up this step as originally suggested in the original method by Colman (2002).

We have not evaluated if the micro extraction protocol of McLaughlin et al. (2004) can be modified for a the application on pore water samples. However, we believe that this method could be equally refined as the protocol from Colman (2002).

We expect that innovations in mass spectrometry will further decrease the sample amounts needed for isotope analysis, allowing the use of oxygen isotope composition of P_i as a tracer for P cycling in yet unexplored environments. Our refined micro extraction protocol is a first step in the direction to make ultralow amounts of P_i accessible for isotope analysis.

II.6 Acknowledgements

We gratefully acknowledge the technical assistance of Tanja Broder, Silvana Pape and Karsten Enneking, Geochemistry and Hydrogeology Group, University of Bremen. Martin Kölling, shipboard scientific party and crew provided help and support during expedition MSM04-4a. Torsten Vennemann kindly supplied us with silver phosphate standards TU1 and TU2 that were invaluable for method assessment. Tim Ferdelman's critical comments substantially improved an earlier version of this manuscript. This work was funded by German Research Foundation (DFG) through MARUM Center for Marine Environmental Sciences, Project B2.

II.7 References

Benitez-Nelson CR (2000) The biogeochemical cycling of phosphorus in marine systems. Earth-Science Reviews 51:109-135

Blake RE, Alt JC, Martini AM (2001) Oxygen isotope ratios of PO_4: An inorganic indicator of enzymatic activity and P metabolism and a new biomarker in the search for life. PNAS 98:2148-2153

Blake RE, O'Neil JR, Garcia GA (1997) Oxygen isotope systematics of biologically mediated reactions of phosphate: 1. Microbial degradation of organophosphorus compounds. Geochim Cosmochim Ac 61:4411-4422

Blake RE, O'Neil JR, Garcia GA (1998) Effects of microbial activity on the $\delta^{18}O$ of dissolved inorganic phosphate and textural features of synthetic apatites. American Mineralogist 83:1516-1531

Blake RE, O'Neil JR, Surkov AV (2005) Biogeochemical cycling of phosphorus: insights from oxygen isotope effects of phosphoenzymes. American Journal of Science 305:596-620

Colman AS (2002) The oxygen isotope composition of dissolved inorganic phosphate and the marine phosphorus cycle. PhD Thesis, Department of Geology & Geophysics, Yale University, New Haven

Colman AS, Blake RE, Karl DM, Fogel ML, Turekian KK (2005) Marine phosphate oxygen isotopes and organic matter remineralization in the oceans. PNAS 102:13023-13028

Colman AS, Holland HD, Glenn CR, Prévôt-Lucas L, Lucas J, Dalrymple RW (2000) The global diagenetic flux of phosphorus from marine sediments to the oceans: redox sensitivity and the control of atmospheric oxygen levels. In: Marine authigenesis: from global to microbial. SEPM Special Publication 66

Dettmann DL, Kohn MJ, Quade J, Ryerson FJ, Ojha TP, Hamidullah S (2001) Seasonal stable isotope evidence for a strong Asian monsoon throughout the past 10.7 m.y. Geology 29:31-34

Dickens GR, Kölling M, Smith DC, Schnieders L (2007) Rhizon Sampling of Pore Waters on Scientific Drilling Expeditions: An Example from the IODP Expedition 302, Arctic Coring Expedition (ACEX). Scientific Drilling 4:22-25

Firsching FH (1961) Precipitation of silver phosphate from homogenous solution. Analytical Chemistry 33:873-874

Freudenthal T, Meggers H, Henderiks J, Kuhlmann H, Moreno A, Wefer G (2002) Upwelling intensity and filament activity off Morocco during the last 250,000 years. Deep Sea Res II 49:3655-3674

Froelich PN, Bender ML, Luedtke NA, Heath GR, DeVries T (1982) The marine phosphorus cycle. American Journal of Science 282:474-511

Hansen HP, Koroleff F (1999) Determination of nutrients. In: Grasshoff K, Kremling K, Ehrhardt M (eds) Methods of seawater analysis. Wiley, Weinheim New York, pp 159-228

Ingall ED, Van Capellen P (1990) Relation between sedimentation rate and burial of organic phosphorus and organic carbon in marine sediments. Geochim Cosmochim Ac 54:373-386

Karl DM, Tien G (1992) MAGIC: A sensitive and precise method for measuring dissolved phosphorus in aquatic environments. Limnology and Oceanography 37:105-116

Kester DR, Duedall IW, Connors DN, Pytkowic RM (1967) Preparation of Artificial Seawater. Limnology and Oceanography 12:176-&

Kolodny Y, Luz B, Navon O (1983) Oxygen Isotope Variations in Phosphate of Biogenic Apatites. 1. Fish Bone Apatite - Rechecking the Rules of the Game. Earth and Planetary Science Letters 64:398-404

Kornexl BE, Gehre M, Höfling R, Werner RA (1999) On-line d18O Measurement of organic and inorganic substances. Rapid Commun. Mass Spectrom. 13:1685-1693

Laporte D, Holmden C, Patterson W, Prokopiuk T, Eglington B (2009) Oxygen isotope analysis of phosphate: improved precision using TC/EA CF-IRMS. Journal of Mass Spectrometry 44:879-890

Liang Y, Blake R (2009) Compound- and Enzyme-specific Phosphodiester Hydrolysis Mechanisms Revealed by $\delta^{18}O$ of Dissolved Inorganic Phosphate: Implications for marine P cycling. Geochim Cosmochim Ac 73:1-49

Liang Y, Blake RE (2006) Oxygen isotope signature of Pi regeneration from organic compounds by phosphomonoesterases and photooxidation. Geochim Cosmochim Ac 70:3957-3969

Liang Y, Blake RE (2007) Oxygen isotope fractionation between apatite and aqueous-phase phosphate: 20-45°C. Chemical Geology 238:121-133

Longinelli A, Nuti S (1973) Revised phosphate-water isotopic temperature scale. Earth and Planetary Science Letters 19:373-376

McLaughlin K, Cade-Menun BJ, Paytan A (2006a) The oxygen isotopic composition of phosphate in Elkhorn Slough, California: A tracer for phosphate sources. Estuarine Coastal and Shelf Science 70:499-506

McLaughlin K, Chavez F, Pennington JT, Paytan A (2006b) A time series investigation of the oxygen isotopic composition of dissolved inorganic phosphate in Monterey Bay, California. Limnology and Oceanography 51:2370-2379

McLaughlin K, Silva SR, Kendall C, Stuart-Williams H, Paytan A (2004) A precise method for the analysis of $\delta^{18}O$ of dissolved inorganic phosphate in seawater. Limnology and Oceanography: Methods 2:202-212

Murphy J, Riley JP (1962) A modified single solution method for the determination of phosphate in natural waters. Analytica Chimica Acta 27:31-36

O'Neil JR, Roe LR, Reinhard E, Blake RE (1994) A rapid and precise method for oxygen isotope analysis of biogenic phosphate. Israel Journal of Earth Sciences 43:203-212

Paytan A, McLaughlin K (2007) The oceanic phosphorus cycle. Chem Rev 107:563-576

Schink B, Friedrich M (2000) Bacterial metabolism - Phosphite oxidation by sulphate reduction. Nature 406:37-37

Seeberg-Elverfeldt J, Schlüter M, Feseker T, Kölling M (2005) Rhizon sampling of porewaters near the sediment-water interface of aquatic systems. Limnology and Oceanography: Methods 3:361-371

Tudge AP (1960) A method of analysis of oxygen isotopes in orthophosphate - its use in the measurement of paleotemperatures. Geochim Cosmochim Ac 18:81-93

Vennemann TW, Fricke HC, Blake RE, O'Neil JR, Colman AS (2002) Oxygen isotope analysis of phosphates: a comparison of techniques for analysis of Ag_3PO_4. Chemical Geology 185:321-336

III

Phosphate oxygen isotopes: New insights into sedimentary phosphorus cycling in the Benguela upwelling system

Tobias Goldhammer[1], Timothy G. Ferdelman[1,2], Benjamin Brunner[1,2], Stefano Bernasconi[3], Matthias Zabel[1]

[1] MARUM – Center for Marine Environmental Sciences, University of Bremen, Bremen, Germany, [2] Max Planck Institute for Marine Microbiology, Bremen, Germany, [3] Department of Earth Sciences, ETH Zurich, Switzerland

Manuscript in preparation for submission to *Geochimica et Cosmochimica Acta*

Abstract

Marine sediments are the main repositories in the oceanic phosphorus (P) cycle. The activity of benthic microorganisms is decisive for regeneration, reflux, or burial of inorganic phosphate (P_i), which in turn has a strong impact on marine productivity. The Benguela upwelling system comprises a variety of sedimentary environments, and recent formation of phosphorites on the continental shelf make this area prime target for studying biogeochemical P cycling. As yet, it has been difficult to elucidate the role of microbes in benthic P turnover. The oxygen isotope signature of pore water phosphate ($\delta^{18}O_P$) carries information on microbial P cycling. Intracellular turnover of phosphory-

lated biomolecules results in isotopic equilibrium with ambient water, while enzymatic regeneration of P_i from organic matter yields distinct offsets from the equilibrium. A recently refined micro extraction protocol has made pore water P_i, which was previously too limited for isotope analysis, accessible as isotope biosignature.

We present a comprehensive study of sedimentary pore water P cycling from a transect across the Namibian continental shelf and slope. We combine pore water chemistry (sulfate, sulfide, ferrous iron, P_i), steady state turnover rate modeling, and oxygen isotope analyses of P_i and pore water to gain insight into microbial P cycling and regeneration of P_i from organic matter. The balance of these two processes is the major control for $\delta^{18}O_P$, with microbial P cycling enriching P_i in ^{18}O towards isotopic equilibrium with water, whereas mineralization of organic matter causes depletion of P_i in ^{18}O compared to the equilibrium value.

We found $\delta^{18}O_P$ values in a range from 12.8 to 26.2 ‰ that were in equilibrium as well as pronounced disequilibrium with water. We applied a mass balance model to calculate the predominance of regeneration versus microbial turnover signatures. Our results indicate a trend towards regeneration signatures under low mineralization activity and low P_i concentrations, and microbial turnover signatures under high mineralization activity and high P_i concentrations. These findings disagree with our expectation from earlier water column studies and geochemical evidence of preferential P_i regeneration. We suggest that microbial P_i uptake strategies, which are controlled by P_i availability, are decisive for the preservation of the isotope signature. This hypothesis is supported by the observation of efficient microbial P_i turnover in the phosphogenic mudbelt.

The $\delta^{18}O_P$ data elucidated benthic microbial P turnover in greater detail than possible from concentration data and steady state modeling alone. Our results emphasize the potential of the isotopic approach to understanding marine microbial P cycling.

III.1 Introduction

Phosphorus (P) is an essential nutrient for life on land and in the ocean, and occurs almost exclusively in the form of ortho-phosphate (PO_4^{3-}, abbreviated below as P_i). Living cells require phosphorylated biomolecules to mediate replication, transfer of energy and information, and buildup of structure (Pasek 2008). The marine P cycle is thus tightly coupled to global biogeochemical cycles of other elements, such as carbon and oxygen (Berner 1990). In interplay with other nutrients, P_i controls marine primary production

on both geologic and recent time scales (Benitez-Nelson 2000, Berner 1990, Froelich et al. 1982), and is linked to atmospheric oxygen levels in the history of the Earth (Colman et al. 2000, Van Capellen and Ingall 1996). The direct impact of nutrient availability on primary production is particularly evident at those subtropical eastern boundaries of the ocean basins, where a combination of wind systems and oceanic currents force nutrient rich, deep water masses to ascend. The flux of P_i associated with the upwelling water masses may be as high as 95 % of the ocean's standing P_i stock (Föllmi 1996). Though the main upwelling systems at the continental margins of the Pacific (California and Humboldt current) and the Atlantic (Canary and Benguela current) cover only a small fraction (0.1 %) of the global ocean's volume, they do account for 5 % of the marine primary production, with the Benguela upwelling system being the most productive (Carr 2002). As a consequence, the sediments on the continental shelf are mainly comprised by remains of marine organisms and form an elongated sedimentary structure rich in organic matter (OM), which was termed "mudbelt" (Bremner 1981). High mineralization rates are characteristic of the mudbelt sediments (Brüchert et al. 2000).

On Earth, the most important repositories of P are marine sediments. Sedimentary burial of P in refractory OM and phosphorite minerals is perceived as the ultimate sink in the marine P cycle (Blackwelder 1916, Froelich et al. 1982), and it has become evident that this sink also affects present-day P cycling (Benitez-Nelson 2000, Paytan and McLaughlin 2007). In regions of the ocean where external input of P_i is limited, it must be recovered from organic matter (OM) to supply the pelagic and benthic communities. The balance of burial and benthic reflux of regenerated P_i depends on manner and magnitude of the activity of microorganisms inhabiting the seabed. Microbial remineralization of OM is the major source for dissolved P_i in the sediment pore water (Berner 1990).

It has frequently been postulated that the active role of microbes in marine P cycling is not restricted to remineralization, but also involves concentration, formation and sequestration of P_i minerals in the sediments (Baturin and Bezrukov 1979). Modern sites of phosphorite formation are predominantly upwelling zones such as the Benguela system (Föllmi 1996). However, it still remains difficult to characterize the biological contribution to P_i regeneration and sequestration. Since P_i does not change its molecular form when passing from one pool to another and does not undergo significant redox transformations (Schink and Friedrich 2000), it is impossible to reconstruct these transitions from P_i concentration data alone.

Recently, the oxygen isotope signature of dissolved P_i has been shown to carry information on biological P_i cycling (Blake et al. 2001). The P-O bond is stable under ambient

conditions in the ocean, and only the intervention of enzymes can exchange oxygen atoms with surrounding media and alter the P_i oxygen isotope composition ($\delta^{18}O_P$, Blake et al. 1997, Tudge 1960), particularly in phosphoester hydrolysis (Blake et al. 2005, Liang and Blake 2009). Laboratory studies have investigated enzyme mechanisms involved in this cleavage and isotope effects of different cultures (Blake et al. 2005, Liang and Blake 2006), reconstructed signatures of different P_i substrates (Liang and Blake 2009), and distinguished biological processes from geochemical reactions (Blake et al. 1998, Liang and Blake 2007).

From these studies it has become evident that two antagonistic processes are reflected in the oxygen isotope signature of P_i. First, an oxygen isotope equilibrium between P_i and water, caused by a cascade of phosphorylation and dephosphorylation reactions during microbial P_i metabolism, and second, a kinetic fractionation by extracellular, hydrolytic cleavage of P_i from OM, incorporating isotopically lighter oxygen into P_i and driving the isotope signature away from the equilibrium (Blake et al. 2001).

Pioneering field studies of marine, estuary, and riverine water $\delta^{18}O_P$ have disentangled the balance of P_i release and uptake (Colman et al. 2005, McLaughlin et al. 2006a), and identified external P_i sources (McLaughlin et al. 2006b). This new isotope biosignature should thus prove useful for unraveling P_i dynamics in marine sediments, where the pore water P_i pool constitutes the interface between release of P_i by OM mineralization, microbial uptake and release of P_i, and interactions of P_i with the mineral solid phase. With a refined micro extraction protocol (Colman 2002, Goldhammer et al. 2009), we are now able to analyze $\delta^{18}O_P$ on pore water samples, where P_i yields were previously too small for isotope ratio mass spectrometric (IRMS) analysis.

In this contribution, we use a comprehensive approach to tackle the role of microbes in P_i regeneration in the marine subsurface. We measured $\delta^{18}O_P$ in marine sediment pore waters, obtained pore water geochemical data and modeled turnover rates to address the following questions:

(1) Are oxygen isotopes of P_i a suitable tracer for the study of P cycling in marine sediments, as they have proven in the water column?

(2) How do different settings in the seabed (e.g. mineralization activity, P_i concentrations) affect the isotope signatures?

(3) What is the microbial control on P_i regeneration? Do we find (isotopic) evidence for P_i limitation in the seabed?

The Benguela upwelling system offers an ideal natural laboratory to study benthic P cycling. It covers a variety of sedimentary environments from low activity deep-sea sites and intermediate slope sediments to the phosphogenic mudbelt.

III.2 Materials and Methods

III.2.1 Region of the study

At the southwest African and Namibian continental margin, the Benguela current forms, together with trade winds and shelf topography, one of the world's most intense upwelling areas. Driven by persistent, southeasterly and alongshore winds, upwelling cells are found along the entire coast from Cape Point (34.5 °S) in the south to Cape Frio (18.4 °S) in the north (Nelson and Hutchings 1983), and vary in seasonal strength

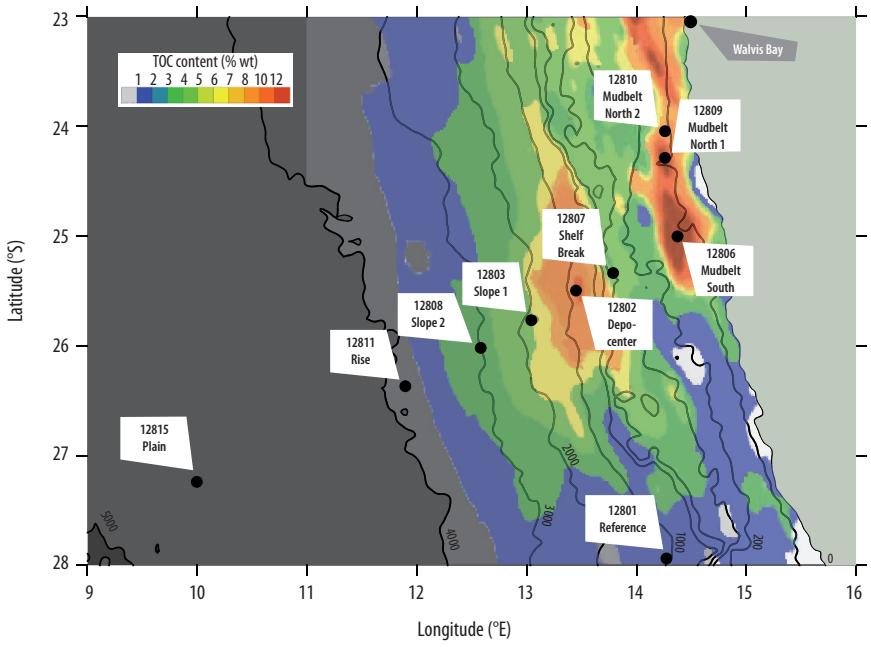

Figure III.1 Bathymetric map of the investigation area displaying the sampling sites on a cross-slope transect and total organic carbon content (TOC) of the surface sediments. TOC data taken from Inthorn et al. (2006b)

(Currie 1953) with peak intensity between March and September (Shannon and Nelson 1996). The Lüderitz cell at 25 to 27 °S is probably the most pronounced and persists throughout the year, while the Walvis Bay cell at 23 °C is strong but only seasonally active (Shannon and Nelson 1996). The upwelled nutrient-rich South Atlantic midwaters supply intense primary productivity in the inner shelf surface waters (Chapman and Shannon 1985), sequestering up to 0.37 Gt C yr^{-1} (Carr 2002).

Beneath this zone of high productivity, the debris of organisms has accumulated in a narrow, near shore band of organic-rich sediment that stretches over 700km alongshore and is up to 14 m thick (Bremner 1981, Emeis et al. 2004). This mudbelt forms a flat lens on the underlying sediments and covers a total area of 18,000 km^2 (Emeis et al. 2004). Sediments on the shelf are usually sandy and contain a large fraction of foraminifera, often interspersed with shell fragments and glauconitic grains. The mudbelt itself consists of a thick layer of organic rich, diatomaceous ooze, which is barely diluted by carbonate or terrestrial material since no rivers discharge from the adjacent desert (Borchers et al. 2005). It often exhibits considerable amounts of fish bones, scales and shell fragments, and the total organic carbon content of the sediments may be as high as 15 % weight (Inthorn et al. 2006b).

Shelf bottom waters are periodically anoxic, and outbreaks of hydrogen sulfide through the water column have been reported (Brüchert et al. 2006). The outcrops of older sediments of the Upper Tertiary at the shelf break (Dingle 1973) may form a barrier for seaward export of organic matter (OM), but nepheloid layers have been found to transport outer shelf material to an OM depocenter on the upper continental slope (Inthorn et al. 2006a). Towards the abyssal plain, the foraminiferal sand fraction of the sediments decreases and is gradually substituted by clays often rich in carbonate.

III.2.2 Retrieval of sediment cores and pore water sampling

During R/V Meteor's expedition M76/1 in April and May 2008, we sampled surface-near and deep sediments along a transect from the mudbelt of the shallow shelf (mean water depth 120 m) across the shelf break (~400 m) and a depocenter of organic matter on the upper continental slope to the abyssal plain (~5000 m), comprising seven singular stations plus an additional reference station outside the upwelling zone (Figure III.1, Table III.1). At each station, two parallel cores were taken with a 6 m gravity corer (diameter of the PVC inner tube 16 cm) for both standard pore water analysis and determination of $\delta^{18}O_P$. Surface sediments were analogously sampled with an 8+4 tube multi corer (diameter 10 cm). After retrieval, the gravity cores were cut into 1 m sections, labeled,

Table III.1 Transect stations with coordinates, water depth and representative bottom water temperatures used for isotope equilibrium calculation. Temperature data from Mohrholz et al. (2008)

Station	Longitude	Latitude	Water depth	Bottom water temperature
	°E	°S	m	°C
12801 Reference	14.301	27.999	1018	4
12802 Depocenter	13.450	25.500	791	4
12803 Slope 1	14.070	25.760	1944	3
12806 Mudbelt South	14.389	25.000	132	12
12807 Shelf Break	13.775	25.344	299	9
12808 Slope 2	11.891	26.369	3794	3
12809 Mudbelt North 1	14.268	24.286	120	12
12810 Mudbelt North 2	14.262	24.053	121	12
12811 Rise	12.573	26.010	2980	3
12815 Plain	10.000	27.237	4672	3

and brought to the ship's 4 °C cool chamber. Pore water was obtained with rhizon micro suction samplers (porous polymer, 0.1 µm filter width, Rhizosphere Research, Wageningen) that were pre-flushed with de-ionized water (H_2O), and inserted into the core after drilling a 3.7 mm hole into the core liner. An evacuated syringe was connected to the Luer adaptor to extract pore water, the first 0.5 mL discarded, and the syringe re-applied. The rhizon technique is advantageous over conventional squeezing as the extracted solution is readily filtered and excludes further microbial P_i turnover. Pore water samples for onboard and onshore analyses were collected in 20 mL scintillation vials, and for $\delta^{18}O_P$ analysis in HDPE bottles, triple washed with nitric acid (suprapur, 1 mol L^{-1}) and rinsed with de-ionized water (H_2O, Millipore Milli-Q).

III.2.3 Quantification of dissolved compounds

Phosphate (P_i) was quantified using a modified protocol after (Murphy and Riley 1962) and (Hansen and Koroleff 1999). One mL of sample was placed in a disposable polystyrene (PS) cuvette (2.5 mL) containing 50 µL ammonium molybdate solution, and amended with 50 µL of ascorbic acid solution. The extinction of the phosphomolybdenum blue complex was measured after 10 min at a wavelength of 820 nm (Hach

Lange DR 5000 photometer). *Ferrous iron* (Fe^{2+}) was measured photometrically (Hach Lange DR 5000 photometer) at 565 nm. An iron sensitive color complex was formed by adding 1 mL of sample to 20 µL of ferrospectral solution in PS cuvettes. Samples with high Fe concentrations were diluted with oxygen free H_2O to match the calibration range. *Sulfate* (SO_4^{2-}) was quantified in filtered samples (0.2 µm nylon syringe micro filter) by ion chromatography (Metrohm 861 Advanced Compact IC, Metrohm A Supp 5 column, 0.8 mL min^{-1}, conductivity detection after chemical suppression). *Dissolved inorganic carbon* (DIC) was measured in pore water samples as liberated CO_2 after treatment with HCl on a TOC analyzer (Shimadzu TOC-V). Dissolved *hydrogen sulfide* (HS^-) was determined in pore water samples fixed with $ZnCl_2$ using the photometric methylene blue method (Cline 1969).

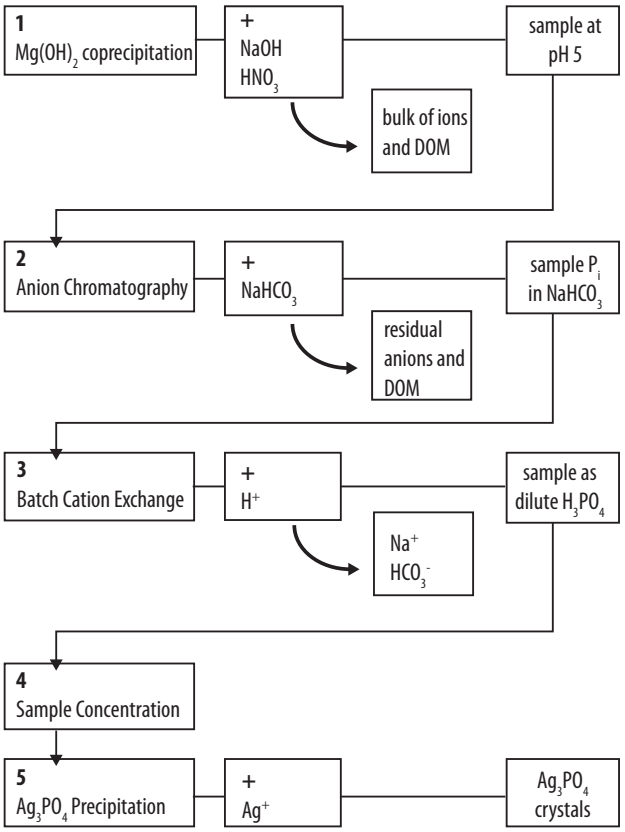

Figure III.2 Flow diagram of the refined P_i micro extraction protocol after Colman (2002). Panels show in sequence: the reagents that were added (+), the components that were removed, and the resulting sample status for each treatment step

III.2.4 Isotopic analyses of phosphate

Micro extraction of pore water P_i and isotope ratio mass spectrometry

We applied a recently refined micro extraction protocol that allowed us to convert very low quantities of P_i (> 0.5 µmol) to silver phosphate (Ag_3PO_4) for the analysis of phosphate oxygen isotopes by isotope ratio mass spectrometry (IRMS, Goldhammer et al. 2009). This protocol is based on an earlier method that comprises a sequence of precipitations, resin treatments, and sample concentrations to isolate P_i from ocean water samples (Colman 2002). Figure III.2 displays an overview of the five major steps in the extraction procedure. First, the plain pore water sample was subjected to a number of co-precipitations of P_i with magnesium hydroxide ($Mg(OH)_2$), induced by adding 1 M NaOH to raise the pH value to 10, with intermediate centrifugation and re-dissolution in 0.1 M HNO_3 (Colman 2002, Karl and Tien 1992). This first step already excluded bulk dissolved organic matter and ions. Second, a preparative anion chromatography with anion exchange resin (Biorad AG1X8, 100 - 200 mesh, HCO_3^- form, 1.4 mL min^{-1} flow rate, $NaHCO_3$ eluent) followed by selected collection of the eluted P_i peak fraction exchanged all remaining contaminant anions for HCO_3^- and eliminated traces of DOM (Colman 2002, Goldhammer et al. 2009). Third, the P_i fraction was stripped from eluent Na^+ and HCO_3^- in batch reaction with a cation exchange resin (Biorad AG50WX8, 100 - 200 mesh, freshly converted to H^+ form with HNO_3) that exchanged Na^+ for H^+ and drove out HCO_3^- as CO_2 (Colman 2002, Goldhammer et al. 2009). Fourth, the sample volume was reduced under gentle heating (60 °C) and Ar flow to concentrate P_i for facile Ag_3PO_4 precipitation. Fifth, Ag_3PO_4 crystals were precipitated according to O'Neil et al. (1994), washed with deionized H_2O (Milli-Q) and dried for IRMS.

We analyzed the oxygen isotope composition of Ag_3PO_4 using a standard setup (Colman 2002, Laporte et al. 2009) comprising a thermal combustion elemental analyzer (Thermo Finnigan TC/EA) linked via a continuous flow interface (Thermo Finnigan ConFlo II) to a mass spectrometer (Thermo Finnigan Delta plus). The layout of the TC/EA's carbon reactor followed Kornexl et al. (1999) and allowed the analysis of sample weights as low as 100 – 200 mg (Goldhammer et al. 2009). Samples of approximately 200 mg Ag_3PO_4 were weighed into silver foil capsules (3.5 mm, Hekatech) that were tightly crimped to exclude atmospheric oxygen, and inserted into the TC/EA's auto sampler. Oxygen was pyrolytically liberated from Ag_3PO_4 at 1450 °C and formed carbon monoxide (CO) with the glassy carbon of the reactor. The CO sample gas passed a H_2O trap and a GC column for separation, and was online measured for its 30/28 ratio in the MS against a CO test gas. Raw $\delta^{18}O_P$ values were retrieved from the instrument's

software (Isodat NT version 2.0), and normalized to ‰ VSMOW by a linear three-point calibration with external Ag_3PO_4 standards TU1, TU2 and $NaNO_3$ standard USGS35, that were run in triplicates before and after each batch of samples.

Determination of water oxygen isotopes and calculation of isotopic equilibrium

Water oxygen isotopes ($\delta^{18}O_w$) were determined by direct injection into a TCEA reactor operated at 1200°C, conversion to CO and continuous flow IRMS. We calculated a temperature dependent, oxygen isotope equilibrium value ($\delta^{18}O_{P\text{-}EQ}$) for microbial phosphate cycling, following the empirical relationship of Longinelli and Nuti (1973)

$$\delta^{18}O_{P-EQ} = \left[(111.4 - T)/4.3\right] + \delta^{18}O_W \qquad \text{Equation III.1}$$

where $\delta^{18}O_P$ is the oxygen isotope signature of dissolved P_i in ‰ VSMOW, *T* the temperature in °C, and $\delta^{18}O_W$ the oxygen isotope signature of pore water in ‰ VSMOW. We used representative bottom water temperatures documented for this region in an earlier study (Table III.1, Mohrholz et al. 2008) and applied a geothermal gradient of 0.02 °C m^{-1}.

III.2.5 Modeling of steady state production of DIC and P_i

We used the PROFILE numerical solution (Berg et al. 1998) to determine one-dimensional, stationary production of DIC and P_i in the pore water profiles. A box model was fitted iteratively to the concentration data by adjusting a number of reactive layers to the calculation domain, and subsequently minimizing this number by merging adjacent zones without losing statistical significance (Berg et al. 1998). By depth integration of these reactive layers, rates of DIC and P_i production were obtained for the entire profile to assess the amount of P_i produced during OM mineralization.

To identify preferential P_i regeneration, we calculated the ratio of DIC and P_i production rates. Usually, we perceive the C:P ratio of organic matter as a bulk indicator for preferential P_i release in mineralization (Anderson et al. 2001, McManus et al. 1997). When P_i is liberated from OM, e.g. with a Redfield composition (C:P = 106), the C:P in the residual OM increases. In turn, the ratio of C and P in the mineralization products, DIC and P_i, will be much smaller than the Redfield ratio. To explore this relationship we calculated the ratio of DIC and P_i production rates for each station of the transect, and presumed that C:P values lower than those of fresh OM indicate preferential regeneration of P_i.

III.3 Results

III.3.1 Pore water geochemistry

The pore water profiles of the Benguela transect (Figure III.1) for dissolved inorganic carbon (DIC), sulfate (SO_4^{2-}), sulfide (HS^-), phosphate (P_i) and dissolved ferrous iron (Fe^{2+}) are displayed in Figures III.3A and III.3B (next pages). Concentrations of DIC increased from the abyssal plain (12815) to the upper shelf (12806), except for the shelf break station 12807. The non-upwelling reference station 12801 resembled the abyssal plain (Figure III.3A). The depth of sulfate consumption decreased towards the shelf, again with the exception of the shelf break. Steepest gradients were found at the depocenter (12802) and mudbelt stations (12806, 12809, 12810). Sulfate bottom water concentrations usually corresponded to the seawater value and were approximately 29 mmol L^{-1} for most of the stations. Surprisingly high bottom water concentrations (up to 33 mmol L^{-1}) were found at stations 12815, 12811 and 12810.

At depths where sulfate becomes strongly depleted, an increase in sulfide (HS^-) concentration was observed. The concentrations of sulfide were rising from the abyssal plain to the continental shelf, and highest concentrations were found in the mudbelt cores (12806, 12809, 12810). We did not encounter sulfidic bottom waters in any of the stations (Figure III.3A).

Likewise, pore water concentrations of P_i were highest on the shelf, and lowest at the non-upwelling site and the abyssal plain. Phosphate concentrations generally increased with core depth at transect stations 12811 to 12802. The mudbelt cores (12806, 12809, 12810) revealed a different and fairly consistent depth profile, with P_i peaks (up to < 500 µmol L^{-1}) in 0.1 – 0.2 m below seafloor, and a sharp decrease below (Figure III.3B). Ferrous iron was very low to absent in the mudbelt cores (12806, 12809, 12810) and the abyssal plain (12815), and played a minor role in the rest of the transect (12811 to 12807), where sharp peaks of Fe^{2+} were consistently observed at around 0.1 m below seafloor. Highest concentrations (up to 70 µmol L^{-1}) were identified at the shelf break (12807). The non-upwelling reference station (12801) had a much broader Fe^{2+} peak in the upper 1 m of the core (Figure III.3B).

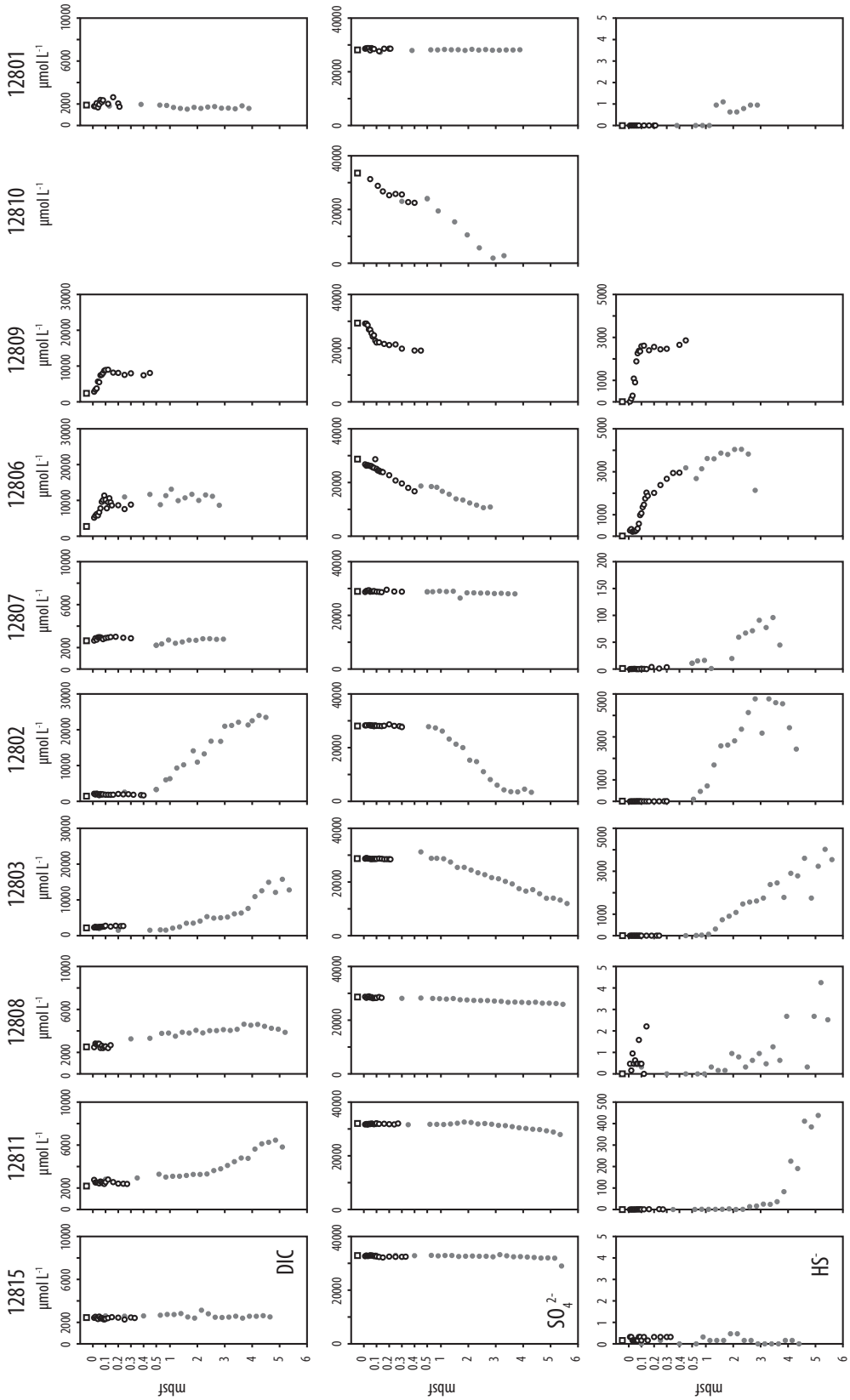
12815
12811
12808
12803
12802
12807
12806
12809
12810
12801
µmol L-1
mbsf
DIC
SO4 2-
HS-

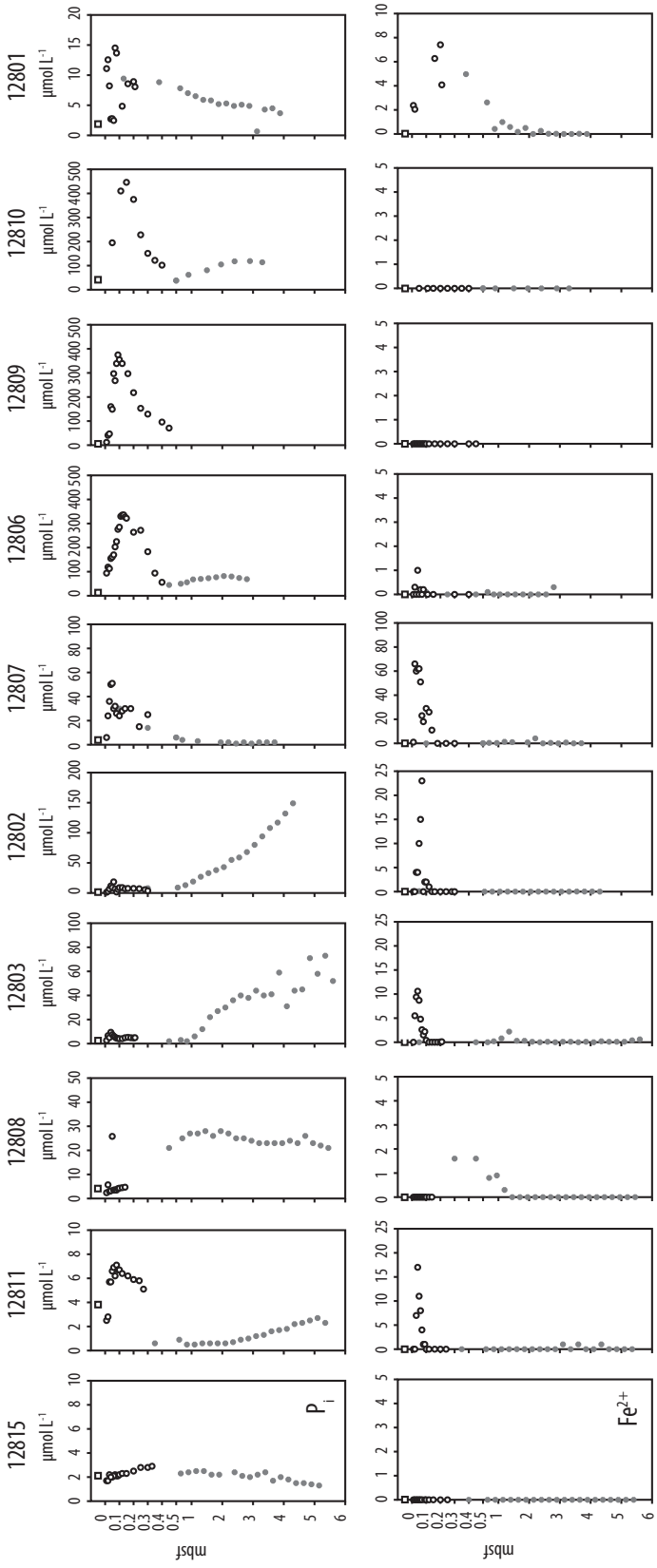

Figures III.3A (left page) and III.3B (this page) Pore water profiles of dissolved inorganic carbon (DIC), sulfate (SO_4^{2-}), and sulfide (HS^-, III.3A, left page), dissolved inorganic phosphate (P_i) and ferrous iron (Fe^{2+}, III.3B, this page) for each station of the transect. Data from bottom water samples (squares), multicorer (circles) and gravity core pore water samples (dots) are given in µmol L^{-1}. At site 12810, sample limitation prevented DIC and HS^- analyses. Note the different scales on the concentration axes and the magnified depth axis for the near-surface layer from 0 to 0.5 m depth

III.3.2 DIC and P_i turnover

We modeled steady state turnover of DIC and P_i for selected stations (12801, 12802, 12803, 12806, 12808, 12809 and 12811) based on pore water concentration data. An example of the model output can be found in Figure III.4. At reference station 12801 outside the upwelling zone, no significant turnover of DIC and P_i was observed. The transect stations showed low rates for DIC and P_i production at the rise, slope, and depocenter (3.12 – 24.64 nmol DIC cm^{-2} d^{-1}, 0.05 to 0.51 nmol P_i cm^{-2} d^{-1}). In the mudbelt, production rates were up to two orders of magnitude higher, with 163.30 and 243.65 nmol DIC cm^{-2} d^{-1} and 4.90 and 5.60 nmol P_i cm^{-2} d^{-1} (Table III.2). At most stations, the main zones of DIC and P_i production overlap (Figure III.4). The ratio between DIC and P_i production is small at the reference (23), rise (8) and lower slope (57) stations, and much higher at the upper slope (290) and depocenter site (147). The mudbelt again was lower with 33 respective 48 (Table III.2).

Table III.2 Results of steady-state pore water modeling with the PROFILE numerical solution. Turnover rates were integrated over the entire profile. Coefficients of determination (R^2) indicate the level of accuracy that the fit achieves with respect to measured data

Station	DIC integrated production (R_{DIC})	DIC main zones		P_i integrated production (R_{Pi})	P_i main zones		Rate ratio R_{DIC}:R_{Pi}
	nmol cm^{-2} d^{-1}	*m*	*R^2*	*nmol cm^{-2} d^{-1}*	*m*	*R^2*	
12811 Rise	4.27	0-0.9, 4.5-5.4	0.97	0.51	0-0.5	0.79	8
12808 Slope 2	3.12	0-1.8	0.90	0.05	0-1.1	0.98	57
12803 Slope 1	24.64	4.5-5.6	0.96	0.08	4.7-5.6	0.96	290
12802 Depocenter	9.33	0-4.5	0.99	0.06	> 4.5	0.99	147
12806 Mudbelt South	163.30	0-0.4	0.51	4.90	0-0.3	0.95	33
12810 Mudbelt North 2	243.65	0-0.5	0.95	5.06	0-0.4	0.86	48
12801 Reference	-0.22	0-3.9	0.82	-0.01	0-3.9	0.56	23

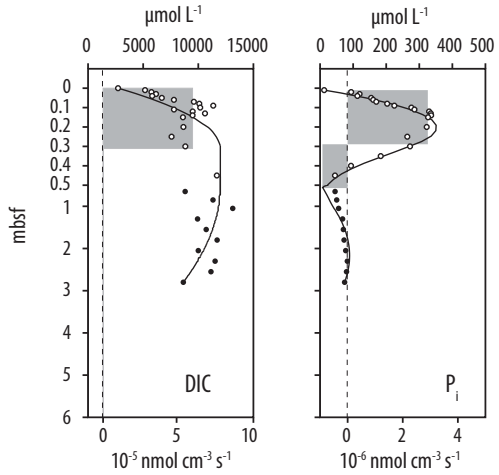

Figure III.4 Example of PROFILE model output for station 12806, DIC production (left panel) and P_i production (right panel). Shown are: pore water concentrations of multicore (circles) and gravity core samples (dots) plotted on the upper x-axis, production rates in reactive layers (greyshades) plotted on the lower x-axis, and the model approximation of the concentration profile (solid line). The dashed line denotes zero turnover. The scaling of the depth axis changes below 0.5 m

III.3.3 Phosphate oxygen isotopes

The analysis of water oxygen isotopes revealed minor variability around 0 ‰ (min - 0.06, max + 0.74, µ + 0.27, 1σ sdev 0.22, n = 79). We did not obtain water $\delta^{18}O$ samples for station 12801 and assumed a value of 0 ‰ for calculation of isotopic equilibria at this station.

The range of pore water $\delta^{18}O_P$ values measured from 12.80 to 26.21 ‰. The profiles displayed characteristic depth patterns of equilibrium signatures and offsets from the calculated isotopic equilibrium. At reference station 12801, phosphate oxygen isotopes were lighter than equilibrium values over the entire core. At the rise and slope stations 12811 and 12803, we found remarkable offsets from equilibrium values of up to – 10 ‰ at the core tops, while values approached calculated equilibrium with greater sediment depth (Figure III.5). At slope station 12808 and the depocenter 12802, these offsets were of the same magnitude, but located deeper in the core. In contrast, the mudbelt stations 12806 and 12810 showed only minor deviations, and the $\delta^{18}O_P$ values were close to the calculated equilibrium in the entire core (Figure III.5). Bottom water $\delta^{18}O_P$ was measured at four stations, and was significantly off equilibrium with H_2O at stations 12801, 12803 and 12806, and closer to equilibrium at station 12810 (Figure III.5).

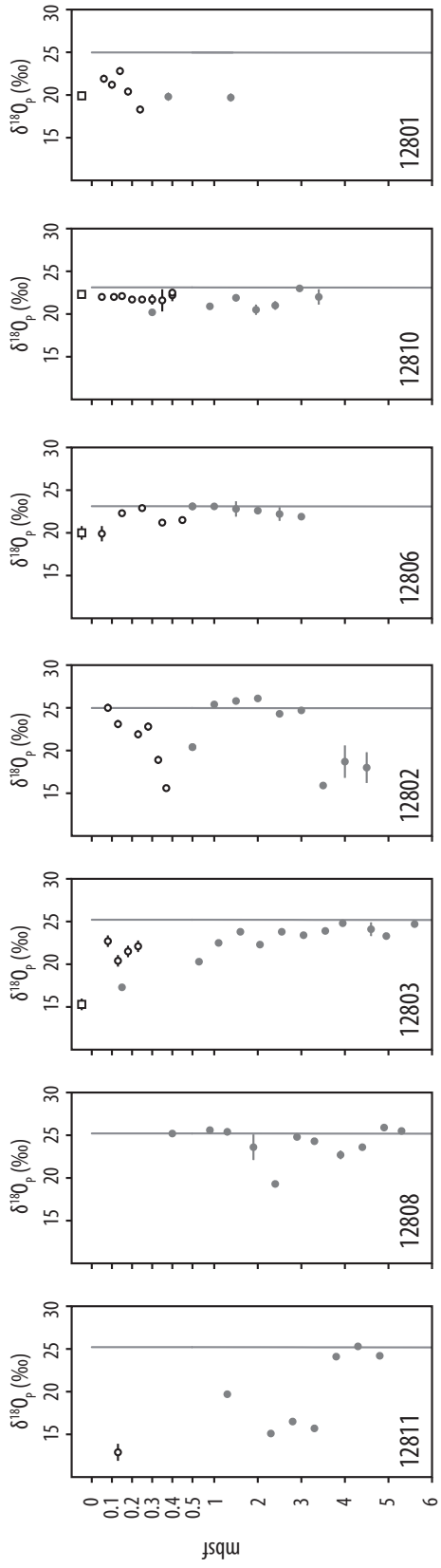

Figure III.5 Pore water profiles of phosphate oxygen isotopes ($\delta^{18}O_p$). Data from bottom water samples (squares), multicorer (circles) and gravity cores (dots) are given in ‰ VSMOW. The grey line represents the isotope equilibrium calculated from the equation of Longinelli and Nuti (1973, Equation III.1) with typical bottom water temperatures (Table III.1) and a geothermal gradient of 0.02 °C m^{-1}. For clarity, we corrected the $\delta^{18}O_p$ for the measured $\delta^{18}O$ of water, and calculated the Longinelli equilibrium for a water $\delta^{18}O$ of 0 ‰VSMOW. The scaling of the depth axis changes below 0.5 m

III.4 Discussion

In the following discussion, we will first comment on the geochemical evidence of P_i cycling and preferential regeneration that were derived from pore water profiles and steady state modeling. We use the results of the steady state model to characterize the transect stations by their geochemical setting and use this classification as background information for the later interpretation of isotope signatures. Second we introduce an oxygen isotope mass balance model that is applied to discriminate P_i regeneration against microbial uptake and turnover, and evaluate the predominant process. We finally show that P_i uptake strategies by microorganisms are crucial for the $\delta^{18}O_P$ signature and may explain characteristic features of the isotope data set.

III.4.1 Organic matter mineralization and rates of P_i regeneration along the transect

Mineralization of organic matter and preferential regeneration of P_i

Besides the re-dissolution of P_i adsorbed to mineral surfaces during early diagenesis, the majority of bioavailable P_i in marine sediments is released by preferential regeneration of P_i from organic matter (Berner 1990). This process can be stimulated under two different environmental conditions, P limitation and OM limitation. Under P limitation, microorganisms scavenge P_i from OM, whereas extracellular enzymes such as alkaline phosphatase (APase) or 5' nucleotidase (5'Nase) liberate P_i from phosphoester bonds. This mechanism is induced by P_i deficiency inside the cells (Benitez-Nelson 2000). On the other hand it is also known that microorganisms in the oligotrophic deep-sea are limited by OM as a carbon (C) source (Sander and Kalff 1993). About 95 % of the cell's C demand is respired, but remaining P_i headgroups prevent C uptake and metabolism. Release of extracellular phosphomonoesterases dephosphorylates OM to obtain C, and will result in a high portion of regenerated P_i as a by-product of C respiration (Colman et al. 2005).

Fe oxyhydroxides as alternative P_i source

As expected from the absence of riverine input (Borchers et al. 2005), reduction of ferric iron plays a marginal role in C mineralization along the transect. The sharp peaks of dissolved Fe^{2+} coincide with minor increases in P_i concentration at station 12811, 12803, 12802, 12807 and 12801, as a result of release from OM during iron reduction or by desorption of P_i during reductive dissolution of ferric oxyhydroxides (Krom and Berner

1981, van der Zee et al. 2003). We believe that the contribution of this process to the dissolved P_i pool in the sediment pore waters of the investigated stations is minor.

Carbon-to-phosphorus ratios of organic matter

Particulate organic matter undergoes microbial degradation during sinking through the water column. The OM reaching the sediment surface is thus already depleted in P compared to the pristine material produced in photosynthesis. Its C:P ratio is therefore higher than e.g. 106 (Redfield 1958) or 174 (Takahashi et al. 1985), and will be further increased by preferential P_i regeneration. For example, sedimentary C:P ratios of > 300 have been reported from the Benguela region (K. Küster-Heins, personal communication). We therefore consider C:P ratios of mineralization products (DIC and P_i) indicative of preferential P_i release, when they are much smaller than the C:P of the OM source (Anderson and Sarmiento 1994). This is the case for all stations except 12802 (147) and 12803 (290).

Classification of stations with similar geochemical setting

On the basis of steady state DIC production as indicator for the total mineralization activity, and the ratio between DIC and P_i production (Table III.2), we classified the stations into three groups of P_i remineralization regimes.

The first group consists of the low activity stations 12801, 12811 and 12808, with zero to minor DIC production, and extraordinary small DIC to P_i production ratios of 8 to 57 (Table III.2). At these input-limited deep-sea sites, we expected preferential P_i regeneration.

The second group includes the high activity stations 12802 and 12803 that are related to the shelf depocenter (Figure III.1) and exhibit high DIC production, but also high DIC to P_i production ratios of 290 and 147 (Table III.2) that probably exceed the C:P of the deposited OM. These ratios point to less preferential P_i release during OM degradation.

The third group spans the mudbelt stations 12806 and 12810, which show the highest DIC production rates of the transect, but have ratios of DIC to P_i production in the same range as the low activity stations (33 and 48, Table III.2). This indicates highly preferential P_i regeneration from OM. In light of the high P_i concentrations (up to 470 µmol L^{-1}, Figure III.3B), it seems unlikely that it is limitation in P_i that drives the preferential regeneration.

In the following, we will use these classifications for the evaluation of the oxygen isotope composition of pore water P_i.

III.4.2 The phosphate oxygen isotope balance of regeneration and microbial turnover

Two processes primarily control the oxygen isotope composition of P_i in aquatic systems: microbial P_i turnover (uptake, cycling, and release), and extracellular, enzymatic hydrolysis of phosphoesters during regeneration of P_i from OM. In this section, we discuss important aspects of these two pathways and introduce, based on earlier experimental results, a two-endmember-model for the isotope mass balance.

Endmember 1: Isotope equilibrium in microbial P_i metabolism

Microbial P_i uptake, use, and subsequent release drive the oxygen isotope composition of pore water P_i towards isotopic equilibrium between P_i and ambient water. This is due to the action of intracellular phosphoenzymes, involved in synthesis and cleavage of biomolecules, such as adenosine mono-, di- and triphosphates (AMP, ADP, ATP) and ribonucleic (RNA) and desoxyribonocleic acid (DNA). Recurring intracellular turnover of these molecules completely exchanges the P_i oxygen atoms with water oxygen. The ubiquitous inorganic pyrophosphatase (PPase) has been identified as the key enzyme involved in this rapid equilibration (Blake et al. 2005), which is largely controlled by temperature and follows the earlier empirical equation of Longinelli and Nuti (1973, Equation III.1). Studies on cultures of *Escherichia coli* have revealed a similar relationship (Blake et al. 1997, Equation III.2)

$$\delta^{18}O_{P-EQ} = \left[(155.8 - T)/6.4\right] + \delta^{18}O_W \qquad \text{Equation III.2}$$

We subtract Equation (III.1) from (III.2) to obtain the potential difference $\Delta(\delta^{18}O_{P\text{-}EQ})$ of resulting equilibrium signatures:

$$\Delta(\delta^{18}O_{P-EQ}) = \left[(155.8 - T)/6.4\right] - \left[(111.4 - T)/4.3\right] = -1.56 + 0.08T$$

Equation III.3

For the temperature range of 3 to 12 ° C, the deviation is -1.3 to -0.6 ‰. This is slightly larger than the analytical error of our $\delta^{18}O_P$ measurements (1σ sdev: 0.6 ‰). We consider the Longinelli equation more representative for our study, since it has been obtained from field samples and not microbial pure cultures, and use it for the calculation of the equilibrium endmember.

Endmember 2: Kinetic fractionation and incorporation of water-oxygen during extracellular P_i regeneration from organic matter

In contrast to microbial P_i cycling, the enzymatic hydrolysis of P_{org} involves kinetic isotope fractionation and incorporation of water oxygen that depends on substrate type and enzymatic systems. In general, these isotope effects drive the isotope composition of pore water P_i away from the isotope equilibrium between P_i and ambient water, towards lighter values. Experimental studies have revealed that P_i regeneration pathways (Liang and Blake 2006), enzymatic systems (Blake et al. 2005), and substrate characteristics (Liang and Blake 2009) yield distinct isotope effects.

Consideration of substrate and enzyme systems for calculation of the regeneration endmember

Phosphoesters are the main form of P_{org} in marine sediments that is available for microbial degradation (Ingall et al. 1990). In the case of a phosphomonoester (PME) substrate, one oxygen atom is exchanged with ambient H_2O, and the resulting $\delta^{18}O_{PME}$ will depend on the kinetic fractionation F_{ME} imposed by the phosphomonoesterase enzyme involved, and follows Equation III.4:

$$\delta^{18}O_{PME} = 0.25 \times \left(\delta^{18}O_W + F_{ME}\right) + 0.75 \times \delta^{18}O_{P_{org}} \qquad \text{Equation III.4}$$

Common phosphomonoesterases in aquatic environments are alkaline phosphatase (APase) and 5' nucleotidase (Blake et al. 2005). APase is most abundant, attacks a wide range of P monoesters, and its production by the cell is stimulated by P_i limitation (Benitez-Nelson 2000). The kinetic fractionation F_{APase} accompanying APase activity is -30 ‰ (Liang and Blake 2006). In contrast, 5' nucleotidase (5'Nase) targets nucleotides exclusively, is correlated with high growth rates of bacteria, and is not affected by high P_i concentrations. The associated fractionation $F_{5'Nase}$ is -10 ‰ (Liang and Blake 2006) (Table III.3).

In the case of a phosphodiester (PDE) substrate, the $\delta^{18}O_{PDE}$ is additionally dependent on the substrate type. Naturally occurring phosphodiesters are the nucleic acids RNA and DNA, which may account for up to 50 % of the sedimentary P_{org} (Minear 1972). The hydrolysis exchanges two oxygen atoms with H_2O in a two-step mechanism, in which a phosphodiesterase (PDase) cracks the terminal nucleotide off the polynucleotide backbone, and a phosphomonoesterase (APase or 5'Nase) attacks the free nucleotide. The kinetic fractionations of diesterases (F_{DE}) and monoesterases (F_{ME}) are combined as follows (Liang and Blake 2009):

$$\delta^{18}O_{PDE} = 0.25 \times \left(\delta^{18}O_W + F_{DE}\right) + 0.25 \times \left(\delta^{18}O_W + F_{ME}\right) + 0.5 \times \delta^{18}O_{P_{org}}$$

Equation III.5

The fractionation of the PDase step is for DNA -20 ‰ and for RNA +20 ‰, largely due to molecular structure (Liang and Blake 2009). The resulting fractionations for phosphomono- and phosphodiester hydrolysis are summarized in Table III.3.

Composition of phosphorus bound to organic matter

In light of these distinct isotope effects, we have to estimate the composition of the P_{org} material. Organic P in marine sediments comprises phosphomonoesters (e.g. phospholipids, mononucleotides, or phosphosugars), and phosphodiesters (mainly nucleic acids RNA and DNA). The latter form up to 50 % of the P_{org} pool (Minear 1972). Since RNA is more rapidly degraded than DNA (Kolowith et al. 2001, Novitsky 1986), the ratio of RNA to DNA depends largely on the amount of detrital DNA, which is usually enhanced under high sedimentation of organic matter (Dell'anno et al. 1998). Field investigations offshore the island of Crete have revealed decreasing RNA/DNA ratios with decreas-

Table III.3 Isotopic fractionation during P_i regeneration for phosphomonoester (PME) and phosphodiester (RNA, DNA) substrates and the enzymes alkaline phosphatase (APase), 5' nucleotidase (5'Nase), and phosphodiesterase (PDase). Data from Liang and Blake (2006 and 2009)

Substrate	Enzyme	F	Calculation of resulting $\delta^{18}O_p$
		‰	$\delta^{18}O_p =$
PME	APase	-30	$= 0.25 \times (\delta^{18}O_w + F_{APase}) + 0.75 \times \delta^{18}O_{Porg}$
	5'Nase	-10	$= 0.25 \times (\delta^{18}O_w + F_{5'Nase}) + 0.75 \times \delta^{18}O_{Porg}$
RNA	(1) PDase	+20	$= 0.25 \times (\delta^{18}O_w + F_{RNA+PDase}) + 0.25 \times (\delta^{18}O_w + F_{APase}) + 0.5 \times \delta^{18}O_{Porg}$
	(2) APase	-30	
	(1) PDase	+20	$= 0.25 \times (\delta^{18}O_w + F_{RNA+PDase}) + 0.25 \times (\delta^{18}O_w + F_{5'Nase}) + 0.5 \times \delta^{18}O_{Porg}$
	(2) 5'Nase	-10	
DNA	(1) PDase	-20	$= 0.25 \times (\delta^{18}O_w + F_{DNA+PDase}) + 0.25 \times (\delta^{18}O_w + F_{APase}) + 0.5 \times \delta^{18}O_{Porg}$
	(2) APase	-30	
	(1) PDase	-20	$= 0.25 \times (\delta^{18}O_w + F_{DNA+PDase}) + 0.25 \times (\delta^{18}O_w + F_{5'Nase}) + 0.5 \times \delta^{18}O_{Porg}$
	(2) 5'Nase	-10	

ing benthic microbial activity from the shelf (~1) to the open sea (~0.1, Dell'anno et al. 1998). For the Benguela transect we assume that there is a similar relationship, with a RNA/DNA ratio of 1 for the shelf stations (12806, 12810), 0.5 for the slope stations (12802, 12803), and 0.1 for the plain and rise stations (12801, 12808, 12811). We therefore assume a "model P_{org}" for our calculation of the $\delta^{18}O_{P\text{-}REG}$ signature. The portion r of phosphomonoesters (PME), RNA, and DNA is based on Dell'anno et al. (1998) and displayed in Table III.4. The regeneration endmember signature $\delta^{18}O_{P\text{-}REG}$ is then calculated from the relation of phosphomonoester (PME), RNA and DNA regeneration (see Equations III.5 and III.6, and Table III.4)

$$\delta^{18}O_{P-REG} = r_{PME}\,\delta^{18}O_{PME} + r_{RNA}\,\delta^{18}O_{P-RNA} + r_{DNA}\,\delta^{18}O_{P-DNA} \qquad \text{Equation III.6}$$

We further assumed a $\delta^{18}O_{Porg}$ signature of sinking OM from the photic zone of 23 ‰, which was inferred from Equation III.1 using a temperature of 13 °C annual average of sea surface temperatures in the Benguela system (Mohrholz et al. 2008s).

Table III.4 Model composition of P_{org} after Dell'Anno et al. (1998)

Station	r_{PME}	r_{RNA}	r_{DNA}
12801, 12811, 12808	0.5	0.05	0.45
12802, 12803	0.5	0.16	0.34
12806, 12810	0.5	0.25	0.25

Construction of the isotope mass balance model

Under stationary conditions, the mass balance of important P_i sources and sinks can be described as:

regeneration + desorption from oxyhydroxides + microbial release = microbial uptake + adsorption onto oxyhydroxides + authigenic mineral formation

In the following mixing model, we did not consider inorganic processes, such as adsorption and desorption of P_i with iron and manganese oxyhydroxides (Blake et al. 2001) or precipitation and dissolution of apatite (Blake et al. 1998, Liang and Blake 2007), for the $\delta^{18}O_P$ signature. Pore water data suggested that iron cycling was of minor importance (Figure III.3B), and ongoing precipitation or re-dissolution of biogenic apatite is almost

non-selective in isotopes (the shift for dissolved P_i accounts to ~ -1 ‰, Liang and Blake 2007) and will thus not invalidate our interpretation. However, it is reasonable to assume that such phases have an isotope composition averaging the values for full equilibrium and maximum disequilibrium, and P_i release from these phases will thus not strongly impact the isotope mass balance.

Isotope mass balance model

The effective phosphate oxygen isotope signature we measure in the pore water ($\delta^{18}O_P$) is the sum of fractions (x) of the regeneration ($\delta^{18}O_{P\text{-}REG}$) and equilibrium signature ($\delta^{18}O_{P\text{-}EQ}$)

$$\delta^{18}O_P = x\delta^{18}O_{P-REG} + (1-x)\delta^{18}O_{P-EQ} \qquad \text{Equation III.7}$$

In an alternative formulation of Equation III.7, we determine the ratio η_P between P_i regeneration and microbial turnover to

$$\eta_P = \frac{\delta^{18}O_{P-EQ} - \delta^{18}O_P}{\delta^{18}O_P - \delta^{18}O_{P-REG}} \qquad \text{Equation III.8.}$$

The smaller the difference in the enumerator (respective the denominator), the more important is the equilibrium imprint (respective the regeneration imprint). The ratio thus indicates the predominance of P_i regeneration (for $\eta_P > 1$) or microbial turnover (for $\eta_P < 1$) and may be perceived as the P_i cycling efficiency by the microbial community.

Results of the mass balance model: efficiency of microbial P_i cycling

Figure III.6 illustrates the downcore variability of the η_P ratio. It is conspicuous that stations similar in mineralization activity and ratio of DIC and P_i production do not necessarily resemble in $\delta^{18}O_P$ and η_P. We focus on three remarkable observations based on the isotope data.

Preservation of regeneration signature (disequilibrium) at low activity, low P_i sites

Geochemical evidence of the low activity stations 12801, 12808, and 12811 suggests preferential P_i release induced by low P_i concentrations. In contrast to the expectation, the efficiency of P_i cycling seems less pronounced as indicated by η_P around 1, and a considerable portion of the regeneration signal is preserved (Figure III.6).

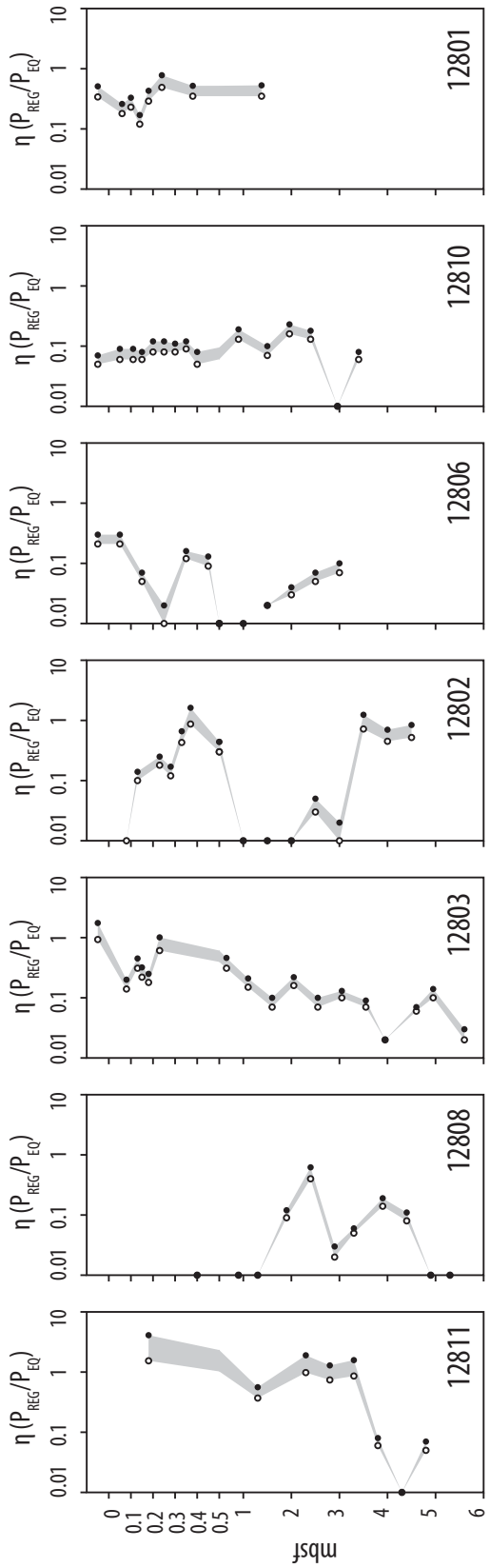

Figure III.6 Ratio η_P between P_i regeneration and microbial turnover, calculated from the isotope mass balance and Longinelli equilibrium (see text). Values of $n_P > 1$ indicate predominance of P_i regeneration, values of $\eta_P < 1$ indicate predominance of microbial turnover. For $n_P = 1$ the proportion is 1:1. The ratio calculated for the APase reaction pathway is denoted with black dots, for the 5′ NAse reaction pathway with circles. The grey area represents the range we expect from a combination of both reaction pathways. Note that η_P values are plotted on a log-transformed x-axis, and all values $n_P \leq 0.01$ are displayed as 0.01. The scaling of the depth axis changes below 0.5 m

Equilibrium signature at high activity, high P_i mudbelt sites

The mudbelt stations 12806 and 12810 exhibit the highest DIC and P_i production rates, and release DIC and P_i in a ratio much smaller than the Redfield ratio (Table III.2). Nevertheless, the P_i regeneration signature is poorly preserved, and η_P values below 0.2 suggest highly efficient microbial turnover.

Unequal display of slope sites with intermediate DIC production

The stations 12802 and 12803 with intermediate mineralization activity show variable patterns of P_i regeneration. The slope station 12803 suggests a model where low microbial activity in the top of the sediments corresponds to surplus regenerated P_i, similar to stations 12801 or 12811, and with increasing depth, η_P decreases due to more efficient recycling within the microbial community (Figure III.6). At the depocenter (12802), two distinct zones of P_i regeneration prevail. It is difficult to evaluate this pattern, since the quality of the deposited OM may differ in the core. Degraded material is exported from the shelf in nepheloid layers with transport intensities that might vary over time (Inthorn et al. 2006b) and result in different OM quality in these layers.

Apparent inconsistencies between geochemical evidence and isotope mass balance

These inconsistencies of geochemical evidence and isotope mass balance results point to sophisticated relations between P_i availability and demand of benthic communities in low activity sediments. We believe that results from the water column, where P_i limitation induced pronounced equilibrium signatures (Colman et al. 2005, Liang and Blake 2009), cannot easily be transferred to sediment pore waters. In the Benguela transect, we observe large offsets from the isotopic equilibrium (Figure III.5) in many of the samples. It is striking that the few bottom water samples (stations 12803, 12806, 12810, 12801) are also in isotopic disequilibrium with ambient water because deep water samples from earlier studies were always in isotopic equilibrium with ambient water (Table III.5). This suggests that either processes within the benthic boundary layer control these disequilibria, or that the signature of regenerated P_i diffusing out of the sediments is preserved in the bottom water.

Microbial P_i transport systems: consequences for phosphate isotope biosignatures

The isotopic expression of P_i regeneration versus cycling in the sediment pore water is strongly affected by microbial P_i uptake strategies that are controlled by ambient P_i concentrations (Jansson 1988, van Veen 1997). Under low P_i availability, microorganisms use P_i specific transport systems (Pst) for the cross-membrane transfer of P_i into the cell.

Table III.5 Comparison of phosphate oxygen isotope signatures measured in the water column of ocean sites, and in bottom water of the Namibian shelf

Site	Sample ID	Water depth	$\delta^{18}O_P$ sample	$\delta^{18}O_P$ equilibrium	Reference
		m	*‰VSMOW*	*‰VSMOW*	
Hawaii Ocean Time Series / ALOHA	H113-2-15-9	3000	24.07	25.33	Colman et al. 2005
Bermuda Atlantic Time Series / BATS	B146-5-23	4000	24.54	25.50	
Long Island Sound	LISS-J2-1AB	2	21.30	21.35	
San Francisco Bay transect	Ocean Endmember Station 19 (10/2002)	surface	20.1	21.6	McLaughlin et al. 2006
Benguela transect	12803 Slope 1 BW	1944	15.56	25.44	*this study*
	12806 Mudbelt South BW	132	20.61	23.80	
	12810 Mudbelt North 2 BW	121	22.84	23.68	
	12801 Reference BW	1018	19.87	24.98	

Along with generally reduced activity and community turnover, the active release of P_i is prevented in living cells, and may occur only after cell death, where P_{org} from cell debris is instantly attacked by synchronous enzyme release (Jansson 1988). Such a strategy will preserve the regeneration isotope signature even under low P_i concentrations. In contrast, high P_i concentrations induce the development of unspecific P_i cross-membrane transport systems (Pit, Jansson 1988), and P_i that has undergone microbial metabolism and is in isotopic equilibrium with water can also diffuse out of living cells (Jansson 1988, van Veen 1997). High community turnover rates thus easily equilibrate the P_i pool in the pore water.

The mudbelt as a unique environment for marine P cycling

The mudbelt setting (at stations 12806, 12810) is striking for two reasons: the extraordinary magnitude of pore water P_i concentrations, that form a sharp peak in the upper 0.5 m of the sediments, and the predominance of the microbial turnover imprint on the $\delta^{18}O_P$ signature (Figures III.5 and III.6). Limitation of P and C is rather unlikely, since the input of fresh organic matter is massive under average sedimentation of 0.5 cm a^{-1} (Inthorn et al. 2006b), and the high DIC production rates indicate high microbial activity. We assume that these conditions are favorable of the unspecific microbial P_i uptake,

and this is exactly reflected in the predominance of isotope equilibrium (Figure III.6). Additionally, the continuous P_i uptake and release is corroborated by the occurrence of bacteria with a special P physiology.

The Benguela mudbelt is considered as a modern region with recent phosphorite formation (Bremner and Rogers 1990), in which bacteria have been proposed to play an active role (Nathan et al. 1993). Evidence has accumulated that large sulfur bacteria of the genera *Beggiatoa* and *Thiomargarita*, inhabiting the shelf sediments (Brüchert et al. 2003), carry physiological prerequisites to mediate this process (Schulz and Schulz 2005). We encountered significant cell numbers of *Thiomargarita namibiensis* in the upper layers of the sediments at stations 12806 and 12810. This non-motile sulfur bacterium has to renew an internal nitrate reservoir during periods of oxygenated bottom waters to sustain its capability of oxidizing sulfide when bottom water anoxia prevail (Schulz 2006). Under such conditions *Thiomargarita* take up excess P_i that is stored as polyphosphates. During anoxic periods, hydrolysis of the polyphosphates liberates energy (Kornberg 1995) that is used for the uptake and storage of a carbon source such as acetate (Schulz 2006). Phosphate produced in this process is released to the pore water. This phenomenon supports the hypothesis that *Thiomargarita* control interstitial P_i enrichment, and are directly involved in apatite formation (Schulz and Schulz 2005).

The finding of $\delta^{18}O_P$ signatures close to or in equilibrium with H_2O perfectly supports this peculiar microbial P_i cycling mechanism. Synthesis and breakdown of intracellular polyphosphates requires activity of PPase, and the high concentrations of equilibrated P_i suggest continuous uptake, temporary storage, and release of P_i by the microorganisms.

III.5 Conclusion

With this comprehensive study, we have extended the oxygen isotope record of dissolved P_i into the pore water of marine sediments. In contrast to open ocean water column samples, where isotope signatures close to a temperature-dependent equilibrium with water prevail, the sediments of the Benguela upwelling system display also significant disequilibrium signatures. They indicate a dominance of P_i regeneration over microbial P_i uptake and turnover. We have found that the combination of concentration profiles and steady state modeling of mineralization and P_i turnover does not suffice to reveal the peculiarities of P_i cycling in these sediments. Using the $\delta^{18}O_P$ isotope data and a differentiated mass balance model, it was possible to distinguish the predominance of P_i regeneration from microbial turnover signatures. The preservation of these signatures

is most likely controlled by microbial P_i uptake strategies that depend on the bioavailability of ambient P_i.

Our calculations revealed that even sites with low P_i concentrations are not necessarily P limited. Furthermore, we found variability in oxygen isotope composition that was not expected from the characterization of the geochemical setting. The investigation of mudbelt sediments unfolded isotope signatures and P_i cycling efficiency that are in line with concepts of the peculiar P_i turnover of large sulfur bacteria, that may contribute to authigenic phosphorite formation.

We conclude that investigations of P_i oxygen isotopes have a great potential to deliver detailed insights into benthic P cycling. For future endeavors, we suggest to improve the parameterization of the isotope mass balance model. It would be beneficial to integrate the molecular characterization of sedimentary P_{org} in monoesters, DNA, and RNA. Seabed temperatures are needed to derive exact equilibrium models, and the quality and isotopic signature of organic bound P_i reaching the sediment surface – likely varying within coastal upwelling ecosystems - must be examined. Finally, the effect of interaction of dissolved and solid-bound P_i in various mineral phases, as well as the contribution of high turnover rates and fluxes in the benthic boundary layer where water column and sediments are coupled has not yet been evaluated *in situ*.

III.6 Acknowledgements

We are indebted to captain, crew and scientific party of RV Meteor for manifold support during expedition M76/1. Silvana Pape and Simone Sauer greatly helped in the laboratory off- and onshore, and Thomas Max provided support with IRMS analyses. Torsten Vennemann provided silver phosphates TU1 and TU2 for external calibration. This study was funded by German Research Foundation (DFG) through MARUM Center for Marine Environmental Sciences, Project B2.

III.7 References

Anderson LA, Sarmiento JL (1994) Redfield ratios of remineralization determined by nutrient data analysis. Global Biogeochemical Cycles 8:65-80

Anderson LD, Delaney ML, Faul KL (2001) Carbon to phosphorus ratios in sediments: Implications for nutrient cycling. Global Biogeochemical Cycles 15:65-79

Baturin GN, Bezrukov PL (1979) Phosphorites on the sea floor and their origin. Mar Geol 31:317-332

Benitez-Nelson CR (2000) The biogeochemical cycling of phosphorus in marine systems. Earth-Science Reviews 51:109-135

Berg P, Risgaard-Petersen N, Rysgaard S (1998) Interpretation of measured concentration profiles in sediment pore water. Limnology and Oceanography 43:1500-1510

Berner RA (1990) Diagenesis of phosphorus in sediments from non-upwelling areas. Phosphate Deposits of the World 3:27-33

Blackwelder E (1916) The geologic role of phosphorus. PNAS 2:190-495

Blake RE, Alt JC, Martini AM (2001) Oxygen isotope ratios of PO_4: An inorganic indicator of enzymatic activity and P metabolism and a new biomarker in the search for life. PNAS 98:2148-2153

Blake RE, O'Neil JR, Garcia GA (1997) Oxygen isotope systematics of biologically mediated reactions of phosphate: 1. Microbial degradation of organophosphorus compounds. Geochim Cosmochim Ac 61:4411-4422

Blake RE, O'Neil JR, Garcia GA (1998) Effects of microbial activity on the $\delta^{18}O$ of dissolved inorganic phosphate and textural features of synthetic apatites. American Mineralogist 83:1516-1531

Blake RE, O'Neil JR, Surkov AV (2005) Biogeochemical cycling of phosphorus: insights from oxygen isotope effects of phosphoenzymes. American Journal of Science 305:596-620

Borchers S, Schnetger B, Böning P, Brumsack H (2005) Geochemical signatures of the Namibian diatom belt: Perennial upwelling and intermittent anoxia. Geochem Geophys Geosyst 6

Bremner JM (1981) Shelf morphology and surficial sediment off Central and Northern South West Africa (Namibia). Geo-Marine Letters 1:91-96

Bremner JM, Rogers J (1990) Phosphorite deposits on the Namibian continental shelf. Phosphate Deposits of the World 3:143-152

Brüchert V et al. (2006) Biogeochemical and physical control on shelf anoxia and water column hydrogen sulphide in the Benguela coastal upwelling system off Namibia. In: Neretin LN (ed) Past and present water column anoxia. Springer, Dordrecht, The Netherlands, pp 161-193

Brüchert V, Jørgensen B, Neumann K, Riechmann D, Schlösser M, Schulz HN (2003) Regulation of bacterial sulfate reduction and hydrogen sulfide fluxes in the central namibian coastal upwelling zone. Geochim Cosmochim Ac 67:4505-4518

Brüchert V, Perez ME, Lange CB (2000) Coupled primary production, benthic foraminiferal assemblage, and sulfur diagenesis in organic-rich sediments of the Benguela upwelling system. Mar Geol 163:27-40

Carr ME (2002) Estimation of potential productivity in Eastern Boundary Currents using remote sensing. Deep-Sea Res II 49:59-80

Chapman P, Shannon L (1985) The Benguela ecoystem part II. Chemistry and related processes. Oceanography Marine Biology Annual Review 23:183-251

Cline JD (1969) Spectrofluorometric determination of hydrogen sulfide in natural waters. Limnology and Oceanography 14:454-458

Colman AS (2002) The oxygen isotope composition of dissolved inorganic phosphate and the marine phosphorus cycle. PhD Thesis, Department of Geology & Geophysics, Yale University, New Haven

Colman AS, Blake RE, Karl DM, Fogel ML, Turekian KK (2005) Marine phosphate oxygen isotopes and organic matter remineralization in the oceans. PNAS 102:13023-13028

Colman AS, Holland HD, Glenn CR, Prévôt-Lucas L, Lucas J, Dalrymple RW (2000) The global diagenetic flux of phosphorus from marine sediments to the oceans: redox sensitivity and the control of atmospheric oxygen levels. In: Marine authigenesis: from global to microbial. SEPM Special Publication 66

Currie R (1953) Upwelling in the Benguela current. Nature 171:497-500

Dell'anno A, Fabiano M, Duineveld GCA, Kok A, Danovaro R (1998) Nucleic acid (DNA, RNA) quantification and RNA/DNA ratio determination in marine sediments: comparison of spectrophotometric, fluorometric, and high-performance liquid chromatograpyh methods and estimation of detrital DNA. Applied and Environmental Microbiology 64:3238-3245

Dingle RV (1973) The geology of the continental shelf between Luderitz and Cape Town (Southwest Africa), with special reference to Tertiary strata. Journal of the Geological Society 129:337-362

Emeis K et al. (2004) Shallow gas in shelf sediments of the Namibian coastal upwelling ecosystem. Continental Shelf Research 24:627-642

Föllmi KB (1996) The phosphorus cycle, phosphogenesis and marine phosphate-rich deposits. Earth-Science Reviews 40:55-124

Froelich PN, Bender ML, Luedtke NA, Heath GR, DeVries T (1982) The marine phosphorus cycle. American Journal of Science 282:474-511

Goldhammer T, Max T, Einsiedl F, Brunner B, Zabel M (2009) Marine Sediment pore water profiles of phosphate oxygen isotopes using a refined micro extraction technique. Submitted to Limnology and Oceanography: Methods (Chapter II of the dissertation)

Hansen HP, Koroleff F (1999) Determination of nutrients. In: Grasshoff K, Kremling K, Ehrhardt M (eds) Methods of seawater analysis. Wiley, Weinheim New York, pp 159-228

Ingall ED, Schroeder PA, Berner RA (1990) The nature of organic phosphorus in marine sediments: New insights from ^{31}P-NMR. Geochim Cosmochim Ac 54:2617-2620

Inthorn M, Mohrholz V, Zabel M (2006a) Nepheloid layer distribution in the Benguela upwelling area offshore Namibia. Deep Sea Res I 53:1423-1438

Inthorn M, Wagner T, Scheeder G, Zabel M (2006b) Lateral transport controls distribution, quality, and burial of organic matter along continental slopes in high-productivity areas. Geology 34:205

Jansson M (1988) Phosphate uptake and utilization by bacteria and algae. Hydrobiologia 170:177-189

Karl DM, Tien G (1992) MAGIC: A sensitive and precise method for measuring dissolved phosphorus in aquatic environments. Limnology and Oceanography 37:105-116

Kolowith LC, Ingall ED, Benner R (2001) Composition and cycling of marine organic phosphorus. Limnology and Oceanography 46:309-320

Kornberg A (1995) Inorganic polyphosphate: toward making a forgotten polymer unforgettable. Journal of Bacteriology 177:491-496

Kornexl BE, Gehre M, Höfling R, Werner RA (1999) On-line δ^{18}O Measurement of organic and inorganic substances. Rapid Commun. Mass Spectrom. 13:1685-1693

Krom M, Berner RA (1981) The diagenesis of phosphorus in a nearshore marine sediment. Geochim Cosmochim Ac 45:207-216

Laporte D, Holmden C, Patterson W, Prokopiuk T, Eglington B (2009) Oxygen isotope analysis of phosphate: improved precision using TC/EA CF-IRMS. Journal of Mass Spectrometry 44:879-890

Liang Y, Blake R (2009) Compound- and Enzyme-specific Phosphodiester Hydrolysis Mechanisms Revealed by $\delta^{18}O$ of Dissolved Inorganic Phosphate: Implications for marine P cycling. Geochim Cosmochim Ac 73:1-49

Liang Y, Blake RE (2006) Oxygen isotope signature of Pi regeneration from organic compounds by phosphomonoesterases and photooxidation. Geochim Cosmochim Ac 70:3957-3969

Liang Y, Blake RE (2007) Oxygen isotope fractionation between apatite and aqueous-phase phosphate: 20-45°C. Chemical Geology 238:121-133

Longinelli A, Nuti S (1973) Revised phosphate-water isotopic temperature scale. Earth and Planetary Science Letters 19:373-376

McLaughlin K, Chavez F, Pennington JT, Paytan A (2006a) A time series investigation of the oxygen isotopic composition of dissolved inorganic phosphate in Monterey Bay, California. Limnology and Oceanography 51:2370-2379

McLaughlin K, Kendall C, Silva SR, Young M, Paytan A (2006b) Phosphate oxygen isotope ratios as a tracer for sources and cycling of phosphate in North San Francisco Bay, California. Journal of Geophysical Research-Biogeosciences 111

McManus J, Berelson WM, Coale KH, Johnson KS, Kilgore TE (1997) Phosphorus regeneration in continental margin sediments. Geochim Cosmochim Ac 61:2891-2907

Minear RA (1972) Characterization of Naturally Occurring Dissolved Organophosphorus Compounds. In: Environ Sci Technol, vol. 6, pp 431-437

Mohrholz V, Bartholomae C, van der Plas A, Lass H (2008) The seasonal variability of the northern Benguela undercurrent and its relation to the oxygen budget on the shelf. Continental Shelf Research 28:424-441

Murphy J, Riley JP (1962) A modified single solution method for the determination of phosphate in natural waters. Analytica Chimica Acta 27:31-36

Nathan Y, Bremner JM, Loewenthal RE, Monteiro P (1993) Role of bacteria in phosphorite genesis. Geomicrobiology Journal 11:69-76

Nelson G, Hutchings L (1983) The Benguela upwelling area. Progress in Oceanography 12:333-356

Novitsky JA (1986) Degradation of dead microbial biomass in a marine sediment. Applied and Environmental Microbiology 52:504-509

O'Neil JR, Roe LR, Reinhard E, Blake RE (1994) A rapid and precise method for oxygen isotope analysis of biogenic phosphate. Israel Journal of Earth Sciences 43:203-212

Pasek MA (2008) Rethinking early Earth phosphorus geochemistry. PNAS 105:853-858

Paytan A, McLaughlin K (2007) The oceanic phosphorus cycle. Chem Rev 107:563-576

Redfield AC (1958) The biological control of chemical factors in the environment. American Scientist 46:205-221

Sander BC, Kalff J (1993) Factors controlling bacterial production in marine and freshwater sediments. Microbial Ecology 26:79-99

Schink B, Friedrich M (2000) Bacterial metabolism - Phosphite oxidation by sulphate reduction. Nature 406:37-37

Schulz HN (2006) The genus Thiomargarita. Prokaryotes 6:1156-1163

Schulz HN, Schulz HD (2005) Large sulfur bacteria and the formation of phosphorite. Science 307:416-418

Shannon LV, Nelson G (1996) The Benguela: Large scale features and processes and system variability. In: Wefer G, Berger WH, Siedler G, Webb DJ (eds) The South Atlantic: Present and past circulation. Springer, New York, pp 163-210

Takahashi T, Broecker WS, Langer S (1985) Redfield ratio based on chemical data from isopycnal surfaces. Journal of Geophysical Research 90:6907-6924

Tudge AP (1960) A method of analysis of oxygen isotopes in orthophosphate - its use in the measurement of paleotemperatures. Geochim Cosmochim Ac 18:81-93

Van Capellen P, Ingall ED (1996) Redox stabilization of the atmosphere and oceans by phosphorus-limited marine productivity. Science 271:493-496

van der Zee C, Roberts D, Rancourt D, Slomp C (2003) Nanogoethite is the dominant reactive oxyhydroxide phase in lake and marine sediments. Geology 31:993-996

van Veen HW (1997) Phosphate transport in prokaryotes: molecules, mediators and mechanisms. Antonie van Leeuwenhoek 72:299-315

IV

Bacteria disrupt a positive phosphorus feedback loop in the Benguela upwelling system

Tobias Goldhammer[1], Volker Brüchert[2], Timothy G. Ferdelman[1,3], and Matthias Zabel[1]

[1]MARUM Center for Marine Environmental Science, University of Bremen, Bremen, Germany, [2]Department of Geochemistry and Geology, Stockholm University, Stockholm, Sweden, [3]Max Planck Institute for Marine Microbiology, Bremen, Germany

Manuscript submitted to *Nature*, 02.10.2009

Note: To keep the specific structure of the manuscript according to the Nature submission, Chapter IV comprises the main manuscript text (IV.1), the methods section (IV.2), the supplementary discussion (IV.3), and supplementary table and figures (IV.4). References follow each section.

IV.1 Main manuscript

First paragraph

As an essential nutrient, phosphorus (P) is a key player in marine biogeochemical cycling (Berner 1990). Its effective sequestration from the oceanic cycle controls primary productivity and is linked to the regulation of atmospheric oxygen levels over geologic time (Van Capellen and Ingall 1996). The most relevant mechanisms of phosphorus are burial of organic matter and the authigenic precipitation of phosphorite minerals (e.g. apatite) in sediments of upwelling regions of the World's oceans (Föllmi 1996, Froe-

lich 1988), a process which bacteria have long been suspected to mediate (Nathan et al. 1993). Here we present direct evidence of microbial participation in phosphorite formation. In sediment incubation experiments conducted during a recent research cruise to the Benguela upwelling system, we retrieved significant portions of ^{33}P in the authigenic apatite fraction only when living large sulfur bacteria –*Thiomargarita* and *Beggiatoa* - were present. The instantaneous conversion of inorganic phosphate (P_i) to apatite and the magnitude of the transfer rates indicate an effective phosphate removal mechanism. Large sulfur bacteria may thus interrupt a positive feedback loop of enhanced P_i regeneration, ocean productivity, and bottom water anoxia in the Benguela upwelling system.

IV.1.1 Main text

Phosphorus (P) is an essential and often limiting macronutrient for living organisms. Phosphorylated biomolecules provide replication, information, energy transfer and structure of living cells (Pasek 2008) in the terrestrial and marine domain. P source-sink balance in the global ocean controls marine primary productivity on geological timescales (Berner 1990, Froelich et al. 1982), and is closely coupled to the regulation of atmospheric oxygen concentrations (Colman et al. 2000, Van Capellen and Ingall 1996). Burial of P in marine sediments is the ultimate sink in the marine P cycle (Blackwelder 1916, Froelich et al. 1982), and evidence has grown that this sink also regulates present-day P cycling (Benitez-Nelson 2000, Paytan and McLaughlin 2007). Recent formation of phosphate minerals, mostly fine-grained modifications of apatite, has been documented in continental margin sediments under upwelling conditions (Baturin 1988, Föllmi 1996). Yet, the actual removal mechanism remains elusive.

There is a growing consensus that the role of microorganisms is not only limited to diagenetic release of inorganic phosphate (P_i) from organic matter to the sedimentary environment (Baturin and Bezrukov 1979), but also includes an active engagement in P_i concentration and precipitation, e.g., by precipitation of apatite on ubiquitous polyphosphate (poly-P) grains of planktonic origin (Diaz et al. 2008, Nathan et al. 1993, Schulz and Schulz 2005). With this study, we present geochemical and experimental evidence for a direct link between abundant large sulfur bacteria and the authigenic formation of apatite in shelf sediments of the high productivity area off the Namibian coast.

The coastal Benguela upwelling system off Namibia is one of the oceanic regions with modern phosphorite formation (Bremner 1980, Bremner and Rogers 1990). The continental shelf is characterized by a diatomaceous mudbelt with sedimentation rates exceeding 0.5 cm per year (Inthorn et al. 2006). Bottom waters are episodically anoxic

(Copenhagen 1953), and high concentrations of porewater hydrogen sulfide support a large biomass of sulfide-oxidizing bacteria of the genera *Thiomargarita* (Schulz et al. 1999) and *Beggiatoa* (Brüchert et al. 2003), which cover a surface area of more than 30,000 km^2 on the continental shelf (Brüchert et al. 2006). The non-motile large sulfur bacterium *Thiomargarita namibiensis* can store poly-P in its vacuoles, which it takes up during short periods, when bottom waters are oxidized and contain nitrate (Schulz 2006). During anoxic periods, the bacteria may gain energy by hydrolysis of the poly-P molecules which can be used for the uptake and storage of a carbon source such as acetate (Schulz 2006).

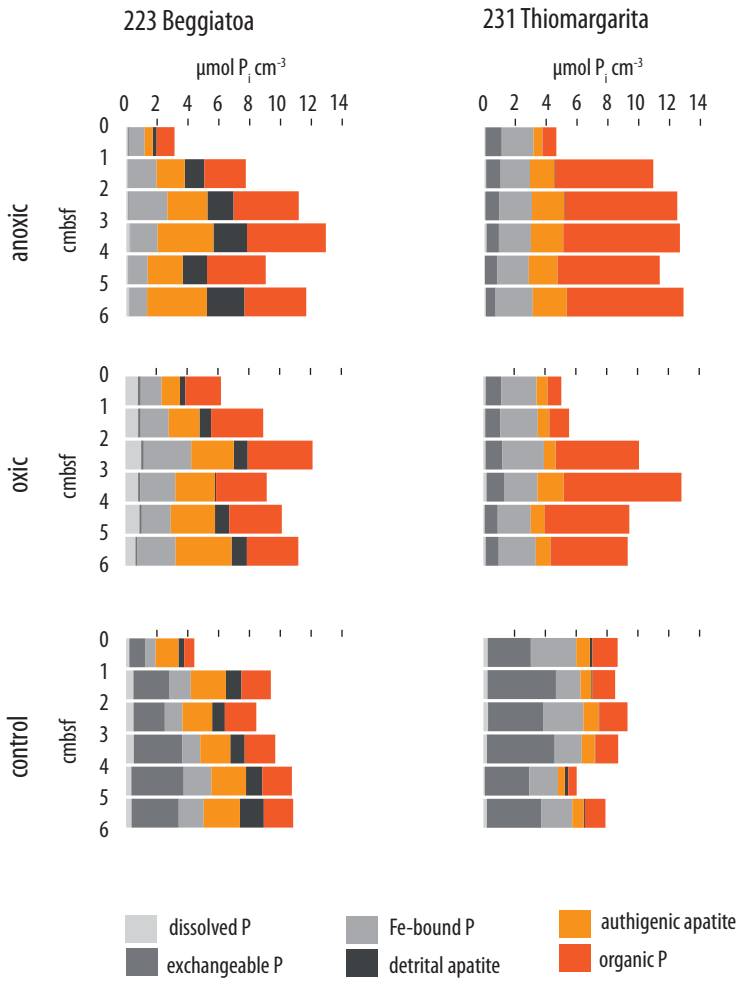

Figure IV.1 Total inventories of P as sequentially extracted from the two 6 cm cores, 223 (left column) and 231 (right column). The panels are from top to bottom: anoxic incubation, oxic incubation and control. The pool size of is given in µmol Pi cm-3 wet sediment. The fractions are displayed in stacked bars for each cm depth slice: dissolved, iron-bound, exchangeable phosphorus, detrital apatite (greyscales), authigenic apatite (orange) and organic/cell internal P (red)

The peculiarity of this P_i cycling has generated the hypothesis that *Thiomargarita* may be directly involved in porewater supersaturation with respect to apatite (Schulz and Schulz 2005). The wider spread phylogenetically related genus *Beggiatoa* also carries the ecophysiological prerequisites for this P metabolism (Mußmann et al. 2007).

On cruise M76-2 of R/V Meteor to the Namibian shelf, we conducted short-term ^{33}P and ^{35}S incubations, P speciation analysis, and microscopic bacterial counting with sediment from the upper 6 cm at two sites in the diatom mud belt (see Methods section). Core top samples contained significant numbers of *Beggiatoa* (site 223) or *Thiomargarita* (site 231, Supplementary Figure IV.S1). The ^{33}P incubation permitted us to track pathways and partitioning of P_i in two living assays under anoxic and oxic treatment, and a killed control (see Methods section). The sequential P extraction protocol was modified to enable quantification of individual ^{33}P-labeled phosphate ($^{33}P_i$) pools and revealed slight differences between the two sites: higher mean contents of authigenic apatite and minor amounts of detrital apatite at site 223, and higher exchangeable/Fe-bound P_i at site 231 (Figure IV.1).

The operational fractions of the extraction protocol distinguish between "abiogenic" components (generally bioavailable inorganic pools such as dissolved, exchangeable, and Fe-bound P_i) plus detrital apatite, and "biogenic" components as products of biological P cycling (authigenic apatite and organic bound P_i). Significant portions of the latter were characteristic in the sediment. At the end of the experiments, P_i speciation of controls and living assays revealed a reallocation of P from the abiogenic to the biogenic pool. For authigenic apatite this change was very pronounced at site 231. We also found remarkable increases in organic-bound P_i during incubation at both sites (Figure IV.1). However, the formation of authigenic apatite and organic-bound phosphorus alone does not proof microbial activity and could, for instance, simply be attributed to abiogenic diagenetic processes, captured by random sampling.

Direct evidence for active microbial P_i cycling comes from the distribution of the radiolabel among the P fractions (Figure IV.2). All living assays showed significant incorporation of ^{33}P into authigenic apatite and organic-bound P. Authigenic apatite contained 11 ± 5 % of spike ^{33}P in the anoxic, 5.1 ± 1.4 % in the oxic incubation at site 223, and 1.6 ± 0.9 % and 0.7 ± 0.2 % in the anoxic and oxic incubation at site 231, respectively. Organic P accounted for 2.9 ± 1.4 % of spike ^{33}P in anoxic, 4.8 ± 1.4 % in oxic incubations at site 223, and 0.4 ± 0.3 % in anoxic and 0.6 ± 0.1 % in oxic incubations at site 231 (Figure IV.2). In contrast, the majority of the ^{33}P phosphate recovered from the killed

control experiments was distributed exclusively between the abiogenic pools. No significant amount of ^{33}P was found in authigenic apatite and organically bound fractions in killed controls from either site (< 0.1 % of the spike, Figure IV.2).

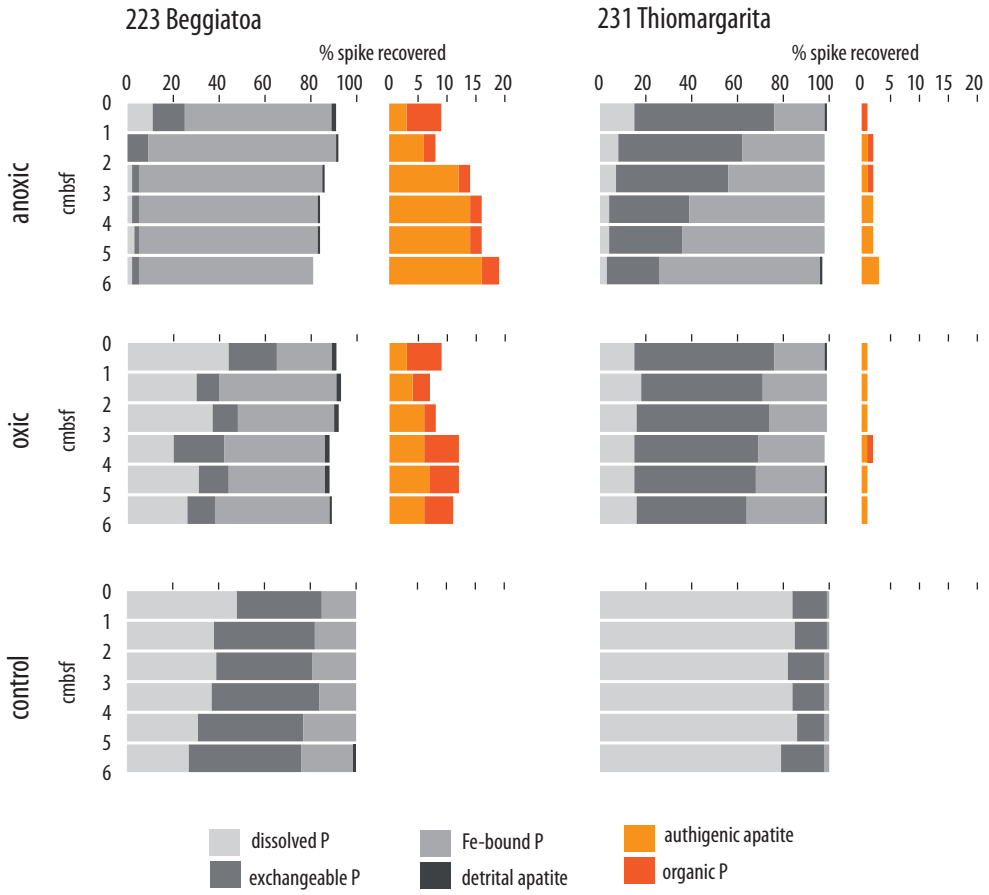

Figure IV.2 Distribution of the recovered ^{33}P spike after incubation between sedimentary P pools from the two 6 cm cores, 223 (left column) and 231 (right column). The panels are from top to bottom: anoxic incubation, oxic incubation and control. Note that the stacked bars for abiotic and biotic pools are plotted on split axes for better perceptibility: on the left x-axis (0-100 %), dissolved, iron-bound, exchangeable phosphorus and detrital apatite (greyscales), on the right x-axis (0-20 %) authigenic apatite (orange) and organic/cell internal P (red). Combined, each bar sums up to 100 %

To evaluate the response of *Thiomargarita*-specific P_i turnover to experimental treatment, we produced digital autoradiographs (beta-images) of handpicked chains and single cells of *Thiomargarita namibiensis* from incubated samples of site 231 (see Methods section). Chains and cells of *Thiomargarita* from oxic incubations incorporated significantly more radiolabel compared to the anoxic incubations, whereas killed controls showed no incorporation above background (Figure IV.3).

In the experiment, on average 80 and 16 pmol P_i $cell^{-1}$ d^{-1} were taken up under oxic and anoxic conditions. The depth-integrated bacterial P_i uptake rates were 25 and

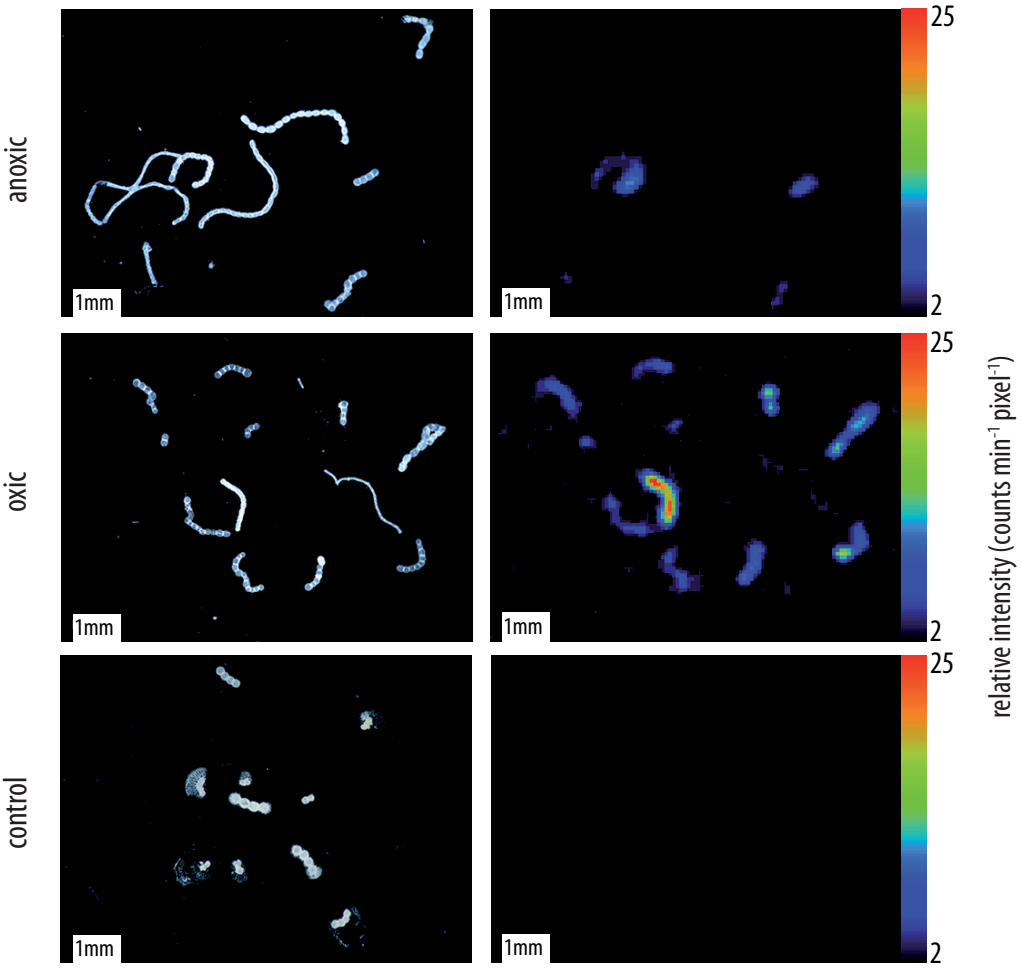

Figure IV.3 Microscopic images (left) and digital autoradiographs (right) of living cells of Thiomargarita namibiensis after incubation: anoxic (top), oxic (middle), and control (bottom). Photographs and radiographs are from the same object slide, scale is identical (scale bar 1 mm). Color range of the radiographs is 2 - 25 counts per minute and pixel. Background noise was < 2 cpm pi^{-1} and subtracted from the radiographs

120 nmol cm^{-2} d^{-1} for the anoxic and oxic treatment, respectively. Note that although these experiments were conducted at room temperature in the laboratory and not at in situ conditions, these rates compare well with the calculated apatite sequestration rates and are at least in the same order of magnitude (see below), which lends support to the important role of these bacteria in the proposed phosphate sequestration mechanism.

Hydroxyapatite (HAp, $Ca_5(PO_4)_3OH$) is a common constituent of phosphorites in Namibian shelf sediments (Schulz and Schulz 2005). Geochemical modelling using PHREEQC indicated that the pore waters at sites 223 and 231 were oversaturated with respect to HAp (see Supplementary Discussion and Figure IV.S5). It is noteworthy that despite oversaturation, neither HAp nor any other authigenic phosphate precipitated in the killed controls as indicated by zero recovery of ^{33}P from the biogenic P extract. The combination of our ^{33}P-labeled P_i speciation analysis results and the digital autoradiographs of *Thiomargarita* chains strongly suggest that incorporation of $^{33}P_i$ into authigenic apatite requires the presence of living bacteria.

The process involved uptake of $^{33}P_i$ into the organic-bound and cell-internal P_i fraction, both at *Beggiatoa* and *Thiomargarita* sites. This pattern was most pronounced at site 223. Although site 231 seemed less active due to lower biomass of sulfur bacteria, our data support a model of phosphorus uptake under oxic conditions by *Beggiatoa* and *Thiomargarita* and polymerization of P_i to poly-P. This scenario is reflected by the enhanced recovery of ^{33}P from the organic and cell-internal fraction under oxic conditions (Figure IV.2). Under anoxic conditions, poly-P can be hydrolyzed, and P_i is released from the cell via inorganic phosphate transfer to the surrounding medium (Gächter and Meyer 1993). There, the concentration is raised until apatite can precipitate and incorporate $^{33}P_i$. In light of this concept, it may seem surprising that $^{33}P_i$ was found in authigenic apatite of the oxic assays. We assume that anoxic fractions have persisted in the aerated sediments, so that both uptake and release of P_i have occurred in the same sample.

Rates for P_i sequestration into the authigenic apatite fraction (see Method section) showed that at both stations less apatite was produced under oxic than under anoxic conditions (Table IV.3). The corresponding rate profiles were parallel for anoxic and oxic treatments (Supplementary Figure IV.S3). Integrated over 6 cm sediment thickness, $^{33}P_i$ sequestration rates into apatite were 78 nmol cm^{-2} d^{-1} at site 223 under anoxic and 35 nmol cm^{-2} d^{-1} under oxic conditions, and 69 and 21 nmol cm^{-2} d^{-1} under anoxic and oxic conditions at site 231 (Table IV.1). These experimental gross rates exceed the steady state net P_i production modelled from pore water P_i concentrations (9 and

12 nmol cm^{-2} d^{-1} for sites 223 and 231, Table IV.1). They also exceed potential P_i release (20 and 36 nmol cm^{-2} d^{-1} at sites 223 and 231, Table IV.1), calculated from bacterial sulfate reduction rates (SRR) and a production C:P ratio of 77 (see Methods Section and Supplementary Discussion).

Table IV.1 Comparison of depth integrated P_i release and sequestration. Depth integration for 0 – 11 cm (*), 0 – 6 cm (**) sediment depth

site	integrated P_i release*		integrated P_i sequestration**	
	estimate from	nmol cm^{-2} d^{-1}	assay	nmol cm^{-2} d^{-1}
223	P_i profile	9	anoxic	78
$C_{DIC}:P_{Pi} = 77$	BSR	20	oxic	35
231	P_i profile	12	anoxic	69
$C_{DIC}:P_{Pi} = 77$	BSR	36	oxic	21

The calculated apatite formation rates are therefore larger than the diffusive loss of phosphate to the overlying water and indicate the sequestration of a significant fraction of mineralized P_i in the sediments. The disagreement between the rates of P_i mineralization and the rates of apatite formation under anoxic conditions indicates significant non-stationary behaviour of dissolved P_i in these porewaters alternating between periods of active P_i uptake by bacteria and release. Apatite formation thus becomes an important P sink in the Namibian mudbelt under anoxic conditions.

Earlier research on redox dependent P cycling has led to the acknowledged paradigm that benthic regeneration and reflux of P_i to the water column is enhanced under conditions of suboxic to anoxic bottom waters (Föllmi 1996, Ingall and Jahnke 1994, Van Capellen and Ingall 1994), due to synergistic effects of bacterial P_i release and reductive dissolution of iron oxides coated with adsorbed P_i (Slomp et al. 1996). Consequently, a positive feedback mechanism of anoxic bottom waters, high P_i return flux, stimulated productivity and thus intensified anoxia has been postulated (Benitez-Nelson 2000, Ingall and Jahnke 1994). These studies are from regions where sedimentary iron cycling plays a major role in mineralization (McManus et al. 1997). In this respect, they differ

from the Benguela upwelling system where iron cycling is minor, and if so, it may be that uptake by large sulfur bacteria keeps P_i away from that particular iron trap.

We did not finally resolve the exact mechanism that allows large sulfur bacteria to overcome the kinetic barrier preventing HAp from abiotic precipitation. Most probably, the unique physiology of large sulfur bacteria combines intense P_i concentration in the pore water with synthesis of poly-P nodules, readily providing crystallization templates (Diaz et al. 2008).

The different scales of P sequestration under the short experimental treatments point to the fact that microbial formation of apatite is not only relevant on integrated, geologic timescales, but also susceptible to short-term changes in redox conditions. Our experiments reveal apatite sequestration rates of a previously unknown magnitude that exceed those of P_i regeneration from organic matter, indicating that the intermediate poly-P stored in large sulfur bacteria creates sediment phosphate fluxes that are strongly out of steady state with respect to organic matter mineralization. We suggest that this observation also holds true for other highly productive upwelling regions. Under such circumstances, an escape from the positive feedback loop of enhanced P_i regeneration, primary productivity, and bottom water anoxia, is possible.

IV.1.2 Methods summary

Surficial sediment was sampled during a research cruise with German RV Meteor with a multi-core sampler. Sediment slurries were prepared from 1 cm slices of the 6 cm core tops, cut with bottom water, spiked with carrier-free $^{33}P_i$ and incubated under anoxic and oxic conditions for 48 h at 4°C, together with killed controls. After incubation, samples were fixed with zinc chloride, immediately frozen and transported to Bremen for sequential extraction of sedimentary P_i pools. For each of the sequential fractions, we recorded P_i concentrations by photometry and inductively coupled plasma optic emission spectrometry and calculated the size of individual P pools.

The redistribution of $^{33}P_i$ radiolabel among the different P fractions was quantified by liquid scintillation counting of the extractant solutions, and recalculation of the initial activity assuming exponential decay. We calculated phosphate sequestration rates in the authigenic apatite fraction, using a method similar to the calculation of ^{35}S sulfate reduction rates, taking into account specific activities of dissolved and apatite pools and incubation time. These rates were compared to potential P_i release derived from integrated turnover on the basis of P_i profiles and ^{35}S sulfate reduction rates.

Single cells and strings of Thiomargarita namibiensis were picked from incubated sediments of site 231, washed repeatedly to remove external $^{33}P_i$ and placed on object slides. A microscopic photograph was taken and the distribution of beta radiation captured and quantified with a digital autoradiograph, and cell-specific P_i uptake rates were calculated.

IV.1.3 Acknowledgements

We thank Kay-Christian Emeis for cruise coordination, Verena Salman and Heide Schulz-Vogt for providing additional samples and microscope imaging, and Heinz Filthuth for support and advice in using the digital autoradiograph.

IV.1.4 References

Baturin GN (1988) Disseminated phosphorus in oceanic sediments - a review. Mar Geol 84:95-104

Baturin GN, Bezrukov PL (1979) Phosphorites on the sea floor and their origin. Mar Geol 31:317-332

Benitez-Nelson CR (2000) The biogeochemical cycling of phosphorus in marine systems. Earth-Science Reviews 51:109-135

Berner RA (1990) Diagenesis of phosphorus in sediments from non-upwelling areas. Phosphate Deposits of the World 3:27-33

Blackwelder E (1916) The geologic role of phosphorus. PNAS 2:190-495

Bremner JM (1980) Concretionary phosphorite from SW Africa. Journal of the Geological Society 137:773-786

Bremner JM, Rogers J (1990) Phosphorite deposits on the Namibian continental shelf. Phosphate Deposits of the World 3:143-152

Brüchert V et al. (2006) Biogeochemical and physical control on shelf anoxia and water column hydrogen sulphide in the Benguela coastal upwelling system off Namibia. In: Neretin LN (ed) Past and present water column anoxia. Springer, Dordrecht, The Netherlands, pp 161-193

Brüchert V, Jørgensen B, Neumann K, Riechmann D, Schlösser M, Schulz HN (2003) Regulation of bacterial sulfate reduction and hydrogen sulfide fluxes in the central namibian coastal upwelling zone. Geochim Cosmochim Ac 67:4505-4518

Colman AS, Holland HD, Glenn CR, Prévôt-Lucas L, Lucas J, Dalrymple RW (2000) The global diagenetic flux of phosphorus from marine sediments to the oceans: redox sensitivity and the control of atmospheric oxygen levels. In: Marine authigenesis: from global to microbial, vol 66

Copenhagen WJ (1953) The periodic mortality of fish in the Walvis region. Division of Fisheries, Investigational Report 14, Pretoria

Diaz J et al. (2008) Marine polyphosphate: A key player in geologic phosphorus sequestration. Science 320:652-655

Föllmi KB (1996) The phosphorus cycle, phosphogenesis and marine phosphate-rich deposits. Earth-Science Reviews 40:55-124

Froelich PN (1988) Kinetic Control of Dissolved Phosphate in Natural Rivers and Estuaries - a Primer on the Phosphate Buffer Mechanism. Limnology and Oceanography 33:649-668

Froelich PN, Bender ML, Luedtke NA, Heath GR, DeVries T (1982) The marine phosphorus cycle. American Journal of Science 282:474-511

Gächter R, Meyer JS (1993) The role of microorganisms in mobilization and fixation of phosphorus in sediments. Hydrobiologia 253:103-121

Ingall ED, Jahnke R (1994) Evidence for enhanced phosphorus regeneration from marine sediments overlain by oxygen depleted waters. Geochim Cosmochim Ac 58:2571-2575

Inthorn M, Wagner T, Scheeder G, Zabel M (2006) Lateral transport controls distribution, quality, and burial of organic matter along continental slopes in high-productivity areas. Geology 34:205

McManus J, Berelson WM, Coale KH, Johnson KS, Kilgore TE (1997) Phosphorus regeneration in continental margin sediments. Geochim Cosmochim Ac 61:2891-2907

Mußmann M et al. (2007) Insights into the Genome of Large Sulfur Bacteria Revealed by Analysis of Single Filaments. PloS Biology 5:e230

Nathan Y, Bremner JM, Loewenthal RE, Monteiro P (1993) Role of bacteria in phosphorite genesis. Geomicrobiology Journal 11:69-76

Pasek MA (2008) Rethinking early Earth phosphorus geochemistry. PNAS 105:853-858

Paytan A, McLaughlin K (2007) The oceanic phosphorus cycle. Chem Rev 107:563-576

Schulz HN (2006) The genus Thiomargarita. Prokaryotes 6:1156-1163

Schulz HN, Brinkhoff T, Ferdelman TG, Hernández Mariné M, Teske A, Jørgensen B (1999) Dense populations of a giant sulfur bacterium in Namibian shelf sediments. Science 284:493-495

Schulz HN, Schulz HD (2005) Large sulfur bacteria and the formation of phosphorite. Science 307:416-418

Slomp CP, Epping EHG, Helder W, Van Raaphorst W (1996) A key role for iron-bound phosphorus in authigenic apatite formation in North Atlantic continental platform sediments. . Journal of Marine Research 54:1179-1205

Van Capellen P, Ingall ED (1994) Benthic phosphorus regeneration, net primary production, and ocean anoxia: A model of the coupled marine biogeochemical cycles of carbon and phosphorus. Palaeoceanography 9:677-692

Van Capellen P, Ingall ED (1996) Redox stabilization of the atmosphere and oceans by phosphorus-limited marine productivity. Science 271:493-496

IV.2 Methods section

IV.2.1 Onboard incubation experiments

Two sediment core tops of 6 cm were recovered from multicorer deployments at sites 223 and 231 (19°1.01'S 12°13.75'E, 119 m water depth, and 21°0.47'S 13°15.20'E, 123 m water depth) during cruise M76-2 of German R/V Meteor in May 2008. From one cm layers, slurries were prepared blending sediment with bottom water. We spiked the samples with 50 kBq (site 223) and 100 kBq (site 231) of a carrier-free ^{33}P-phosphate radiolabel solution prepared from $H_3{}^{33}PO_4$ (Hartmann Analytic) and bottom water, and incubated the slurries for 48h in 20 mL Zinsser vials. Sediment poisoned with a 4 % formaldehyde solution served as an abiotic control and was treated similar to the assays. After incubation, 2 mL of slurry was transferred to glass Exetainer vials, fixed with 2 mL of 20 % zinc chloride solution, immediately frozen and stored at -20 °C until further analysis in Bremen.

IV.2.2 Sequential extraction of phosphate fractions

The frozen sediment samples were thawed, transferred to 30 mL centrifuge tubes and centrifuged to separate solid phase from interstitial water. The residual sediment pellet

was subject to a sequential extraction following a modified SEDEX protocol (Ruttenberg 1992, Supplementary Figure IV.S2). Phosphate (P_i) concentrations of supernatant solutions were obtained either by a modified phosphomolybdenum blue spectral photometric method (Murphy and Riley 1962, Hansen and Koroleff 1999), or by elemental analysis as phosphorus with inductively coupled plasma optical emission spectrometry (ICP-OES, Perkin Elmer Optima 3300R, cross-flow nebulizer). The total size of phosphate fractions was calculated from concentrations of subfractions for each extraction step, and referenced to the initial volume of wet sediment utilized.

IV.2.3 Determination of ^{33}P radiolabel activity in SEDEX fractions

The decanted supernatant solutions were again centrifuged to settle potentially remaining radioactive particles. Seven mL of SEDEX solution were pipetted, mixed with 14 mL of a liquid scintillation cocktail (Perkin Elmer Lumasafe Plus) and counted in a liquid scintillation counter (Packard Tri-Carb 2900TR). Counting time was < 10 min. Backgrounds were determined from blank extraction solutions, and quench correction was neglected. Analytical error of scintillation counting was < 2 % on a 2 σ level. To evaluate radiolabel partitioning during incubation, the hypothetical activity for t = 0 (*i.e.*, start of incubation) A_0 was calculated from measured activity A_t at time t and half-life $t_{1/2}$ assuming exponential decay (Equation IV.M1)

$$A_0 = A_t \times 2^{\frac{t}{t_{1/2}}} \qquad \text{Equation IV.M1}$$

The calculated activities for extraction and rinse steps of each fraction were summed and finally normalized to the percentage of the total amount of radiolabel recovered from the extractions.

IV.2.4 Digital autoradiographing of *Thiomargarita* cells

Several chains of multiple cells were picked from incubated sediment samples using an microliter pipette (Thermo Finnigan) and subsequently rinsed in six steps in plastic Petri dishes: triple in artificial seawater (Kester et al. 1967) to remove sediment and particles sticking to the mucus, twice in a 0.35 mol L^{-1} $MgCl_2$ solution to dissolve potentially adsorbed ^{33}P-labeled P_i (Ruttenberg 1992), and finally once in deionised water for facile transfer onto microscope glass slides. The cells were slightly dried at room temperature to fix them onto the slides, and were photographed through a binocular microscope (Zeiss Stemi 2000 / Canon Powershot A640). The two-dimensional distri-

bution of beta-radiation on the glass slides was captured with a real-time radio-imaging system (BioSpace Mesures Micro Imager). Counting time was 6 h, background noise on a 2 cpm level was subtracted. The specific activity of single *Thiomargarita* chains, identified by comparison of microscope image and autoradiograph, was integrated by the instrument software (BetaVision) after manually specifying the corresponding region of interest (Supplementary Figure IV.S7, and Supplementary Table IV.S1). Cell specific uptake *R* was calculated to Equation IV.M2

$$R = \frac{a_c}{c} \times \frac{1}{A_0} \times 2^{\frac{t_i}{t_{1/2}}} \qquad \text{Equation IV.M2}$$

with a_c the sum of counts (Bq) and c the number of cells on the slide, A_0 the concentration specific activity of dissolved $^{33}P_i$ before incubation (Bq nmol^{-1}), t_i the incubation time and $t_{1/2}$ the half-life of ^{33}P (25.4 d). The integrated uptake rate was inferred from cell specific rates and an approximate *Thiomargarita* abundance of 1500 cells cm^{-2} at station 231.

IV.2.5 Calculation of saturation state of hydroxyapatite

We employed the geochemical computing package PHREEQC (Parkhurst and Appelo 1999, Version 2.15) to calculate hypothetical saturation indices for HAp for our measured P_i data in a pore water surrogate. For a minimum-maximum estimate, we assumed a range of pH (6.5 to 8.5) and calcium concentrations (5000 to 11000 µmol L^{-1}) plausible for a marine environment, and introduced seawater ionic strength by means of a 0.675 mol L^{-1} NaCl solution. PHREEQC calculations were performed for P_i concentrations of 60, 100, 210 and 540 µmol L^{-1}, representing the range encountered in our sample profiles. The PHREEQC input file is given in Supplementary Figure IV.S4.

IV.2.6 Estimation of P_i transfer rates to authigenic apatite

Similar to the calculation of gross sulfate reduction rates derived from ^{35}S incubation experiments (Fossing and Jørgensen 1989), we calculated sequestration rates (ASR) for the transfer of P_i to the authigenic apatite fraction on the basis of P_i equivalents:

$$ASR = \frac{c(P_i) \times a \times 24}{(A + a) \times t} \qquad \text{Equation IV.M3}$$

Since there is no previously documented data on ^{33}P isotopic fractionation during apatite precipitation, we did not introduce a correction factor (*e.g.* as for ^{35}S in the original Fossing equation). With the pore water phosphate concentration $c(P_i)$ in µmol L^{-1}, the activity of the authigenic apatite pool a in Bq, the activity of the remaining dissolved phosphate A, and the incubation time t in h we obtained gross rates of P_i transferred to the apatite pool in nmol P_i cm^{-3} d^{-1}. Since a significant portion of dissolved P_i was precipitated in the experiment by adding $ZnCl_2$ to stop incubation, we hypothesized that the missing portion of $^{33}P_i$ spike (100% minus recovery) corresponded to the Zn-bound fraction which was not affected by the SEDEX protocol (see Supplementary Discussion), and included it in the remainder activity A.

IV.2.7 Estimation of P_i release rates from organic matter remineralization

We calculated potential P_i release from mineralization in two manners. First, we calculated depth integrated, steady state P_i production by fitting a turnover box model to the pore water P_i profiles with the PROFILE numerical solution (Berg et al. 1998). This two-step procedure iteratively adjusts a number of reactive zones (production or consumption) to the calculation domain and minimizes it by merging adjacent zones without losing statistical significance (Berg et al. 1998), and calculates depth integrated turnover for the zones. Second, we estimated P_i release rates from gross bacterial sulfate reduction rates (SRR) determined with the ^{35}S method (Fossing and Jørgensen 1989). Based on a N:P ratio of 11 found in the Benguela upwelled waters (Chapman and Shannon 1985), and a C:N of 6.6 (Redfield 1958), we inferred a C:P ratio for mineralization products of 77. Phosphate production R_{Pi} was calculated from SRR (Equation IV.M4):

$$R_{Pi} = SRR \times \frac{2}{C:P} \qquad \text{Equation IV.M4}$$

P_i release was integrated over depth for the upper 6 cm of the profile.

IV.2.8 References

Berg P, Risgaard-Petersen N, Rysgaard S (1998) Interpretation of measured concentration profiles in sediment pore water. Limnology and Oceanography 43:1500-1510

Chapman P, Shannon L (1985) The Benguela ecoystem part II. Chemistry and related processes. Oceanography Marine Biology Annual Review 23:183-251

Fossing H, Jørgensen B (1989) Measurement of bacterial sulfate reduction in sediments: Evaluation of a single-step chromium reduction method. Biogeochemistry 8:205-222

Hansen HP, Koroleff F (1999) Determination of nutrients. In: Grasshoff K, Kremling K, Ehrhardt M (eds) Methods of seawater analysis, 3rd edn. Wiley-VCH, Weinheim, pp 159-228

Kester DR, Duedall IW, Connors DN, Pytkowic RM (1967) Preparation of Artificial Seawater. Limnology and Oceanography 12:176-&

Murphy J, Riley JP (1962) A modified single solution method for the determination of phosphate in natural waters. Analytica Chimica Acta 27:31-36

Parkhurst DL, Appelo CAJ (1999) User's guide to PHREEQC (Version 2) - a computer program for speciation, batch-reaction, one-dimensional transport, and inverse geochemical calculations. USGS Water-Resources Investigations Report 99-4259:1-326

Redfield AC (1958) The biological control of chemical factors in the environment. American Scientist 46:205-221

Ruttenberg KC (1992) Development of a sequential extraction method for different forms of phosphorus in marine sediments. Limnology and Oceanography 37:1460-1482

IV.3 Supplementary Discussion

IV.3.1 Bacterial biomass and distribution of large sulfur bacteria

We encountered significant cell numbers of large sulfur bacteria in the 6 cm core tops. At site 223 we exclusively found examples of the filamentous genus *Beggiatoa*, and at site 231 of the spherical species *Thiomargarita namibiensis*. Quantification of bacterial biomass suggested that *Beggiatoa* and *Thiomargarita* did not coexist, but rather excluded each other in our samples (Supplementary Figure IV.S1). Depth integrated bacterial biomasses ranged from around 10 to around 60 mg m^{-2}, and were thus two to three orders of magnitude smaller than encountered on earlier cruises to the Benguela upwelling system (Brüchert et al. 2003, Schulz et al. 1999). At station 231, *Thiomargarita* abundance integrated over the top 6 cm of the sediment was 1535 and 1638 cells cm^{-2} in the oxic and anoxic incubation.

IV.3.2 Incomplete recovery of ^{33}P radiolabel

Total recovery of the radiolabel was high in killed controls (92 ± 7 % at 223 and 82 ± 7 % at 231) and much lower in living assays (39 ± 15 % in 223 anoxic, 31 ± 6 % in 223 oxic, 62 ± 4 % in 231 anoxic and 59 ± 5 % in 231 oxic). We attribute this to the zinc chloride preservative addition to the living assays at the end of the incubation. A significant amount of dissolved P_i may have precipitated as zinc phosphate ($Zn_3(PO_4)_2$), which is insoluble under the conditions of the sequential extraction, and hence not considered in subsequent calculations. In light of the substantial recoveries in the control samples, we infer that our method collected all important P fractions. Apart from formation of $Zn_3(PO_4)_2$, only underestimation of authigenic apatite and organically bound P could explain the lowered ^{33}P recovery rates. However, an incomplete recovery of ^{33}P from the dissolved pool does not compromise the finding of ^{33}P in authigenic apatite and organic bound P phases, and we thus conclude that this does not conflict with our interpretation.

IV.3.3 Recovery of ^{33}P from exchangeable and Fe-bound P_i in living assays

The relative distribution of ^{33}P among exchangeable and Fe-bound phases appears to be elevated in living assays compared to controls (Figure IV.2). Due to the incomplete recovery of ^{33}P from the dissolved pool that was caused by the zinc phosphate precipitation discussed above, the solid phase components are comparatively overestimated in the graphic display. We hence consider this a phenomenon from calculation, and not representing processes characteristic of the sediment dynamics.

IV.3.4 Oversaturation of pore waters with respect to hydroxyapatite

Hydroxyapatite (HAp, $Ca_5(PO_4)_3OH$) is prevalent in Namibian shelf sediments, formed during phosphorite authigenesis (Schulz and Schulz 2005), and extracted with the authigenic apatite fraction in the SEDEX protocol (Supplementary Figure IV.S2). From a calculation of hypothetical saturation indices for HAp with PHREEQC (Parkhurst and Appelo 1999) in a range of pH, calcium (Ca^{2+}) concentrations and measured pore water P_i data (Supplementary Fig. IV.S5), we infer that all measured P_i concentrations indicate HAp oversaturation under plausible field conditions (pH above 7, Ca^{2+} around 11000 μmol L^{-1}).

IV.3.5 Potential P_i release during OM remineralization

Interpretation of the ^{33}P gross rates of P_i sequestration in the authigenic apatite fraction and the relevance of apatite formation as a benthic P sink required a minimum of information on the magnitude of potential P_i supply to the sediment pore water. We calculated depth integrated P_i turnover rates from pore water P_i concentrations using the PROFILE numerical solution (Supplementary Figure IV.S6 and Methods section). We compared these rates to potential P_i release from bulk remineralization of organic matter (OM), simplifying that all interstitial P_i is liberated during the early diagenetic degradation of OM in a given stoichiometry of C and P. Since bacterial sulfate reduction account for as much as 90 % of total mineralization of organic matter in the Namibian shelf sediments (Brüchert et al. 2003), we based our calculation on sulfate reduction rates (SRR) determined from ^{35}S incubations (Supplementary Figure IV.S6 and Methods section). The underlying C:P ratio of the mineralization products (HCO_3^- and P_i) in near-surface sediment layers should be orders of magnitude smaller than that of the deposited OM (e.g. around Redfield's 106 (Redfield 1958)), since P-rich compounds such as proteins and nucleic acids are preferentially decomposed (Algeo and Ingall 2007). We estimated a C:P ratio of 77 from a C:N ratio of 6.6 (Redfield 1958) and a N:P ratio of 11 for Benguela current upwelled waters (Chapman and Shannon 1985), and considered it representative for new mineralization in our calculations.

The corresponding potential P_i release rates to the pore water amounted thus to 9 and 20 nmol cm^{-2} d^{-1} (PROFILE resp. SRR based) at site 223, and 12 and 36 nmol cm^{-2} d^{-1} at site 231 (Table IV.1). These data may represent a lower and upper end of potential P_i release. The PROFILE solution delivers a steady-state, net production rate derived from the profile and thus also includes sedimentary P_i sink processes, whereas bacterial SRR were determined as gross rates in short-term radiotracer incubation experiments (Fossing and Jørgensen 1989) and are likely more representative of P_i release from mineralization.

IV.3.6 References

Algeo TJ, Ingall ED (2007) Sedimentary C_{org}:P ratios, paleocean ventilation, and Phanerozoic atmospheric pO_2. Palaeogeography, Palaeoclimatology, Palaeoecology 256:130-155

Brüchert V, Jørgensen B, Neumann K, Riechmann D, Schlösser M, Schulz HN (2003) Regulation of bacterial sulfate reduction and hydrogen sulfide fluxes in the central namibian coastal upwelling zone. Geochim Cosmochim Ac 67:4505-4518

Chapman P, Shannon L (1985) The Benguela ecoystem part II. Chemistry and related processes. Oceanography Marine Biology Annual Review 23:183-251

Fossing H, Jørgensen B (1989) Measurement of bacterial sulfate reduction in sediments: Evaluation of a single-step chromium reduction method. Biogeochemistry 8:205-222

Grasshoff K, Kremling K, Ehrhardt M (1999) Methods of seawater analysis. Wiley, Weinheim New York

Miller TE (1969) Killing and lysis of gram-negative bacteria through the synergistic effect of hydrogen peroxide, ascorbic acid, and lysozyme. Journal of Bacteriology 98:949-955

Murphy J, Riley JP (1962) A modified single solution method for the determination of phosphate in natural waters. Analytica Chimica Acta 27:31-36

Parkhurst DL, Appelo CAJ (1999) User's guide to PHREEQC (Version 2) - a computer program for speciation, batch-reaction, one-dimensional transport, and inverse geochemical calculations. USGS Water-Resources Investigations Report 99-4259:1-326

Redfield AC (1958) The biological control of chemical factors in the environment. American Scientist 46:205-221

Ruttenberg KC (1992) Development of a sequential extraction method for different forms of phosphorus in marine sediments. Limnology and Oceanography 37:1460-1482

Schulz HN, Brinkhoff T, Ferdelman TG, Hernández Mariné M, Teske A, Jørgensen B (1999) Dense populations of a giant sulfur bacterium in Namibian shelf sediments. Science 284:493-495

Schulz HN, Schulz HD (2005) Large sulfur bacteria and the formation of phosphorite. Science 307:416-418

IV.4 Supplementary Table and Figures

Supplementary Table IV.S1 Results of cell-specific $^{33}P_i$ uptake by analysis of digital autoradiographs. Individual chains are labelled in Supplementary Figure IV.S7. Total uptake (*) was calculated for 1500 cells cm^{-3}

chain ID	cell number	area	recalculated activity		P_i uptake	
		mm^2	*Bq mm^{-2}*	*Bq $cell^{-1}$*	*nmol $cell^{-1}$ d^{-1}*	*nmol cm^{-3} d^{-1}*
Anoxic A1	16	0.67	238	9.89	0.0819	82
Anoxic A2	4	0.29	224	16.33	0.1352	135
Anoxic A3	11	0.11	121	1.22	0.0101	10
Anoxic A4	10	0.21	152	3.22	0.0267	27
Anoxic A5	21	-	-	0	0	0
Anoxic A6	7	-	-	0	0	0
Anoxic A7	38	-	-	0	0	0
Anoxic A8	29	-	-	0	0	0
Anoxic total	136			1.98	0.0164	25 nmol cm^{-2} d^{-1}*
Oxic O1	7	0.77	131	14.38	0.1191	119
Oxic O2	7	0.42	139	8.42	0.0697	70
Oxic O3	4	0.25	368	23.18	0.1919	192
Oxic O4	16	0.60	270	10.21	0.0845	85
Oxic O5	2	0.07	172	6.07	0.0503	50
Oxic O6	4	0.09	129	2.92	0.0242	24
Oxic O7	27	0.58	12961	1.32	0.0109	11
Oxic O8	9	0.45	242	12.19	0.1009	101
Oxic O9	14	0.73	113	5.88	0.0487	49
Oxic O10	10	0.77	439	33.59	0.2781	278
Oxic O11	12	0.59	115	5.68	0.0471	47
Oxic O12	8	0.37	237	11.06	0.0916	92
Oxic total	120			9.66	0.0800	120 nmol cm^{-2} d^{-1}*

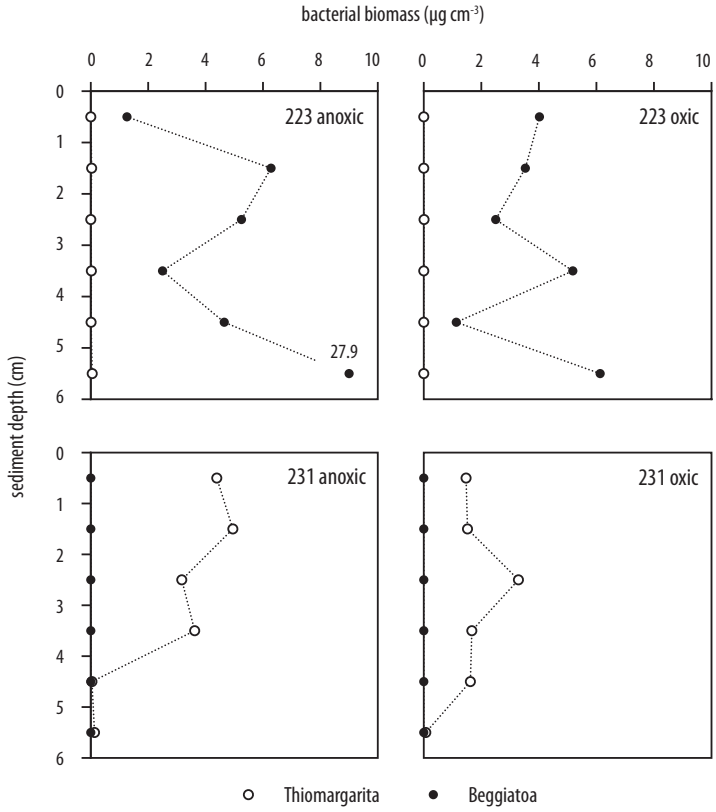

Supplementary Figure IV.S1 Profiles of bacterial biomass of large sulfur bacteria *Beggiatoa* (dots) and *Thiomargarita* (circles) in the upper 6 cm sediment layer that was used in anoxic and oxic incubation experiments and controls at sites 223 and 231

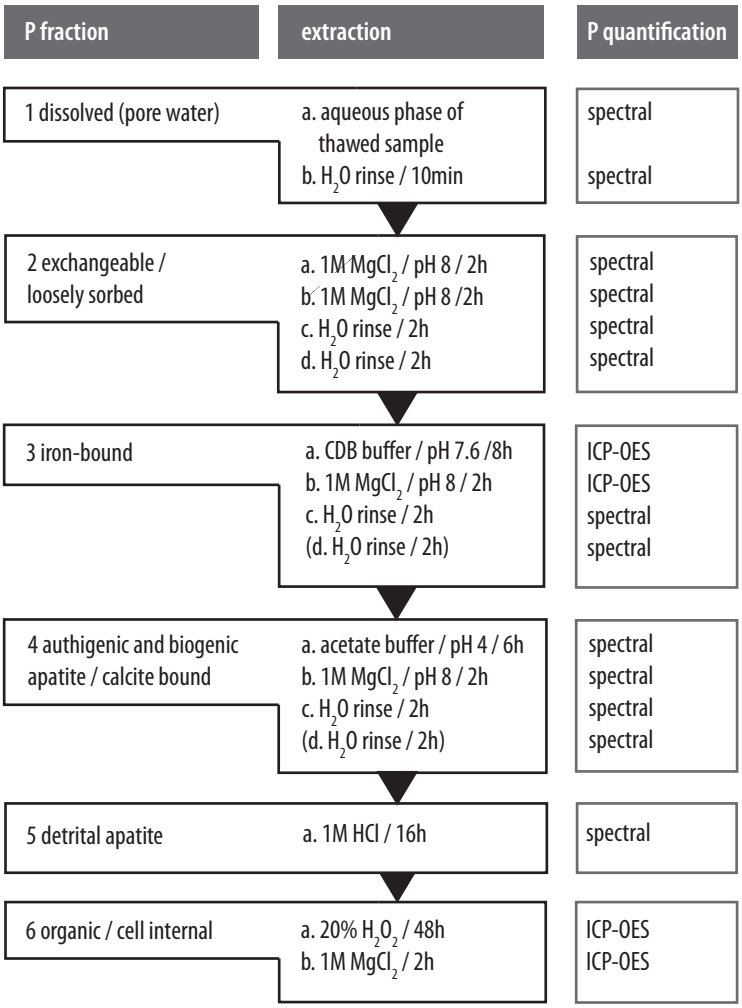

Supplementary Figure IV.S2 Sequential extraction protocol for sedimentary phosphate pools modified after Ruttenberg (1992). Each extraction step after the initial separation of interstitial water and solid phase (Step 1a) is accomplished by adding 10 mL of the given extractant, shaking for the given time on a horizontal shaker plate and finally centrifuging the sample. The supernatant is decanted and the pellet kept for the subsequent extraction step. Determination of phosphate concentration in the supernatant was accomplished either by a modified spectral photometric method (Murphy and Riley 1962, Grasshoff et al. 1999) or by elemental analysis in an inductively coupled plasma optical emission spectrometer (ICP-OES, Perkin Elmer Optima 3000R). In contrast to the original Ruttenberg protocol, we used a low-temperature, wet chemical combustion of organic bound phosphorus (Step 6) with hydrogen peroxide (H_2O_2). Potentially remaining H_2O_2 was boiled off in a 70 °C water bath before centrifugation. This method yielded between 92 and 99 % of recovery compared to the original incineration technique (tested on non-radioactive sediment, data not shown) and could be entirely operated in the isotope lab where no furnace was available. Hydrogen peroxide lyses cell membranes in the presence of oxidizing agents (Miller 1969) and thus includes internally stored P_i into this fraction

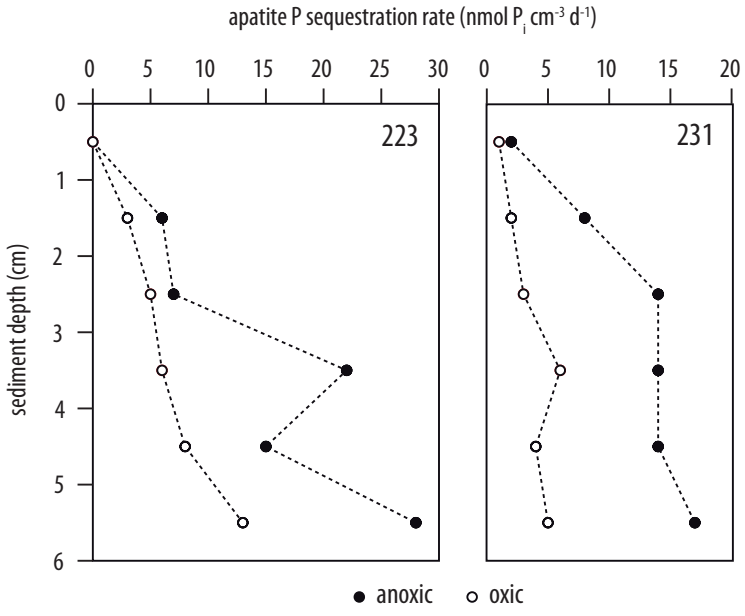

Supplementary Figure IV.S3 Transfer rates of P_i to the authigenic apatite fraction as calculated similar to Fossing and Jørgensen (1989). Left panel for incubations of site 223, right panel for incubations of site 231. Anoxic treatments are displayed as dots, and oxic treatments as circles. Note that apatite formation rates are calculated for each 1 cm depth slice, so the profiles represent integrated values and not discrete point data

```
SELECTED_OUTPUT
        -file     selected.out
        -saturation_indices       Hydroxyapatite
SOLUTION 1 Namibian shelf pore water
        temp     10
        pH               6.5    < adjust
        units    mol/l
        density  1.023
        Ca               0.011 ^< adjust
        P                0.0001 < adjust
        Na               0.675
        Cl               0.675
        -water   1 # kg
END
```

Supplementary Figure IV.S4 PHREEQC input file for calculation of hypothetical saturation indices for hydroxyapatite, "< adjust" denotes input parameters for the variation of pore water conditions

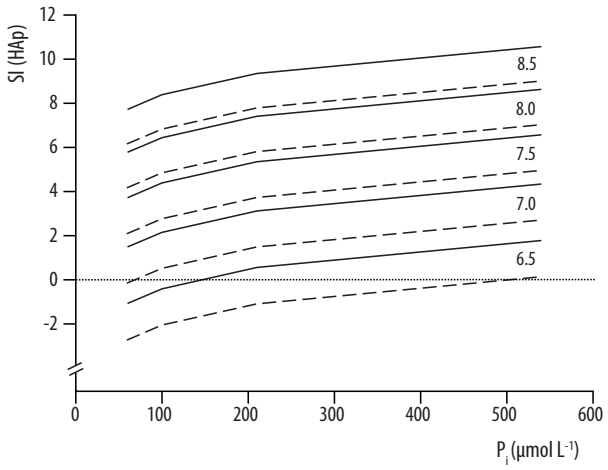

Supplementary Figure IV.S5 Minimum-maximum assessment for a hypothetical saturation field for hydroxyapatite (HAp) in a pore water surrogate solution. Shown are HAp saturation indices (SI) calculated with PHREEQC for five different pH (from bottom to top, 6.5 to 8.5) and two Ca^{2+} concentrations (dashed line 5000 µmol L^{-1}, solid line 11000 µmol L^{-1}), versus corresponding P_i concentrations that were taken from measured data. Zero line (dotted) marks equilibrium with a HAp solid phase, negative values indicate undersaturated, positive values oversaturated conditions

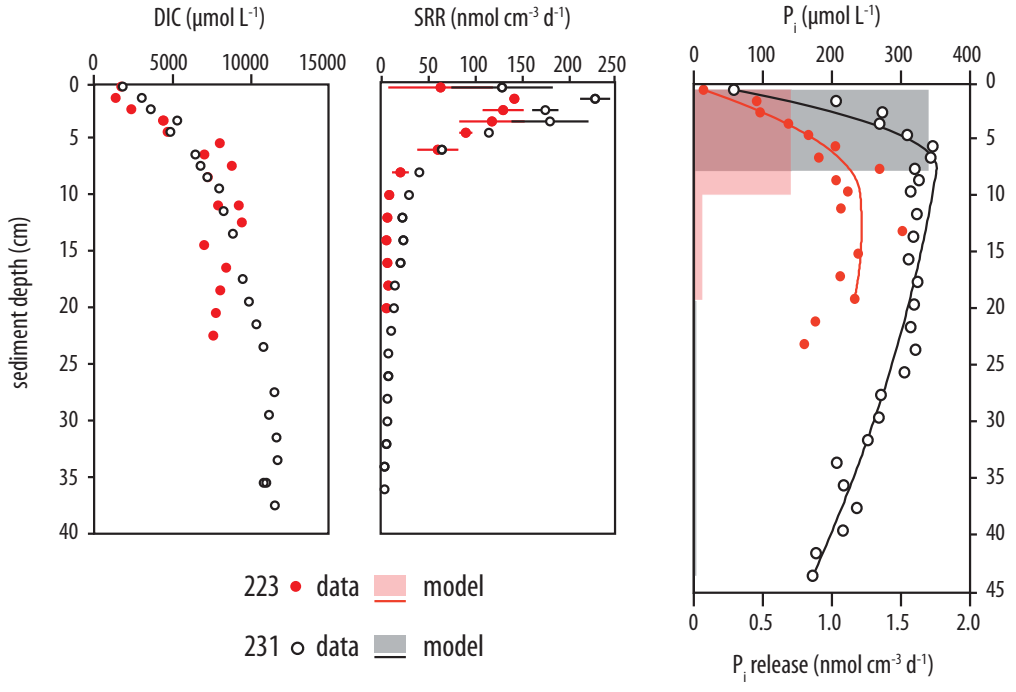

Supplementary Figure IV.S6 Dissolved inorganic carbon (DIC) concentration (left), bacterial sulfate reduction rates (SRR, middle), and phosphate (P_i) concentration profiles (right) for sites 223 (red dots) and 231 (circles). PROFILE model results for P_i production zones are included in the right panel.

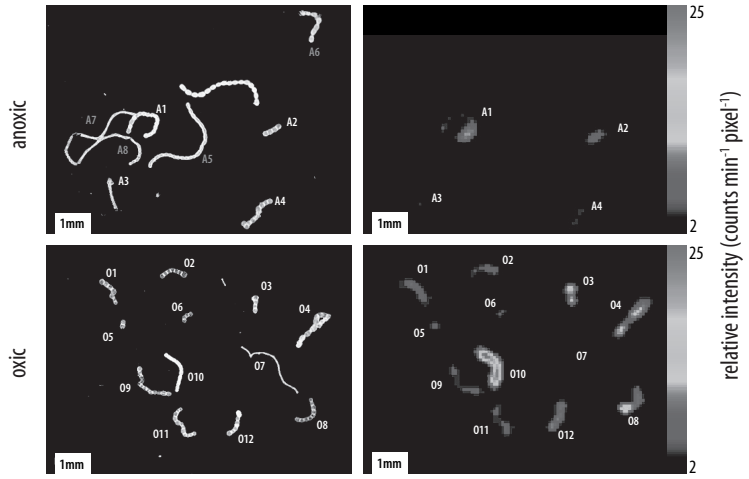

Supplementary Figure IV.S7 Chain identification for cell specific P_i uptake quantification in digital autoradiographs. Note that items A5 to A8 did not produce a signal on the autoradiograph.

V

Concluding remarks and future perspectives

V.1 Contribution to the understanding of benthic phosphorus biogeochemistry

In the present dissertation, we have investigated the role of microorganisms in biogeochemical transformations of phosphorus in the seabed. In particular, we have examined the major source for dissolved phosphate (P_i) in the sediments, the regeneration of P_i during remineralization of organic matter (Berner 1990), and the ultimate burial mechanism of oceanic P that controls marine productivity (Benitez-Nelson 2000), the authigenic formation of phosphorites (Föllmi 1996). We have successfully developed and applied a set of novel isotopic methods on the laboratory and field scale to trace the pathways that the P_i molecule takes in these transformations.

V.1.1 Regeneration and microbial cycling of P_i in the sediments

The stable oxygen isotope composition of dissolved P_i served as an isotopic biosignature (Blake et al. 2001) for P_i regeneration and microbial cycling in the sediments. Recent water column studies have suggested the potential of this parameter for obtaining information of biological P cycling (Colman et al. 2005; Liang and Blake 2009; McLaughlin et al. 2006).

In Chapter II, we have shown that it is possible to determine this parameter also in sediment pore water samples, where P_i quantities were previously too small for the application of stable isotope ratio mass spectrometry (Colman 2002). We have presented a refined micro-extraction protocol in detail, which we believe to be reproducible and robust enough for a routine application in future investigations.

Chapter II also includes a highly novel dataset of $\delta^{18}O_P$ in pore water samples of two sediment cores of the Morocco margin. These two cores revealed a pattern of pronounced isotopic disequilibria and equilibria of P_i with ambient water, in a range of + 19.5 to + 27.3 ‰ VSMOW. Disequilibria have been generally perceived to represent dominance of P_i regeneration, while equilibria were indicative of intense microbial P_i uptake and release (Blake et al. 2005; Colman et al. 2005). We could therefore determine the percentage of regenerated P_i in the pore water pool with a simple isotope-mixing model, and found it enhanced in the upper parts of the cores close to the sediment surface, in line with the expectation of high mineralization rates in these sediment layers.

In Chapter III, we presented an extensive, integrated field study of benthic P cycling across a continental slope and shelf transect in the Benguela upwelling region offshore Namibia. We combined established methods of marine geochemistry, such as pore water profiling and steady state modeling, with the pioneering investigation of P_i oxygen isotopes. We aimed to validate a hypothesis that distinct P_i regeneration regimes, which were identified by mineralization activity and ratio of DIC and P_i production on the basis of the geochemical investigation, are reflected by the $\delta^{18}O_P$ in the pore water samples. We also questioned whether benthic microbial communities are P_i or substrate limited, which are both main drivers of P_i regeneration, but have different implications for the livelihood of the microbial community (Van Mooy et al. 2006). Phosphate limitation has frequently been observed in pelagic bacterioplankton (Thingstad et al. 1998), and we searched for isotopic evidence of such limitation.

We found a much more complex pattern of $\delta^{18}O_p$ in the sediment pore waters than expected from the classification of geochemical settings. Sites with similar mineralization characteristics revealed distinct isotopic signatures. We found preservation of isotope disequilibria, indicative of regeneration, at deep-sea stations low in P_i concentrations, and often fully equilibrated P_i in sites with high mineralization and P_i concentration. In contrast to the expectations from earlier water column $\delta^{18}O_P$ studies, where deep-sea P_i was in equilibrium with water and indicated intensive microbial turnover (Colman et al. 2005; McLaughlin et al. 2006), we observed significant disequilibria in the bottom waters of the Benguela upwelling system. This points to a discontinuity of water column and sediment P_i in the benthic boundary layer, where often high mineralization rates prevail (Jørgensen and Revsbech 1985).

A sophisticated isotope mass balance model that considers enzymatic systems and the composition of organic-bound P allowed us to introduce a parameter for the P_i recycling efficiency of the microbial community.

We believe that different P_i uptake strategies in microorganisms, that are controlled by ambient P_i concentrations, have a strong influence on the preservation of pore water $\delta^{18}O_P$ signatures. We argued that P_i limitation induces a specific P_i crossmembrane transport system (Jansson 1988), keeping equilibrated P_i within the cell and leaving the isotopic disequilibrium, regeneration signature in the pore water behind. In contrast, high P_i concentrations cause unspecific crossmembrane transport and rapid exchange of extra- and intracellular P_i (Jansson 1988; van Veen 1997), which is reflected in thorough equilibration of the P_i pool. This effect was previously unaccounted, but has important consequences for future studies of $\delta^{18}O_P$ in marine ecosystems.

V.1.2 Microbial contribution to the authigenic formation of phosphorites

In Chapter IV, we have used a combination of radiotracer labeling and experimental fractionation of sedimentary P_i pools, to track sedimentary P_i transfers on the time scale of incubation experiments, and reveal the microbial role in the authigenic formation of phosphorites. This role is suspected to be active and not only restricted to P_i enrichment in the pore waters due to high mineralization activity (Nathan et al. 1993; Schulz and Schulz 2005). In the Benguela upwelling system, where recent phosphogenesis takes place, large sulfur bacteria of the genus *Thiomargarita namibiensis* have been the prime suspects, since they are able to store and release P_i in significant amounts, a mechanism that is induced by redox conditions at the sediment surface (Schulz 2006; Schulz and Schulz 2005).

With the incubation of sediments from the Namibian mudbelt we provided the first direct evidence for this intensely debated microbial activity in phosphorite formation in the seabed. In our experiments, the presence of live bacteria was pivotal to phosphorite precipitation, though pore water chemistry indicated oversaturation with respect to apatite also in sterile control assays. We showed that the P_i sequestration rates easily outbalanced P_i regeneration under anoxic conditions. Phosphate uptake rates by *Thiomargarita namibiensis* strongly suggests that these bacteria provide a transient P_i reservoir, and their unique physiology may antagonize the earlier postulated, positive feedback between enhanced anoxic P_i regeneration (Ingall et al. 1993), stimulated primary production, and anoxia in bottom waters (Diaz and Rosenberg 2008). We believe that such a P_i shunt may also exist in other habitats of large sulfur bacteria, *e.g.* at the continental margin off Chile and Peru and in the Gulf of Mexico (Schulz and Jorgensen 2001). How the peculiar P cycle of these regions will react – or has already reacted - to anthropogenic coastal eutrophication and global warming (Diaz and Rosenberg 2008) is highly unclear.

V.2 Future research perspectives

Chapter II and III have shown that the interpretation of $\delta^{18}O_P$ is not that straightforward, but yields insights into sedimentary P cycling that are beyond the scope of classic geochemical investigations of P_i concentration and distribution. In our studies, it has become evident that concepts of P_i turnover in the water column are not easily applied to P_i turnover in marine sediments. It remains to be resolved whether this is due to fundamentally different microbial strategies of P_i metabolism, or different geochemical boundary conditions of both domains.

Chapter IV has highlighted the great potential of a radiotracer-based rate determination in the marine P cycle. We suggest three topics for future studies that have potential to advance the understanding of the P_i oxygen isotope signature, and the transformation rates and fluxes between important pools of P in the ocean.

V.2.1 Role of P transformations and exchange in the benthic boundary layer

Concentration gradients of dissolved P_i across the sediment-water interface stimulate diffusive exchange, and bioturbation and sediment relocation on the seafloor promote advective transport. Thus, it is likely that dissolved P_i in the sediments is not entirely disconnected from the water column. It will therefore be crucial to investigate the isotopic nature of P_i transformations across and in the benthic boundary layer that is the interface of both domains. Recently developed, dedicated equipment will help in obtaining undisturbed water samples, and quantitative information on diffusive and advective flux rates from the benthic boundary layer.

V.2.2 Tracking composition and transformation of P_{org} through the water column into the sediments

The initial oxygen isotopic signature of the organic bound phosphate, as well as the substrate composition of the organic matter itself, will have a significant impact on the characteristic of $\delta^{18}O_P$ in the compartment of interest. For example, the isotopic mass balance model introduced in Chapter III relies heavily on a hypothetical P_{org} composition. To better constrain such mass balance models we suggest determining the composition of OM with respect to important substrates for microbial P_i cycling. In particular, this should involve the quantification of RNA, DNA, and unspecific phosphomonoesters in the organic portion of marine particulate matter and sediments, for which a broad

range of methods exists (Dell'anno et al. 1998). The unbiased, direct determination of $\delta^{18}O_P$ has become feasible with a recent UV-based extraction method (Liang and Blake 2006). Such investigations would also elucidate P_i regeneration from particulate OM during the sinking process, which is pronounced in pelagic oxygen minima below the photic zone.

V.2.3 Determination of P_i turnover rates in different compartments of the marine P cycle

Earlier investigations have focused on the assessment and quantification of standing stocks of P_i in the ocean and have determined large scale residence times (Benitez-Nelson 2000). In contrast, only little is known about the temporal scale on which P_i is biologically moved between the pools. We believe that the framework that we have presented for the application of the ^{33}P radiotracer is ideal to visualize and quantify P_i transfer in biogeochemical systems – provided that the target pools are easily to separate. Another advantage is that radiolabel experiments can be carried out in intact sediment samples, which are probably more accurate in representing in situ dynamics than microbial cultures or artificial substrates.

Two yet uninvestigated examples illustrate the potential of P_i radiolabel applications. First, the uptake and incorporation rate of $^{33}P_i$ into microbial DNA should be a useful estimate of growth or stagnation of a benthic microbial population. Second, adsorption and desorption kinetics of P_i on iron oxyhydroxide surfaces during redox controlled iron cycling could be easily investigated with $^{33}P_i$ and should provide insights into the effectiveness of the "iron trap" often observed in a wide range of marine settings.

V.3 References

Benitez-Nelson CR (2000) The biogeochemical cycling of phosphorus in marine systems. Earth-Science Reviews 51:109-135

Berner RA (1990) Diagenesis of phosphorus in sediments from non-upwelling areas. Phosphate Deposits of the World 3:27-33

Blake RE, Alt JC, Martini AM (2001) Oxygen isotope ratios of PO_4: An inorganic indicator of enzymatic activity and P metabolism and a new biomarker in the search for life. PNAS 98:2148-2153

Blake RE, O'Neil JR, Surkov AV (2005) Biogeochemical cycling of phosphorus: insights from oxygen isotope effects of phosphoenzymes. American Journal of Science 305:596-620

Colman AS (2002) The oxygen isotope composition of dissolved inorganic phosphate and the marine phosphorus cycle. PhD Thesis, Department of Geology & Geophysics, Yale University, New Haven

Colman AS, Blake RE, Karl DM, Fogel ML, Turekian KK (2005) Marine phosphate oxygen isotopes and organic matter remineralization in the oceans. PNAS 102:13023-13028

Dell'anno A, Fabiano M, Duineveld GCA, Kok A, Danovaro R (1998) Nucleic acid (DNA, RNA) quantification and RNA/DNA ratio determination in marine sediments: comparison of spectrophotometric, fluorometric, and high-performance liquid chromatograpyh methods and estimation of detrital DNA. Applied and Environmental Microbiology 64:3238-3245

Diaz RJ, Rosenberg R (2008) Spreading dead zones and consequences for marine ecosystems. Science 321:926-929

Föllmi KB (1996) The phosphorus cycle, phosphogenesis and marine phosphate-rich deposits. Earth-Science Reviews 40:55-124

Ingall ED, Bustin RM, Van Capellen P (1993) Influence of water column anoxia on the burial and preservation of carbon and phosphorus in marine shales Geochim Cosmochim Ac 57:303-316

Jansson M (1988) Phosphate uptake and utilization by bacteria and algae. Hydrobiologia 170:177-189

Jørgensen BB, Revsbech NP (1985) Diffusive boundary layer and the oxygen uptake of sediments and detritus. Limnology and Oceanography 30:111-122

Liang Y, Blake R (2009) Compound- and Enzyme-specific Phosphodiester Hydrolysis Mechanisms Revealed by $\delta^{18}O$ of Dissolved Inorganic Phosphate: Implications for marine P cycling. Geochim Cosmochim Ac 73:1-49

Liang Y, Blake RE (2006) Oxygen isotope composition of phosphate in organic compounds: Isotope effects of extraction methods. Organic Geochemistry 37:1263-1277

McLaughlin K, Kendall C, Silva SR, Young M, Paytan A (2006) Phosphate oxygen isotope ratios as a tracer for sources and cycling of phosphate in North San Francisco Bay, California. Journal of Geophysical Research-Biogeosciences 111

Nathan Y, Bremner JM, Loewenthal RE, Monteiro P (1993) Role of bacteria in phosphorite genesis. Geomicrobiology Journal 11:69-76

Schulz HN (2006) The genus Thiomargarita. Prokaryotes 6:1156-1163

Schulz HN, Jorgensen BB (2001) Big bacteria. Annual Review of Microbiology 55:105-137

Schulz HN, Schulz HD (2005) Large sulfur bacteria and the formation of phosphorite. Science 307:416-418

Thingstad TF, Zweifel UL, Rassoulzadegan F (1998) P limitation of heterotrophic bacteria and phytoplankton in the northwest Mediterranean. Limnology and Oceanography 43:88-94

Van Mooy BAS, Rocap G, Fredricks HF, Evans CT, Devol AH (2006) Sulfolipids dramatically decrease phosphorus demand by picocyanobacteria in oligotrophic marine environments. PNAS 103:8607-8612

van Veen HW (1997) Phosphate transport in prokaryotes: molecules, mediators and mechanisms. Antonie van Leeuwenhoek 72:299-315

VI

Appendix

This appendix contains four abstracts of published or submitted manuscripts that resulted from other research activities before or during the dissertation project. All were published or edited within the period of the project. An overview of (co-)supervised student projects is given at the end of the chapter.

VI.1 In situ determination of sulfate turnover in peatlands: A down-scaled push–pull tracer technique

Tobias Goldhammer[1,2], Florian Einsiedl[3], Christian Blodau[2]

[1] MARUM Center for Marine Environmental Research, University of Bremen, Bremen, Germany, [2] Limnological Research Station, Dept. of Hydrology, University of Bayreuth, Bayreuth, Germany, [3] Institute of Groundwater Ecology, GSF National Research Center for Environment and Health, Neuherberg, Germany

published in *Plant Nutrition and Soil Science* 171, pp. 740-750, 2008

Abstract

Bacterial sulfate reduction (BSR) is a key process in anaerobic respiration in wetlands and may have considerable impacts on methane emissions. A method to determine sulfate production and consumption in situ is lacking to date. We applied a single-well, injection-withdrawal tracer test for the in situ determination of potential sulfate turnover in a northern temperate peatland. Piezometers were installed in three peat depth levels (20, 30, and 50 cm) during summer 2004, and three series of injection-withdrawal cycles were carried out over a period of several days. Turnover rates of sulfate, calculated from

first-order-reaction constant k (–0.097 to 0.053 h^{-1}) and pore-water sulfate concentrations (approx. 10 mol L^{-1}), ranged from –1.3 to -9.0 nmol cm–3 d–1 for reduction and from +0.7 to +25.4 nmol cm–2 d–1 for production, which occurred after infiltration of water following a heavy rainstorm. Analysis of stable isotopes in peat-water sulfate revealed slightly increasing d34S values and decreasing sulfate concentrations indicating the presence of BSR. The calculated low sulfur-fractionation factors of <2‰ are in line with high sulfate-reduction rates during BSR. Routine application will require technical optimization, but the method seems a promising addition to common ex situ techniques, as the investigated soil is not structurally altered. The method can furthermore be applied at low expense even in remote locations.

VI.2 Desiccation and product accumulation constrain heterotrophic anaerobic respiration in peats of an ombrotrophic temperate bog

Tobias Goldhammer[1,2], Christian Blodau[2]

[1] MARUM Center for Marine Environmental Research, University of Bremen, Bremen, Germany, [2] Limnological Research Station, Dept. of Hydrology, University of Bayreuth, Bayreuth, Germany

published in *Soil Biology and Biochemistry* 40(8), pp. 2007-2015, 2008

Abstract

To gain insight into the effects of drying and rewetting events on anaerobic respiration in ombrotrophic peat soils, we investigated bacterial sulfate (SO_4) reduction and methane (CH_4) production in anaerobic incubations of intact peat microcores from 30 to 40cm depth of Mer Bleue bog, Ontario/Canada. Concentrations of dissolved SO_4, carbon dioxide (CO_2), CH_4, acetate, and hydrogen (H_2) were recorded and net turnover rates calculated from regression. Gross rates of bacterial sulfate reduction were determined by $^{35}SO_4$ tracer incubation. After incubation, the peat was dried and rewetted, with saturated peat serving as control. CO_2 production was initially rapid (up to < 360 nmol cm^{-3} d^{-1}) and slowed towards an endpoint of 2–3 mmol l^{-1}, which was only partly related to thresholds of Gibbs free energies of the involved processes. Acetate rapidly accumulated to levels of 600–800 µmol L^{-1} and remained constant thereafter. CH_4

production (0 to 2.8 nmol cm^{-3} d^{-1}) was small and delayed, even after SO_4 was depleted, by about 30-40 d. Hydrogenotrophic methanogenesis was endergonic and the process thus likely followed an acetotrophic pathway. Drying and rewetting replenished the SO_4 pool, enhanced SO_4 reduction rates and suppressed methanogenesis. The overall contribution of net SO_4 reduction and methanogenesis to the CO_2 production rate was small (0.5 to 22 %) and only enhanced in replicates subjected to drying (35 to 62 %). The major fraction of respiration in the incubated peat cores thus followed yet unidentified pathways.

VI.3 Electron transfer processes of dissolved organic matter and their potential significance for anaerobic respiration in a northern bog

Tobias Heitmann[1], Tobias Goldhammer[1,2], Julia Beer[1], Christian Blodau[1]

[1] *Limnological Research Station, Dept. of Hydrology, University of Bayreuth, Bayreuth, Germany,* [2] *MARUM Center for Marine Environmental Research, University of Bremen, Bremen, Germany*

published in *Global Change Biology* 13, pp. 1771-1785, 2007

Abstract

We investigated electron transfer processes of dissolved organic matter (DOM) and their potential importance for anaerobic heterotrophic respiration in a northern peatland. Electron accepting and donating capacities (EAC, EDC) of DOM were quantified using dissolved H_2S and ferric iron as reactants. Carbon turnover rates were obtained from porewater profiles (CO_2, CH_4) and inverse modeling. Carbon dioxide was released at rates of 0.2-5.9 mmol m^{-2} d^{-1} below the water table. Methane (CH_4) formation contributed 10%, and oxygen consumption 2% to 40%, leaving a major fraction of CO_2 production unexplained. DOM oxidized H_2S to thiosulfate and was reduced by dissolved ferric iron. Reduction with H_2S increased the subsequently determined EDC compared to untreated controls, indicating a reversibility of the electron transfer. In situ redox capacities of DOM ranged from 0.2 to 6.1 mEq g^{-1} C (EAC) and from 0.0 to 1.4 mEq g^{-1} C (EDC), respectively. EAC generally decreased with depth and changed after a water table drawdown and rebound by 20 and 45 mEq m^{-2}, respectively. The change in EAC during

the water table fluctuation was similar to CH_4 formation rates. In peatlands, electron transfer of DOM may thus significantly contribute to the oxidation of reduced organic substrates by anaerobic heterotrophic respiration, or by maintaining the respiratory activity of sulfate reducers via provision of thiosulfate. Part of the anaerobic electron flow in peat soils is thus potentially diverted from methanogenesis, decreasing its contribution to the total carbon emitted to the atmosphere.

VI.4 The evolution of Saharan dust input on Lanzarote (Canary Islands) – influenced by human activity in the Northwest Sahara during the Early Holocene?

Hans von Suchodoletz[1], Hedi Oberhänsli[2], Dominik Faust[3], Markus Fuchs[1], Cécile Blanchet[4], Tobias Goldhammer[5], Ludwig Zöller[1]

[1] Institute of Geography, University of Bayreuth, Bayreuth, Germany, [2] Section 5.2, GFZ Helmholtz Center, Potsdam, Germany, [3] Institute of Geography, Technical University of Dresden, Dresden, Germany, [4] Sedimentology, IFM-GEOMAR Leibniz Center for Marine Sciences, Kiel, Germany, [5] MARUM Center for Marine Environmental Research, University of Bremen, Bremen, Germany

Manuscript submitted to *The Holocene*, 06.08.2009

Abstract

An overall Holocene increase of Saharan dust input to the Canary Islands and to the North Canary Basin is accompanied by a strong coarsening of Saharan dust in loess-like sediments deposited on Lanzarote from about 7 to 8 ka. No similar coarsening events are indicated in investigations of the sedimentological record for the last 180 ka, therefore a mobilization of dust by anthropogenic activity in the Northwest Sahara east of the Canary Islands is assumed. Although scarce archaeological data from the coastal area of that region does not point to strong anthropogenic activity during the Early Holocene, a high density of unexplored archaeological remains is reported from the coastal hinterlands in the Western Sahara. Thus, the hypothesis of early anthropogenic activity cannot be excluded.

VI.5 Student projects

10 – 11/2008 BSc thesis in Geosciences "Enigmatic hollows at the Namibian continental slope – clues from a geochemical investigation", Simone Sauer, Department of Geosciences, University of Bremen

11/2007 – 01/2008 BA thesis in Geography „Terrigene Sedimente vor der marokkanischen Küste: eine geochemische Untersuchung von Sedimentkern GeoB11804-4" (in German), Tanja Broder, Department of Geography, University of Bremen

07 – 08/2007 Student project "Phosphate speciation in sediments offshore Morocco", Anna Silyakova, Summer Student Fellow at Research Center Ocean Margins, St. Petersburg State University, Russia, and University of Bremen

Acknowledgements

This dissertation would not have been possible without the enduring help, support and contribution of many people. My deepest thanks go to:

Matthias Zabel for his motivation and supervision through the years, for trust, continuous encouragement and for giving me every freedom to develop my research.

Tim Ferdelman for his inspiring enthusiasm, mentoring and many *radiant* ideas.

Kai-Uwe Hinrichs for his steady support and the willingness to review this dissertation.

Benjamin Brunner for thought-provoking discussions and loads of constructive criticism.

Wolfgang Bach, Katrin Heindel, Julia Gottschalk, Gerhard Bohrmann, Julius Lipp and Johan Faust for joining my dissertation committee. Volker Brüchert for sharing the opportunity of an exciting study.

The technical crew at Geochemistry Group and MPI Bremen, especially lab head Martin Kölling, Silvana Pape, Susanne Siemer, Karsten Enneking, Kirsten Imhoff and Thomas Max.

My students and invaluable Hiwis Tanja Broder and Simone Sauer.

All past and present colleagues at the Geochemistry Group, especially Victoria Marek, Christian März, Kathrin Küster-Heins, Jan Hoffmann, Luzie Schnieders, André Gaßner, Jens Gröger, Jörn Tonnius, Wiebke Kallweit, Kay Hamer, Jürgen Schröter, Horst D. Schulz and Gisela Haack.

All friends, colleagues and collaborators at Department of Geosciences, MARUM and MPI Bremen: Cécile Blanchet, Stijn de Schepper, Yu-Shih Lin, Florence Schubotz, Julius Lipp, Verena Heuer, Johan Faust, Vera Bender, Eva Niedermeyer, Tim Freudenthal, Gail Lee Arnold, Alberto Robador, Michael J. Formolo and Laura Wehrmann.

My friends.

My family.

Julia Schwärzle for everything and everything else.

Erklärung gemäß § 6 Abs. 5 der Promotionsordnung der Universität Bremen für die mathematischen, natur- und ingenieurwissenschaftlichen Fachbereiche

Hiermit versichere ich, dass ich die vorliegende Arbeit

1. ohne unerlaubte fremde Hilfe angefertigt habe,

2. keine anderen als die von mir im Text angegebenen Quellen und Hilfsmittel benutzt habe und

3. die den benutzten Werken wörtlich oder inhaltlich entnommenen Stellen als solche kenntlich gemacht habe.

Bremen, 02. Oktober 2009

Tobias Goldhammer